MARIA S. MERIAN-Berichte

FLUID DYNAMICS AND SLOPE STABILITY OFFSHORE W-SPITSBERGEN: EFFECT OF BOTTOM WATER WARMING ON GAS HYDRATES AND SLOPE STABILITY

Cruise No. MSM21/4

August 12, 2012 – September 11, 2012
Reykjavik (Iceland) - Emden (Germany)

C. Berndt, I. Dumke, T. Feseker, C. Graves, P. Franek, K. Hissmann, V. Hühnerbach, S. Krastel, K. Lieser, H. Niemann, L. Steinle,T. Treude

Editorial Assistance:

DFG-Senatskommission für Ozeanographie
MARUM – Zentrum für Marine Umweltwissenschaften der Universität Bremen

2014

The MARIA S. MERIAN-Berichte are published at irregular intervals. They are working papers for people who are occupied with the respective expedition and are intended as reports for the funding institutions. The opinions expressed in the MARIA S. MERIAN-Berichte are only those of the authors.

The MARIA S. MERIAN expeditions are funded by the *Deutsche Forschungsgemeinschaft (DFG)* and the *Bundesministerium für Bildung und Forschung (BMBF)*.

Editor:
DFG-Senatskommission für Ozeanographie
c/o MARUM – Zentrum für Marine Umweltwissenschaften
Universität Bremen
Leobener Strasse
28359 Bremen

Author:
Prof. Dr. Christian Berndt
Marine Geodynamics
GEOMAR
Wischhofstr. 13
24148 Kiel

Telefon: +494316002273
Telefax:+494316002922
e-mail: cberndt@geomar.de

Citation: C. Berndt, I. Dumke, T. Feseker, C. Graves, P. Franek, K. Hissmann, V. Hühnerbach, S. Krastel, K. Lieser, H. Niemann, L. Steinle, T. Treude (2014) FLUID DYNAMICS AND SLOPE STABILITY OFFSHORE W-SPITSBERGEN: EFFECT OF BOTTOM WATER WARMING ON GAS HYDRATES AND SLOPE STABILITY - Cruise No. MSM 21/4 – August 12 – September 11, 2012 – Reykjavik (Iceland) – Emden (Germany). MARIA S. MERIAN-Berichte, MSM21/4, 96 pp., DFG-Senatskommission für Ozeanographie, DOI:10.2312/cr_msm21_4

ISSN 2195-8483

Table of Contents

1 Summary

The main goal of MSM21/4 was the study of gas hydrate system off Svalbard. We addressed this through a comprehensive scientific programme comprising dives with the manned submersible JAGO, seismic and heat flow measurements, sediment coring, water column biogeochemistry and bathymetric mapping. At the interception of the Knipovich Ridge and the continental margin of Svalbard we collected seismic data and four heat flow measurements. These measurements revealed that the extent of hydrates is significantly larger than previously thought and that the gas hydrate system is influenced by heat from the oceanic spreading centre, which may promote thermogenic methane production and thus explain the large extent of hydrates. At the landward termination of the hydrate stability zone we investigated the mechanisms that lead to degassing by taking sediment cores, sampling of carbonates during dives, and measuring the methane turn-over rates in the water column. It turned out that the observed gas seepage must have been ongoing for a long time and that decadal scale warming is an unlikely explanation for the observed seeps. Instead seasonal variations in water temperatures seem to control episodic hydrate formation and dissociation explaining the location of the observed seeps. The water column above the gas flares is rich in methane and methanotrophic microorganisms turning over most of the methane that escapes from the sea floor. We also surveyed large, until then uncharted parts of the margin in the northern part of the gas hydrate province. Here, we discovered an almost 40 km wide submarine landslide complex. This slide is unusual in the sense that it is not located at the mouth of a cross shelf trough such as other submarine landslides on the glaciated continental margins around the North Atlantic. Thus, the most widely accepted explanation for the origin of such slides, i.e. overpressure development due to deposition of glacial sediments on top of water rich contourites, is not applicable. Instead we find gas-hydrate-related bottom simulating reflectors underneath the headwalls of this slide complex, possibly indicating that subsurface fluid migration plays a major role in its genesis.

Zusammenfassung

Das Hauptziel der Ausfahrt MSM21/4 war die Untersuchung des Gashydratsystems vor Spitzbergen. Zur Erreichung dieses Zieles führten wir ein umfangreiches wissenschaftliches Programm durch, das den Einsatz des bemannten Forschungstauchbootes JAGO, seismische und Wärmestrommessungen, Sedimentkernentnahme, Wassersäulen-Biogeochemie, sowie Fächerecholotkartierungen umfasste. Am nördlichen Ende des Knipovich-Rückens sammelten wir seismische Daten und machten Wärmestrommessungen. Diese Daten zeigten, dass sich die Gashydratvorkommen über ein größeres Gebiet erstrecken, als bisher angenommen und dass der mittelozeanische Rücken dem Gashydratgebiet Wärme zuführt, was die große Verbreitung von Gashydraten in diesem Gebiet erklären mag, da sich hierdurch auch thermogen Methan bilden sollte. Im proximalen Bereich der Gashydratstabilitätszone untersuchten wir die Prozesse, die zur Entgasung der Sedimente führen, basierend auf Sedimentkernen und während der Tauchgänge gesammelten Karbonatproben, sowie gemessenen Umsatzraten von Methan in der Wassersäule. Es stellte sich heraus, dass die Gasaustritte schon lange aktiv sein müssen und dass die dekadische Erwärmung eine unwahrscheinliche Erklärung für die beobachteten Gasaustrittsstellen ist. Stattdessen scheint es, dass saisonale Schwankungen der Meeresbodentemperatur episodische Hydratbildung und –dissoziation kontrollieren und somit die Lage der Gasaustritte beeinflussen. Die Wassersäule über den Gasaustritten ist reich an Methan und methanotrophen Mikroorganismen, die einen Großteil des austretenden Methans noch in der Wassersäule umsetzen. Desweiteren kartierten wir ein großes Stück des bislang unbekannten nördlichen Teils der Gashydratprovinz. Hierbei entdeckten wir eine fast 40 km breite Hangrutschung. Diese zeichnet sich dadurch aus, dass sie nicht am Ausgang einer eiszeitlichen Schelfrinne liegt, wie alle anderen bisher gefundenen

großen Rutschungen im Nordatlantik. Demnach treffen die bisherigen Erklärungsmuster für derartige Rutschungen, d.h. Überdruckentwicklung in von glazialen Sedimenten überlagerten hemipelagischen Kontourit-Sedimenten, in diesem Fall nicht zu. Stattdessen beobachten wir gashydratbezogene bodensimulierende Reflektoren unterhalb der Kanten der Rutschung, was darauf hindeuten kann, dass unterirdische Fluidmigration eine wichtige Rolle in der Entstehung der Rutschung spielt.

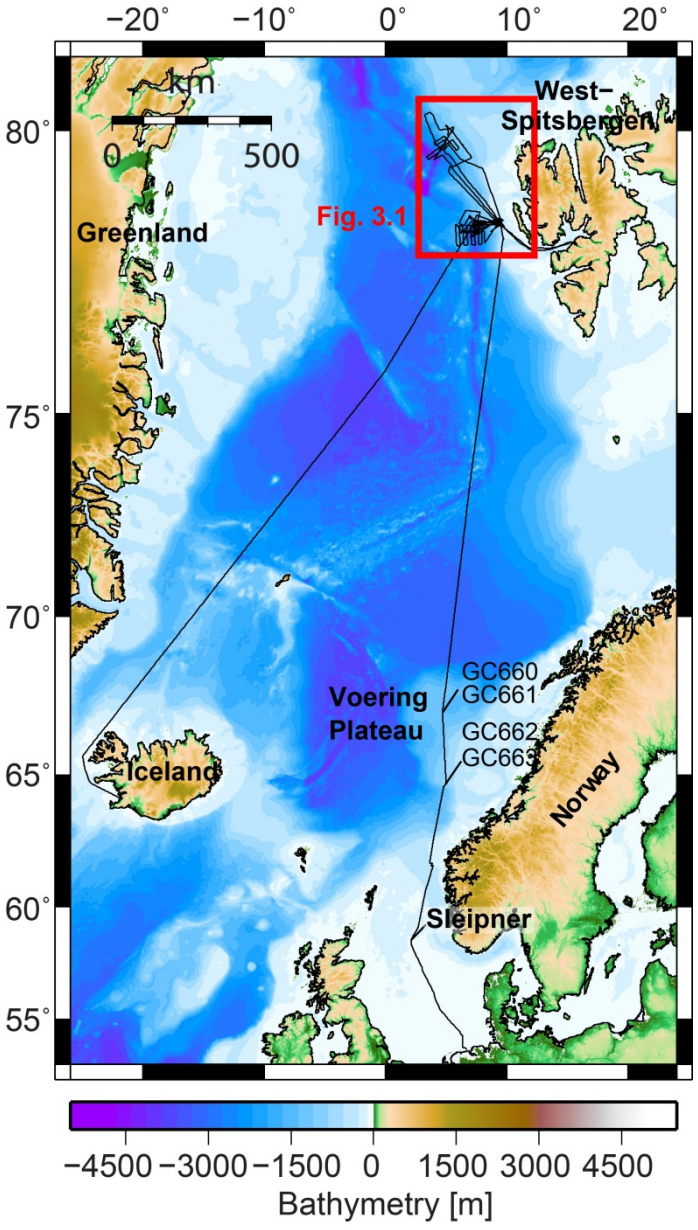

Fig. 1.1 GEBCO 30' bathymetry map showing the cruise track. Cruise MSM21/4 started from Reykjavik, Iceland on 13-8-2012 and finished in Emden, Germany on 11-9-2012. The working areas were the continental margin off Svalbard, the Gjallar Ridge and Nyegga on the Vøring Plateau, and the Sleipner Field in the central North Sea.

2 Participants

Name	Discipline	Institution
Berndt, Christian, Prof.	Chief Scientist	GEOMAR
Krastel, Sebastian, Prof.	Leader Seismics	GEOMAR
Dumke, Ines	Seismics	GEOMAR
Gross, Felix	Seismics	GEOMAR
Lieser, Kathrin	Seismics	GEOMAR
Dünnbier, Karolin	Seismics	GEOMAR
Wetzel, Gero	Seismic Engineer	GEOMAR
Treude, Tina, Prof.	Leader biogeochemistry	GEOMAR
Niemann, Helge, Dr.	Leader water biochemistry	UBasel
Steinle, Lea	Water biochemistry	UBasel
Krause, Stefan, Dr.	Sediment geochemistry	GEOMAR
Kretschmer, Kerstin	Sediment geochemistry	GEOMAR
Bertics, Victoria, Dr.	Sediment geochemistry	GEOMAR
Graves, Carolyn	Sediment geochemistry	NOCS
Hühnerbach, Veit	Observatory	NOCS
Franek, Peter, Dr.	Observatory	UTromsø
Feseker, Tomas, Dr.	Heat flow	MARUM
Hissmann, Karen	JAGO	GEOMAR
Schauer, Jürgen	JAGO	GEOMAR
Fenske, Martin	JAGO	GEOMAR

GEOMAR GEOMAR Helmholtz Centre for Ocean Research, Kiel

NOCS National Oceanography Centre, University of Southampton

UBasel Department of Environmental Sciences, University of Basel

UTromsø Institute of Geology, University of Tromsø

MARUM Center for Marine Environmental Sciences, University of Bremen

3 Research Program

(Christian Berndt)

3.1 Introduction

Gas hydrates are ice-like crystals that form naturally at high pressure and low temperature in continental margin sediments at water depth greater than 300 m and in perma-frost areas, whenever there is enough methane and pore water (Sloan Jr., 1998). Once formed below the seafloor, their stability is mainly governed by temperature variations. Hence, hydrate stability will be strongly affected by warming of the seafloor.

Recent estimates of the total amount of carbon stored in gas hydrates range from 500 to 5000 Gt of carbon (Buffett and Archer, 2004; Milkov, 2004; Kvenvolden and Rogers, 2005). Additionally, gas hydrates are frequently underlain by free gas reservoirs that contain another approximate 1800 Gt of organic carbon (Buffett and Archer, 2004). Together the gas hydrate and underlying free gas reservoirs comprise almost half of the Earth's organic carbon that could enter the atmosphere. Therefore, it is of paramount importance that the mobility of this reservoir is understood. Archer and Buffett (2005) predict that, globally, a change in ocean temperature of 3°C would release ~4000 Gt of carbon into the ocean and atmosphere, while others claim that the amounts would be much smaller (Biastoch et al., 2011) showing that there is a dire need for more information. A large release of methane would have catastrophic effects on climate as most of this carbon as methane is a 25-35% more effective greenhouse gas than CO_2 (Harvey and Huang, 1995; Shindell et al., 2009).

So far, climate models do not include such a scenario but assume flux rates from the seafloor to be constant which is certainly not the case (Hill et al., 2004). Furthermore, climate modellers assume that the present amounts of released carbon are small, and that it therefore does not reach the atmosphere as methane gets oxidised in the water column (IPCC, 2001). However, it is becoming increasingly clear that even at present there are significant amounts of methane venting from the seabed and that up to 20% of this methane reaches the atmosphere even at times of no sudden gas hydrate dissociation due to bottom-water warming (Dimitrov, 2002; Judd et al., 2002; Kastner et al., 2005). In this situation it is important to understand how the gas hydrate reservoirs will react to future increases in bottom-water temperature, and if future bottom-water warming might trigger a sudden release of large amounts of methane leading to accelerated climate warming (Kennett et al., 2003).

Sudden submarine slope failures represent a natural hazard to seafloor infrastructure and to coastal communities due to their ability to generate large-scale tsunamis. Formation and dissociation of hydrate within sediments of continental margins affect the stability of submarine slopes in several ways. Hydrate in the pore space glues the sediment together. Growing bodies of hydrate (e.g. veins and lenses) re-structure the sediment into layers or bodies and ascending fluids and gases that reach this permeability barrier in the sediment may get trapped below the hydrate. The zone of hydrate occurrence, therefore, acts as stabilizing cement within the slope and as a barrier for migrating gases and fluids leading to under-consolidation. Also, the lower boundary may potentially act as a weak layer during slope failure.

Dissociation of gas hydrate (e.g. induced by rising temperatures and/or descending pressure), in contrast, reduces the slope stability (e.g. Kennett et al., 2003; Mienert et al., 2005). Destruction of the cementation between sediment particles and liquefaction of the remaining sediment formerly bound by hydrate leads to loss of structural support and increasing pore pressure. Higher pore pressure may in turn lead to fracturing of adjacent sediment. All these effects could, in combination with gravity and/or seismic acceleration, lead to slope failure.

There are several submarine landslides on glaciated continental margins that have been attributed to be at least partly related to dissociation of gas hydrates and migrating fluids (e.g. Mienert et al., 2005; Winkelmann and Stein, 2007). However, alternative explanations exist for all these slides. The site off Svalbard is perfect for testing the link between hydrates and slope stability as there is a large amount of background information and all the prerequisites for large scale sliding exist (Berndt et al., 2009).

Methane migrating through sediments can lead to a series of complex biogeochemical reactions, which are to a large extent governed by a microbial process called anaerobic oxidation of methane (AOM) (Boetius et al., 2000; Luff et al., 2003; Treude et al. 2003). In diffusive systems, AOM very effectively prevents methane emissions from the seafloor (Hinrichs and Boetius, 2002; Treude et al., 2005a). At advective methane seeps, the effectiveness of microbial methane consumption appears to be governed by the gas and fluid flux (Treude et al. 2003, Niemann et al., 2006). AOM organisms should be able to metabolically adapt to certain changes in these fluxes by regulating their methane turnover (Wegener and Boetius, 2008); however, adaptations might be limited based on the extremely slow growth rate of the organisms (Nauhaus et al., 2007). A prevailing question is how fast the benthic methane filter could respond to rapid increases in methane fluxes caused by the dissociation of gas hydrates.

A characteristic of benthic methane seepage sites is the presence of symbiotic chemoautotrophic communities (Sahling et al., 2002) that are thriving on the hydrogen sulfide that is produced during AOM. These communities serve as indicators for video-guided sampling of seep sediments. Their presence (and size/age) should also give further inside into the genesis of seep areas.

Migrating methane that finally passes the sediment-water interface and enters the water column is subjected to another microbial process, i.e., the aerobic oxidation of methane (AeOM) (Valentine et al. 2001). The ultimate fate of methane (dilution, consumption or degassing into the atmosphere) is still not well understood in marine pelagic environments. In general, methane rising from greater water depths would have greater chances to be consumed before entering the atmosphere than methane rising from shelves and upper slopes. Different to AOM the AeOM consumes oxygen and produces CO_2. Massive gas venting from dissociating gas hydrates could therefore lead to the development or spreading of oxygen minimum zones as well as contribute to ocean acidification.

Most climate models predict a rapid increase in Arctic air and surface water temperatures within the next decades (Dickson, 1999; IPCC, 2001; Johannessen et al., 2004). There are several interlinked processes that lead to a particularly faster rate of warming in the Arctic than elsewhere: (1) lowering of the albedo as ice and snow melt, (2) less trapped energy goes into evaporation, (3) the atmosphere is thinner, and (4) faster ocean-atmosphere heat exchange with less sea ice (Hassol, 2004). As a consequence the Arctic has been warming twice as fast over the last decade as the global average.

With increasing surface temperatures, it is expected that also the bottom-water will warm up, which will affect the stability of shallow gas hydrate, where it exists. The part of the gas hydrate system that is most strongly affected by bottom-water warming is the zone where the base of the gas hydrate stability zone (BGHSZ) intersects the seabed (Jung and Vogt, 2004; Mienert et al., 2005). In the Arctic this zone is approximately at 350 m water depth, a depth which is still affected by surface circulation and thus by increasing surface water temperatures (Vanneste et al., 2005). Because there is no sediment overburden, gas hydrates in this zone are not insulated from bottom water temperature changes and will respond quickly to warming bottom waters; opposed to the deeper parts of the GHSZ for which it will take hundreds to thousands of years (Berndt et al., 2004; Vogt and Jung, 2002). Therefore, past and present changes in gas hydrate stability conditions can best be evaluated in the Arctic. For the same reasons it is important to predict future methane hydrate mobility for this area. Another

important reason for studying gas hydrates in the Arctic is the shallow water depths of gas hydrate-related methane seeps. As the distance that methane has to travel through the water column is only half compared to that in warm oceans, a much higher percentage of methane that escapes from the seabed will make it into the atmosphere.

The Svalbard archipelago with its main island Spitsbergen is situated directly at the eastern boundary of the Fram Strait (Fig. 3.1). Thus, it is favourably positioned to monitor the inflow of Atlantic water into the Arctic Ocean and associated warming.

The research area is located at the shelf break 10 miles off NW-Spitsbergen approximately in the landward continuation of the slow-spreading Knipovich Ridge. It is a segmented, sheared transform margin partly characterized by under-plating of thinned oceanic crust (Ritzmann and Jokat, 2003; Ritzmann et al., 2004). This and magmatic intrusives at the continent-ocean boundary near the Spitsbergen Fracture Zone (Ritzmann et al., 2004) may generate a higher geothermal gradient. The area was repeatedly glaciated and accordingly experienced rapid changes in sea-level, sedimentation and erosion (Landvik et al., 1998, 2005; Mangerud et al., 1998; Svendsen et al., 2004). The ice of the Svalbard-Barents Sea-Ice Sheet (SBIS) of the last major glaciations on Svalbard retreated from this margin app. 13 ka ago (Landvik et al., 2005). The present rate of uplift in Svalbard is 4-5 mm/yr (Sato et al., 2006) which is a combination of post-glacial rebound and acceleration from recent ice loss of retreating glaciers on Svalbard. The continental shelf off NW-Spitsbergen is morphologically characterized by the glacial cross shelf trough of the Kongsfjord, its lateral and terminal morainal ridges and an area of slope-parallel ridges directly to the south (Ottesen et al., 2007). The sedimentary architecture is composed of glacigenic debris flows of the trough mouth fan (TMF), hemipelagic glacio-marine sediments occasional forming contouritic drift deposits and the transitional areas between them. The alternation of hemipelagic deposits with stacked debris flows have been identified to play an important role for preconditioning of submarine slides due to the increase of pore pressure in sediments between less permeable layers under load (Kvalstad et al., 2005; Winkelmann et al., 2006; Winkelmann and Stein, 2007). Fluid and gas migration on this shelf occurs along major geological structures (Knies et al., 2004). The occurrence of large areas with BSRs indicate the presence of gas hydrates (Vogt et al., 1994; Vanneste et al. 2005; Fig. 3.1), pockmarks (Vogt et al., 1994) and active venting at the upper limit of the GHSZ (Westbrook et al., 2009; Fig. 3.2) makes this area a key site in studying ongoing changes in the GHSZ.

The potential relation of hydrate dissociation, fluid flow, seepage and slope failure events has been discussed elsewhere (e.g. Kennett et al., 2003; Mienert et al., 2005; Winkelmann and Stein, 2007) and seems to be an important factor controlling submarine slope stability off Svalbard (e.g. Winkelmann and Stein, 2007). Geological and geophysical data suggest that the Kongsfjorden TMF has an active fluid flow system (Knies et al., 2004; Bünz et al., 2008; Westbrook et al., 2008) and that there is significant seismicity in the area (Ekström et al., 2003). A part of the slope off this TMF that could be affected by a future slope failure is 30 to 130 km wide in east west direction including the Kongsfjorden TMF proper and the continental slope west of it. Numerical tsunami modelling shows that a submarine landslide west of Spitsbergen, 100 m high and 130 km wide (i.e. third of the size of the Storegga Slide) would cause a tsunami capable of reaching northwest Europe and threatening coastal areas (Berndt et al., 2009).

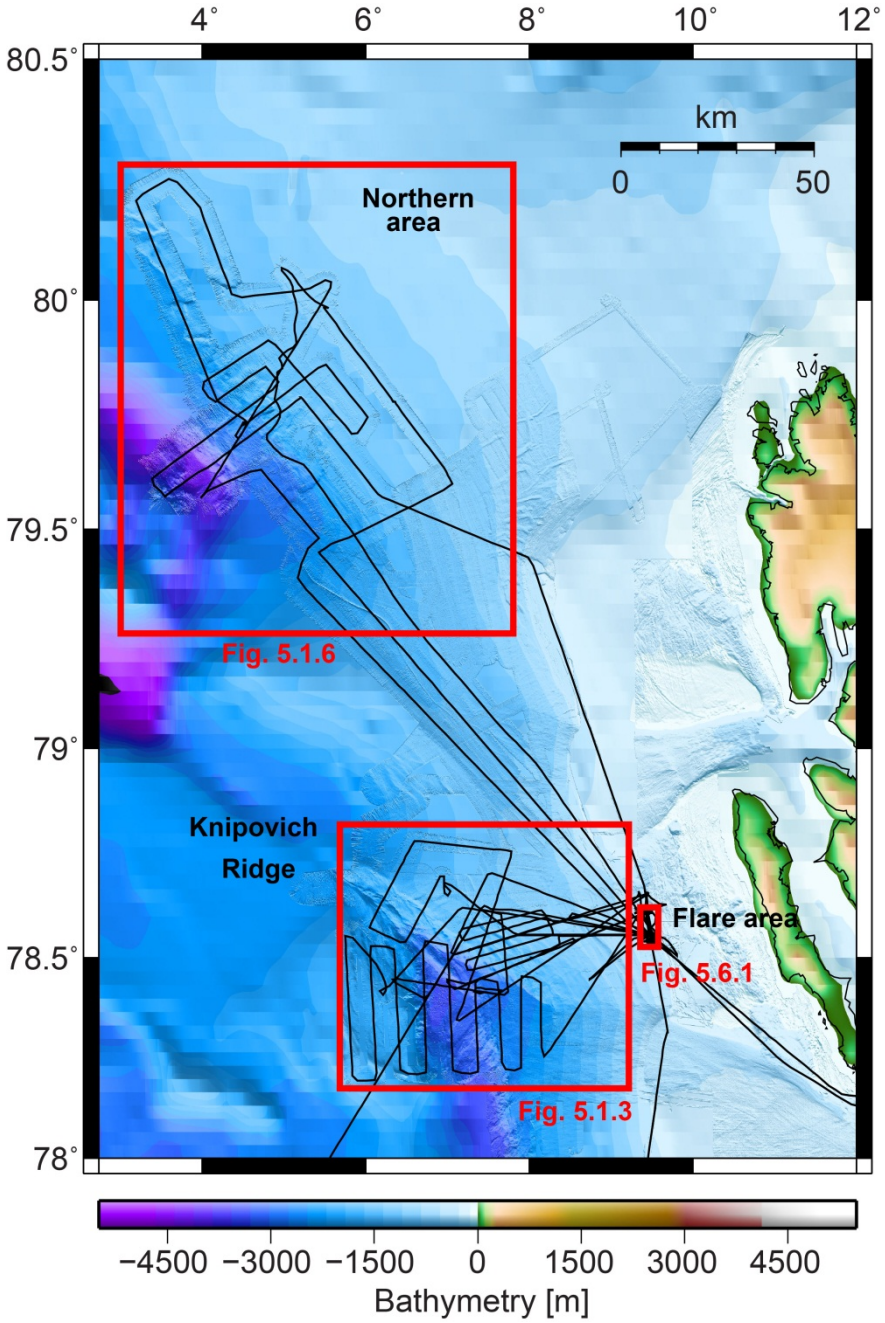

Fig. 3.1 Map showing general bathymetry of the Fram Strait region offshore W-Spitsbergen (IBCAO 2 and multibeam bathymetry compilation from various cruises) and the location of the three working areas. The black lines show the ship track, which is also the coverage for multibeam EM120 and PARASOUND.

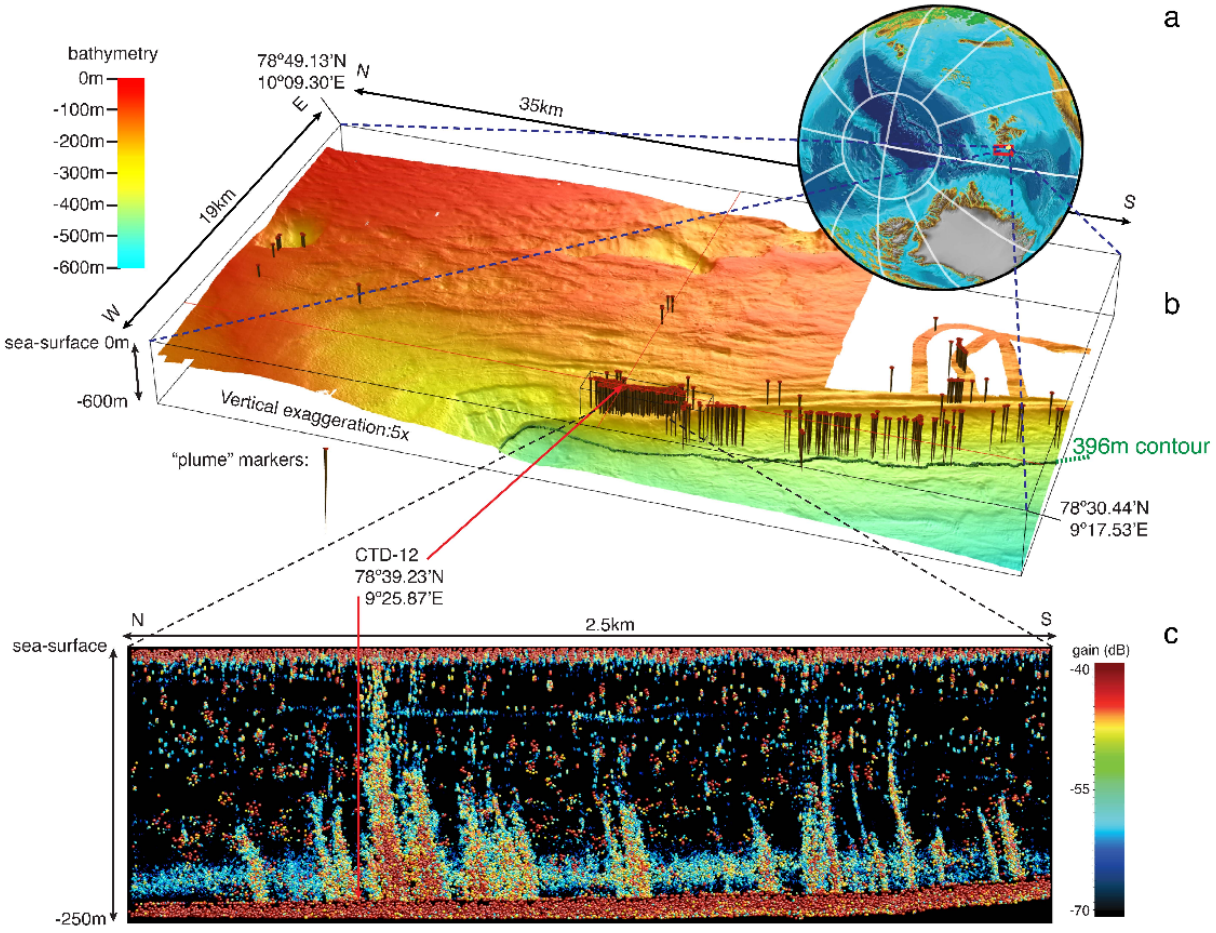

Fig. 3.2 Seepage offshore W-Spitsbergen evidenced by numerous flares (c) seems to be confined to a narrow bathymetric interval (b) coinciding with the upper limit of the gas hydrate stability zone (GHSZ) in the area (from Westbrook et al., 2009).

3.2 Cruise objectives

This cruise was an important part of the MASOX demonstration mission, which is part of the EC funded ESONET network of excellence. MASOX is a collaborative project between the Alfred Wegener Institute for Polar and Marine Research (AWI), Bremerhaven, Germany, the GEOMAR Helmholtz Centre for Ocean Research Kiel, Germany, the Institute for Marine Research (IMR) Bergen, Norway, the Nansen Environmental and Remote Sensing Center (NERSC), Bergen, Norway, the National Oceanography Centre Southampton (NOCS), United Kingdom, and the University of Tromsø (UIT), Norway. It was part of the AOEM (Arctic Ocean ESONET Mission) of the ESONET (The European Seafloor Observatory Network). The MASOX seabed observatory was installed near a vent site at the outcrop of the gas hydrate stability zone in 2010 using the Norwegian vessel G.O. Sars. During this cruise we recovered the seabed observatory and download the data. By the time of recovery, the observatory had monitored the sea-floor offshore W-Spitsbergen for two years to constrain the environmental controls on gas hydrate dynamics. The cruise further contributes to a broader cooperation between the National Oceanographic Centre Southampton (NOCS), UK, the Ifremer (France) and the GEOMAR Helmholtz Centre for Ocean Research Kiel, Germany (G3) again to test the hypothesis that the gas venting of Spitsbergen is caused by hydrate dissociation. This collaboration involves scientists such as Jean-Paul Foucher (Ifremer) and Ian Wright, Doug Connelly, and Rachael James (NOCS).

The goal of cruise MSM21/4 was to quantify the methane flux emitted through the seabed and to find out if the observed venting is indeed the result of bottom water warming-induced gas hydrate dissociation and that it is not due to other geological processes. The main objectives of the cruise were:

- *Recovery and reinstallation of the MASOX observatory*
  The observatory was deployed during an RV Jan Mayen cruise in summer 2010 and was then recovered, maintained, and re-deployed during a NOCS cruise in summer 2011. During our cruise we had to recover this observatory in Svalbard and take down to the Sleipner field for the ECO2 project. The measurements from the Svalbard deployment show the variability of seepage on a seasonal scale and provide insight into the dynamics of the seep system.

- *Acoustic imaging of fluid migration pathways and seep sites*
  We collected 2D-high resolution reflection seismic data to image fluid migration pathways. These data will allow distinguishing between fluid migration along faults and the creation of pathways by hydraulic fracturing. The EA600 multi-frequency echosounder and the PARASOUND system were used for flare imaging in order to identify active seeps and variations in their activity.

- *Surveys of benthic and pelagic methanotrophic activity*
  Sampling with JAGO pushcores facilitates a selective sampling of surface sediments (max 20 cm) in the vicinity of gas vents to study microbial methanotrophic activity and sediment porewater chemistry. If seepage activity was established as a consequence of gas-hydrate dissociation only recently we expected to find relatively low activity and abundance of the methanotrophic community in the sediment. In addition to surface sampling, we will deploy gravity corer to study deeper parts of the sediment with respect to microbiology and geochemistry along transect laid across venting sites. Deeper cores could provide information about past or weaker seepage activities. The fate of methane after passing the benthic biological filter will be investigated with CTD/Rosette casts across venting sites to study the activity of methanotrophic bacteria in the water column and their coupling to hydrographic characteristics.

- *U/Th and ^{14}C dating of sediments from the vent sites*
  Dating of carbonaceous sediments from venting sites will reveal their nature and age of genesis. This obviously depends on suitable field relationships, i.e. the presence of such sediments and the possibility to retrieve them.

- *Analysis of slope stability*
  Further investigation will be focused on the state of slope concerning (in)stability. In particular, we will investigate the presence of precursory phenomena for slope failures that might be caused by hydrate dissociation such as elongated cracks running along the slope within the anticipated bathymetric range. This includes acoustic and seismic surveying and geological sampling by gravity coring.

- *Surveys of methane concentrations and distribution in the water column*
  CTD rosettes were deployed along vertical and horizontal transect in the area of gas venting. Gas flares identified by acoustic techniques were used to guide the sampling. The distribution of methane concentrations around the gas vents provides information about changes of the gas injection into the water column in comparison with earlier data.

3.3 Deviations from the intended cruise schedule

The cruise followed the intended cruise schedule as planned except for an unintended stop in Longyear. We sailed from Reykjavik on 13 August arriving off Svalbard on August 17. As long as weather permitted we conducted JAGO dives during the day and heat flow, CTD and seismic profiles during the nights. Because of bad weather at the JAGO dive sites we sailed to the northern part of study area on August 21. Unfortunately, the streamer was damaged very soon and we had to sail into Longyear (about 12 hours) to get divers. Then we returned to the JAGO dive sites for another 5 days before completing the work in the north on August 25 to 27. During another period of bad weather on September 1 to 3 we surveyed the western part of the gas hydrate province near the Knipovich Ridge before retrieving deployed sensors at the gas flare site and sailing south towards the study area on the Vøring Plateau on September 4. The HyBis ROV was intended as a back up system for the submersible JAGO and as the primary tool recovery of the MASOX observatory. As it was only the second system that the manufacturer has produced delivery was delayed and it could not be shipped in time to Reykjavik.

3.4 Compliance with the regulations for responsible marine research

We complied with the regulations for responsible marine research. None of our activities affected a high percentage of occurring microorganisms in the seep areas adversely, and none of our activities left a long-term impact on the ecosystems. The entire cruise took place outside of the West Svalbard National Park boundaries. We did not take any unnecessary samples. During the entire cruise we held close contact with Dr. Heiko Sahling, chief scientist on board RV Heincke to make sure we do not interfere with their program. Our collected data and samples will be made available to the scientific public after 3 years.

4 Cruise narrative

(Christian Berndt)

Monday 12-08-2012 – Friday 17-08-2012
On 12-8-12 we left Reykjavik heading north towards Svalbard. We made good progress except for some hours on Tuesday afternoon when we had to slow down in fog in order to avoid sea ice. We reached the survey area at 03:30 on Friday morning. At the first station in 1400 m water depth we calibrated the heat flow probe and ran a CTD dip to obtain a water column sound velocity profile. For this we used the CTD because the recently serviced ship's sound velocity probe did not record any data. From 8:30 to 10:30 we ran a multibeam echosounder profile towards the MASOX observatory site filling in gaps in the existing bathymetric data. Because the PARASOUND system did not work due to malfunctioning hardware, we ran the profile at a speed of 10 kts. Having arrived at the observatory site we collected a second CTD using 24 water sampling bottles. This was finished at 12:30. At 14:00 we carried out a JAGO deployment trial that was successfully completed after 30 minutes. Unfortunately, there was a delay afterwards as a crane winch malfunctioned and needed repairs. At 18:30 we deployed the seismic system and started to acquire three seismic profiles towards Vestnesa, down its southern slope and back to the study area.

Saturday 18-08-2012
At 08:30 we retrieved the seismic system and steamed back to the observatory position. Here we deployed the deep sea cable at 10:00 and JAGO at 11:30. JAGO dove along the recovery cable and was positioned right above the observatory using the ship's DP. At 13:30 JAGO

managed to hook the recovery cable to the observatory and everything was hoisted up to the surface where we first recovered JAGO and then the observatory. Before leaving the bottom JAGO took two rock samples and filled a Niskin bottle. Everything was on deck at 17:00. Afterwards we surveyed the observatory position once more with PARASOUND and EA600 echosounder to ensure that there were significant gas flares. Then we started a CTD and heat flow probe transect.

Sunday 19-08-2012
The CTD and heat flow transect continued throughout the night without interruptions. From 10:00 to 15:00 we collected more PARASOUND and MB data to map the flares in the water column hoping that the weather would improve for a second JAGO dive. Unfortunately, the wind did not lessen as forecasted and we had to cancel the dive. Instead we took a gravity core at HF4 and continued seismic surveying of the Knipovich Ridge / Vestnesa transition.

Monday 20-08-2012
During the night the wind picked up reaching 7 Bft with occasional gust of force 9. The seismic data was accordingly bad. It calmed down during the morning hours, but with 2-3 m swell and force 6 JAGO operations were still not possible. After collecting another gravity core at the MASOX observatory site we decided to move north to extend the BSR map into previously seismically uncharted territory taking advantage of this year's exceptionally open sea ice conditions. On the way up north we carried out another calibration of the heat flow lance in 2000 m water depth which was finished after 1 hour at 22:00. At 23:30 we reached the deployment position for the seismic survey.

Tuesday 21-08-2012
The seismic data was deployed at 24:00 and we steamed north towards ODP Site 912. Almost at this site weather conditions deteriorated rapidly with winds of force 7 increasingly dense sea ice and poor visibility due to snow. It was decided to recover the streamer system to avoid damage. Unfortunately, during recovery the streamer got entangled in the starboard propeller and we lost the stretch section, one bird, and four active sections. Fortunately, the tail buoy had enough buoyancy to keep the remaining section afloat and in spite of the poor weather conditions we were able to recover the remaining sections thanks to the excellent manoeuvrability of Maria S. Merian. Inspection of the starboard pod with an underwater camera revealed that parts of the streamer were wrapped around the propeller, and untangling them would require diver assistance. Therefore, we steamed back to Longyear on the port side pod.

Wednesday 22-08-2012
We arrived in Longyear at 13:00 local time and drop anchor at 14:00. The launch picked up three divers and spare parts for the streamer that were kindly provided by the University of Tromsø. The first diver managed to clear the remains (one completely destroyed streamer section and one badly damaged A/D converter bottle) from the starboard pod. This took only 10 minutes. Afterwards he inspected the seal and the portside pod, but could not determine any further damage. We left Longyear at 17:00 ship time (UTC) and sailed back to a flare site that we had discovered during the multibeam and PARASOUND transect 60 m west of the MASOX observatory position. We arrived there at 22:30. A 20 minute PARASOUND transect along the same track as the first down-current profile revealed almost vertical flares where there had been highly tilted one before indicating that the water currents had stalled. Otherwise the same flare sites could be identified. At 23:00 we collected a gravity core at the most pronounced flare. The core smelled strongly of H_2S and showed few drop stones.

Thursday 23-08-2012
Afterwards we steamed north to a site that was occupied for a 24 hour CTD in the previous year and where previous HyBis dives by the British colleagues found strong evidence for seepage. From 00:30 to 01:20 we acquired a PARASOUND profile confirming that active flares existed within the 380 and 390 m depth interval. Upon this we collected a heat flow transect along this profile that had to be terminated at 07:00 when the temperature sensor string was worn off. We sailed back to the southern flare site at the MASOX observatory position and at 08:00 we deployed JAGO in light easterly winds. JAGO operation was smooth and at 11:00 the JAGO team was able to find a flare site approximately 50 m WNW of the MASOX observatory position. The peepers (pore water samplers) and a 40 cm long heat flow probe were deployed and the site marked. Strong zonation of free gas bubbles, beggiatoa mats and pogonophera tube worm fields indicated a highly active seep site. The dive lasted until 14:00 and a second dive was prepared while we carried out further PARASOUND flare imaging along 40-m spaced EW profiles towards the north. The second dive started at 18:00. Its main aim was the deployment of large push cores on the other side of the beggiatoa mat in which the peepers were deployed. This turned out to be very difficult as little pieces of rock prevented the push cores from penetrating into the ground. Only one and half push cores could be deployed and retrieved until 21:00 when JAGO had to be recovered because of increasingly high winds (Force 6). The push cores were of poor quality due to the difficulties with collecting them. At 22:00 JAGO was back on deck after a somewhat more difficult recovery operation than usual due to swell.

Friday 24-8-2012
From midnight onwards we collected water samples at five stations around the main flare site in order to investigate the lateral diffusion of methane away from the gas bubble flares. This was finished by 07:00 in the morning and we prepared JAGO for a fourth dive that started at 08:45. During the dive a different bacterial mat was investigated and it was possible to collect four decent push cores each with slightly more than 10 cm recovery. From 13:00 to 17:00 we collected more PARASOUND data before a second JAGO dive was undertaken. During this dive six small push cores were deployed all working very well and the submersible was back on deck at 20:45. After calibration of a new heat flow string seven more heat flow sites were occupied during the night yielding excellent data quality.

Saturday 25-8-2012
After finishing the heat flow transect we started a PARASOUND survey of the HyBis site at 06:00 which lasted for 2 hours and showed that there are at least four different gas flares in this area. Therefore, we decided to start the next JAGO dive with a transect across each of the positions starting in the south. Upon arrival at the seabed JAGO almost immediately discovered a bacteria mat at an active gas flare. Five push corers and a Niskin bottle were taken and the transect continued. The entire area is rockier than the Masox observatory site. At some of the other four seeps discovered during this dive significant amount of carbonate rocks exist, indicating prolonged seepage. From 13:00 to 17:00 we collected more PARASOUND data to obtain a complete distribution map of flares in the area. At one point we came less than 1 nm close to the research vessel Heincke that was also surveying the area. In the evening we carried out a second JAGO dive to the first seep and collected more push cores and carbonate rock samples. At 22:00 we steamed north completing the multibeam map across the newly discovered landslide on the Yermak Plateau.

Sunday 26-8-2012
We reached the study area at 07:00 and tried to run a CTD dip in order to obtain a sound velocity profile for multibeam echosounder calibration. Unfortunately, the CTD did not work

and we had to carry on. While surveying the first multibeam line the CTD was repaired and the sound velocity profile was measured. As far as possible to distinguish from the preliminary processed data we surveyed the entire slide area before collecting three gravity cores during the night to obtain minimum ages for the slide event.

Monday 27-8-2012
After the last gravity core was on board at 07:00 we surveyed the slope to the north and discovered evidence for another smaller slide that is possibly linked to first one. From 12:00 onwards we shot a seismic profile from ODP Site 912 down the slide headwall to the location of the second gravity core. This profile was finished at 23:00 and we started the transit back to the study area off Prins Karls Forlandet.

Tuesday 28-8-2012
We arrived at 07:00 in the study area and used PARASOUND to verify the location of two reported seeps to the south east of the MASOX observatory position. At 08:00 we started to deploy JAGO to investigate the seep sites. Here, there was less activity then northwest of the MASOX observatory, but it was possible to identify some gas flares and obtain push core samples from a local depression that appeared to be a trawl mark. Starting at 14:00 we carried out further PARASOUND profiling to find a seep site at the deepest part of the flare zone in the hope to identify a site where hydrate could be sampled with a gravity corer. However, only weak indications for deep flares could be found and at 18:00 we decided to carry out a CTD transect from Hybis Site down to lower part of the slope in order to determine the variability of the Spitsbergen current.

Wednesday 29-8-2012
Because of problems with the fibre optic cable the CTD transect took four hours longer than expected. At 08:00 we were finished and we deployed the seismic equipment to carry out a seismic oceanography profile on the way back to the next JAGO dive site. This profile was completed at 15:00. Then we verified the presence of gas flares at a location that was investigated by the R/V Polarstern in 2011 using ROV Kiel 6000. As this was successful we launched JAGO at 17:00. The sea floor was very rocky with large carbonate crusts. At their edges gas flares were discovered. After JAGO was retrieved at 21:00 we carried out a short CTD test and then sailed back to the northern termination of the Knipovich Ridge where we collected a heat flow transect.

Thursday 30-8-2012
It took until 08:00 to collect four heat flow measurements before we came back to the MASOX area where we intended to conduct a further JAGO dive to retrieve the peepers and the short heat flow probe. Unfortunately and contrary to the weather forecast, the winds were too high (force 6-7 instead of 4-5) for safe operation of the submersible and we decided to take gravity core samples from five positions along the lower part of the gas hydrate stability zone / seafloor interception and one below the theoretical interception line. One of the cores had significant shows of methane and sulfide, while the others were probably taken away from the actual seep sites. During the night we repeated the heat flow and water sampling transect across the MASOX observatory site.

Friday 31-8-2012
The heat flow and water sampling transect was completed at 09:00. Due to poor weather conditions (force 7-8 with gusts 9) we were limited to sediment coring and multibeam bathymetry acquisition. Until 14:00 we collected three sediment cores at a flare site reported by Heiko Sahling. However, we were not able to obtain gas rich samples although we

successfully took one core with POSIDONIA positioning (about 5 m away from the reported position). Afterwards we carried out multibeam profiling of the northern termination of the Knipovich Ridge.

Saturday 1-9-2012
At 18:00 on Saturday weather had improved (force 6 with gusts 7) and we decided to deploy the seismic system to survey the transition of the Knipovich Ridge into the Molløy Transform Margin. The aim was to determine if heat from the ridge is causing additional production of gas and is the ultimate reason for the Svalbard gas hydrate province. Seismic surveying continued throughout the rest of the night and into Sunday.

Sunday 2-9-2012
At lunch time we retrieved the seismic system and steamed back to MASOX observatory site where we launched JAGO for a last time to recover the peepers and the temperature probe taking advantage of the only predicted window of calm weather. The dive was successfully completed by 18:00, and JAGO was on deck before the wind picked up again at 02:00 the following morning. Right after the JAGO recovery we sampled the bottom water for analysis of the carbonate crusts, first at the MASOX site then at the HyBis site and then at the 280 m site. At the MASOX site we also had two failed attempts at collecting a gravity core.

Monday 3-9-2012
At 02:00 in the morning we deployed the seismic equipment again to collect further seismic lines across the Knipovich Ridge termination. We discovered a previously unknown area of bottom simulating reflectors, i.e. gas hydrate indications, on the oceanic crust and imaged a large pipe structure in the northern part of the Hydratech area which was discovered in 2008. The wind picked up to force 8 occasionally but the seismic system performed well delivering decent data. After retrieving the seismic system at 17:30 we collected two gravity core samples from the pipe structure and a fault outcrop where the heat flow probe had shown increased fluid migration earlier. Both cores did not show obvious signs of methane advection. But pore water samples were taken for later analysis. Finally we ran a sound velocity profile for calibration of the EM120 multibeam data.

Tuesday 4-9-2012
At midnight we started a last water column sampling programme at three seep sites and at a reference station south of the gas flare area. A final attempt to collect a gravity core from the MASOX observatory site turned out a spectacular success. We retrieved a 3 m-long core with very high sulfide concentration and soupy sediments at the top which will allow an assessment of methane advection rates and their variability. At 08:00 we started the transit towards the Vøring Plateau off mid-Norway.

Wednesday 5-9-2012
With fresh stern winds we had a fast transit to the Vøring Plateau.

Thursday 6-9-2012
We arrived in the northern study area on the Gjallar Ridge at 18:00. First we collected two additional PARASOUND profiles to double-check the location of the coring sites and then we took two gravity cores with POSIDONIA and 12 m core barrels. Both cores are just above 5 m long and consist of stiff grey mud at the bottom and light brown mud at the top. There were no obvious signs of seepage but the cores underwent pore water analysis nonetheless. At 23:00 we steamed on towards the second coring site on the southernmost edge of the Vøring Plateau.

Friday 7-9-2012
At 13:00 we reached Nyegga. Because of strong westerly wind (8 Bft) and waves sometimes breaking onto the deck we decided not to use POSIDONIA for coring. We collected two cores next to faults that appear very recent in the PARASOUND data. The aim of these cores is to find out if there has been recent seafloor movement at the northern Storegga Slide side wall. At the 17:00 we were finished at the second site and we steamed on towards the observatory deployment site at Sleipner.

Saturday 8-9-2012
Transit from Nyegga to Sleipner.

Sunday 9-9-2012
At 07:00 we arrived at the observatory deployment site northwest of Sleipner and took up contact with RRS James Cook. First, we surveyed the deployment site with two perpendicular PARASOUND profiles making sure there were no obstacles at the sea floor. Afterwards we had to wait until 09:15 for the James Cook to recover their AUV, before we deployed the observatory at 09:30. At 09:45 we were on our way back to Emden.

Monday 10-9-2012
We reached Borkum at lunch time and took the pilot on board at 13:00. At 17:00 we docked in Emden.

5 Preliminary Results

5.1 High-resolution 2D multichannel seismic profiling

(Sebastian Krastel)

5.1.1 Introduction

During Cruise MSM21/4 equipment of the Helmholtz Centre for Ocean Research Kiel (GEOMAR) was used to acquire high-resolution multichannel seismic data. Unfortunately parts of the streamer got entangled in the starboard propeller during a recovery action with strong winds, poor visibility and increasingly dense sea ice and we lost the stretch section, one bird, and four active sections. The University of Tromsø kindly provided some spare parts (tow lead, stretch), which allowed to continue seismic data acquisition.

The aim of the seismic survey was to resolve small-scale sedimentary structures and closely spaced layers on a meter scale, which can usually not be resolved by means of conventional seismic systems. During the cruise a 1.7 l GI-Gun was used as source. Data were recorded with a GeoEel digital streamer. Figs. 5.1.1 and 5.1.2 give an outline of the system setup as it was used during Cruise MSM21/4.

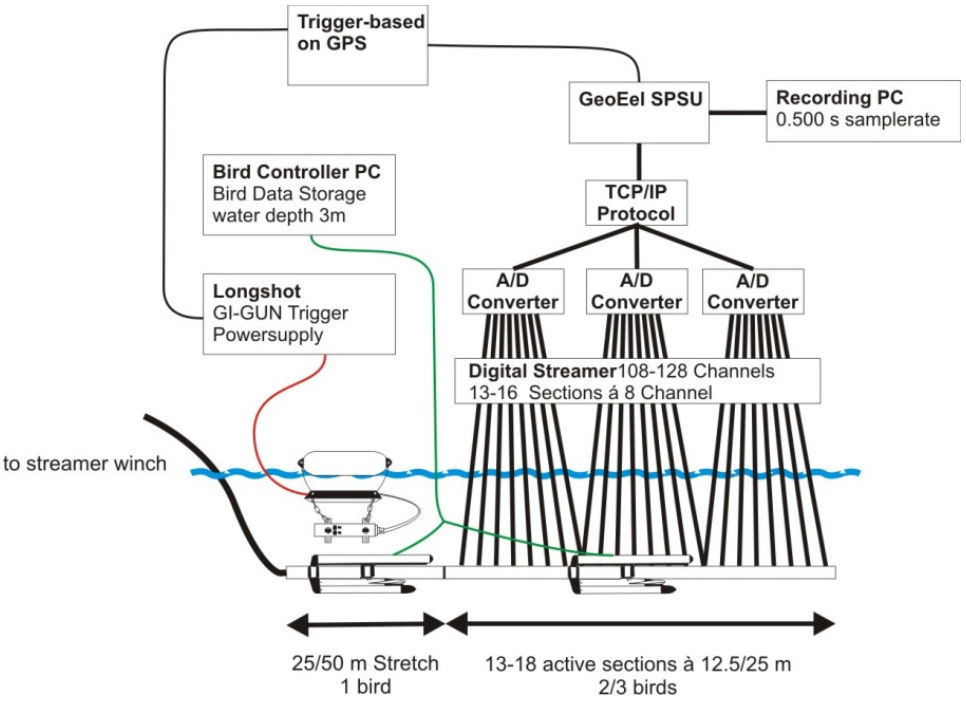

Fig. 5.1.1 Setup of 2D-seismic system during Cruise MSM21/4.

5.1.2 System components

Seismic sources

During seismic surveying a standard GI-Gun was used as source; it was shot in a harmonic mode (2 * 1.7 l). The GI-Gun was deployed at the port rear of the vessel and towed approx. 20 m behind the ship's stern (Fig. 5.1.2). The-GI-gun was connected to a bow with the GI-Gun hanging on two chains 70 cm beneath. An elongated buoy, which stabilized the guns in a horizontal position at a water depth of ~2m, was connected to the bow by two rope loops. The injector of the GI gun was triggered with a delay of 15 ms with respect to the Generator signal, which basically eliminated the bubble signal. The gun was shot at 200 bar. Shooting intervals varied between 6 and 7 seconds (depending on water depth) resulting in a shot point distance of 12 – 15 m at 5 knots. The gun worked very reliable during the entire cruise except for some problems with the umbilical, which caused some short interruptions during shooting.

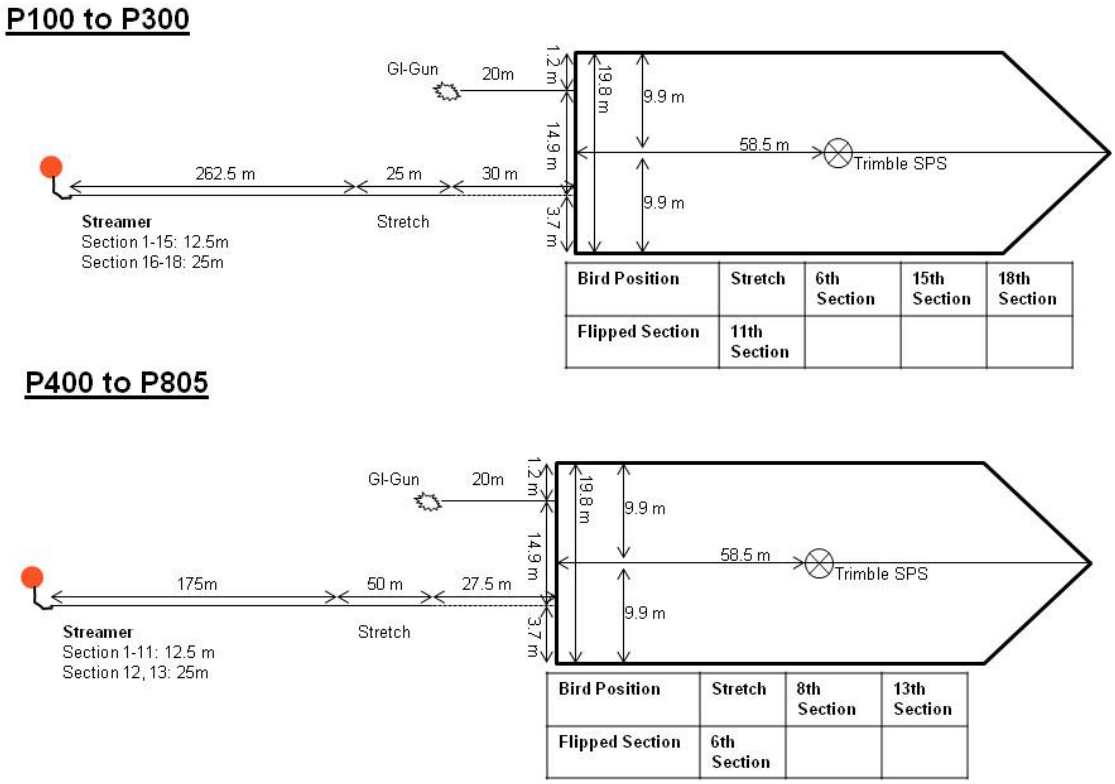

Fig. 5.1.2 Deck and seismic gun setting during Cruise MSM21/4.

Streamer-system

A digital streamer (Geometrics GeoEel) was used for receiving the seismic signals. The system consists of a tow cable, one stretch section and 13 - 18 active sections (each 12.5/25 m). For the first part of the survey, a tow cable and the stretch from GEOMAR was used. The length of the stretch was 25 m. The tow cable has a length of 80 m (30 m in water). Due to the loss of the stretch and two cables, they were replaced by equipment kindly provided by the University of Tromsø from Profile P400 on (see Fig. 5.1.2). From then on, the stretch had a length of 50 m. 27.5 m of the tow cable were in water.

Most of the sections had a length of 12.5 m. Up to three 25 m long sections were placed at the tail of the streamer (Fig. 5.1.2). Some of the 25 m-long sections lost connection to the acquisition unit during profiling. Hence, some of the 25 m-long section has not been recorded for some profiles. An active section contains 8 channels (channel spacing of 1.56 m for 12.5 m sections and 3.25m for the 25 m sections) resulting in 104-144 channels within the streamer. One AD digitizer module belongs to each active section. These AD digitizer module are small Linux computers. Communication between the AD digitizer modules and the recording system in the lab is via TCP/IP. A repeater was located between the deck cable and the tow cable (Lead-In). The SPSU manages the power supply and communication between the recording system and the AD digitizer modules. The recording system is described below. Three to four birds were attached to the streamer (see below). A small buoy was attached to the tail swivel.

Bird Controller
Up to four Oyo Geospace Bird Remote Units (RUs) were deployed at the streamer. The locations of the birds are listed in Fig. 5.1.2. All RUs have adjustable wings. The RUs are controlled by a bird controller in the seismic lab. Controller and RUs communicate via communication coils nested within the streamer. A twisted pair wire within the deck cable connects controller and coils. Designated streamer depth was three meters. It was increased to four meters during bad weather conditions. The RUs thus forced the streamer to the chosen depth by adjusting the wing angles accordingly. The birds were deployed at the beginning of a survey but no scanning of the birds was carried out during the survey because bird scans caused false triggers. However, the birds worked very reliably and kept the streamer at the designated depth.

Data acquisition systems
Data were recorded with acquisition software provided by Geometrics. The analogue signal was digitized with 2 kHz. The data were recorded as multiplexed SEG-D. Recording length was between 5 and 6.5 seconds depending on water depth. One file was generated per shot. The acquisition PC allowed online quality control by displaying shot gathers, a noise window, and the frequency spectrum of each shot. The cycle time of the shots is displayed as well. The software also allows online NMO-Correction and stacking of data for displaying stacked sections. Several logfiles list parameters such as shot time and shot position.

Trigger unit
A long shot was used as gun controller. The Injector was triggered with a delay of 15 ms. The arming point for the gun was set to 80 ms. Due to problems with the hydrophones at the gun, no direct quality control of the source signal was carried out.

5.1.3 First results of 2D seismic survey

Preliminary data processing was carried out for all profiles onboard. Channels 20-23 of each shot were filtered, stacked, and time-migrated. These brute stacks were loaded to a seismic interpretation system (IHS Kingdom Suite) and used for preliminary interpretation. In total we collected about 500 km of seismic 2D profiles off Svalbard (Fig. 5.1.3).
Fig. 5.1.4 shows a profile crossing a newly discovered landslide in the northern most working area (see section 5.3). The north-eastern part (Offset > 15,000 m) shows a thick pile of undisturbed sediments. Slight variations in accumulation rates may point to a partly reworking by contour currents.

A prominent headwall is found at an offset of 15,000 m. The height of the headwall is about 50 m. It cuts well stratified sediments. A hummocky surface beneath the headwall is formed by the slide deposits. The thickness of the deposits, however, seems to be too small to be resolved by the seismic data. A very prominent bottom simulating reflector (BSR) is found in the slide area. It is located about 300 ms TWT beneath the sea floor. High amplitudes beneath the BSR indicate the accumulation of free gas. It is interesting to note that the gas accumulations are thickest directly beneath the headwall. The free gas accumulations continue further upslope as indicated by high amplitude reflectors. A BSR upslope of the headwall region, however, is difficult to identify because it seems to follow the normal stratification.

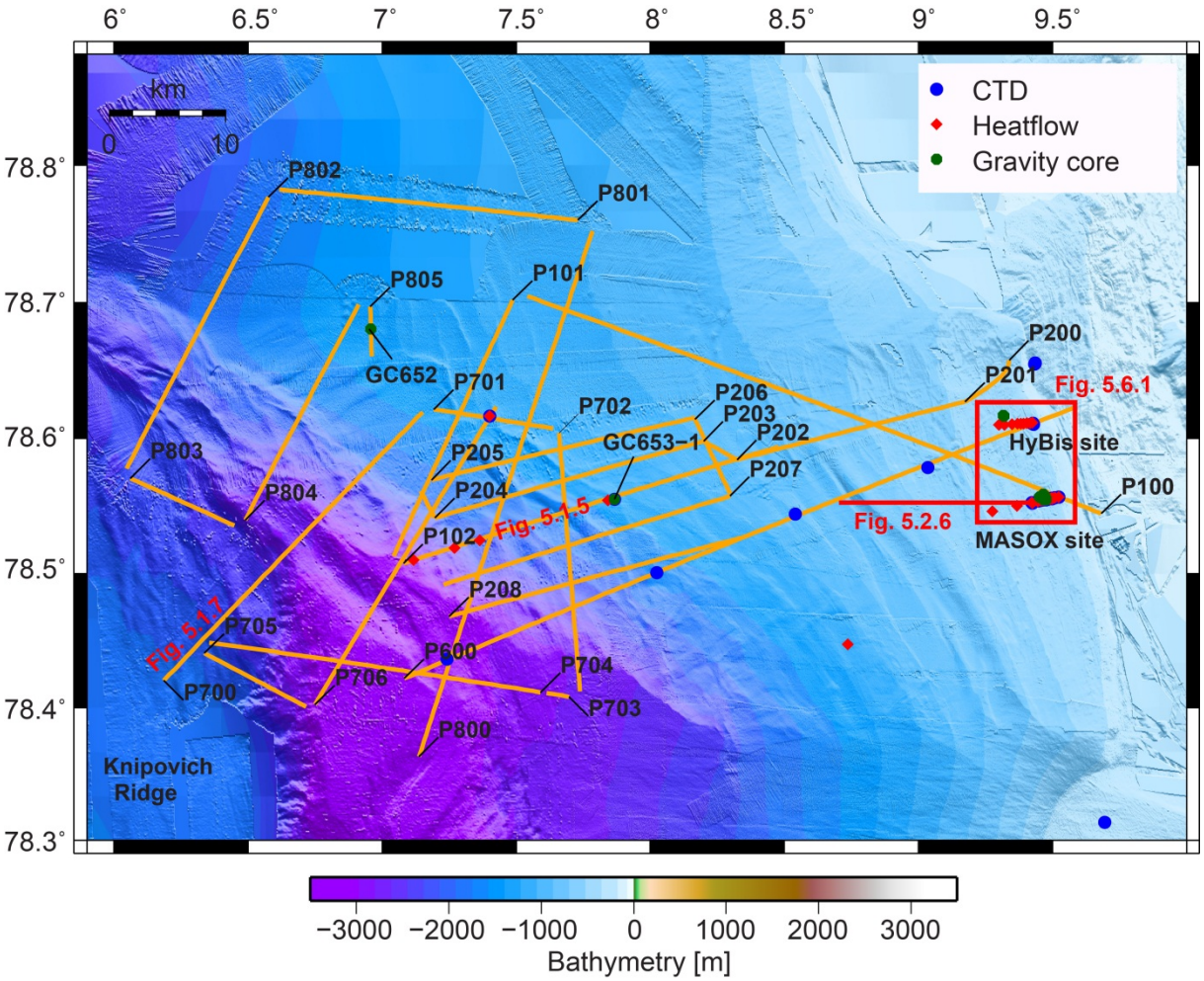

Fig. 5.1.3 Map showing bathymetry (IBCAO 2 and multibeam bathymetry compilation from various cruises) Location of seismic profiles at the northern termination of the Knipovich Ridge. Additionally two profiles were collected in the northern working area at the newly discovered landslide. Map location is shown in Fig. 3.1.

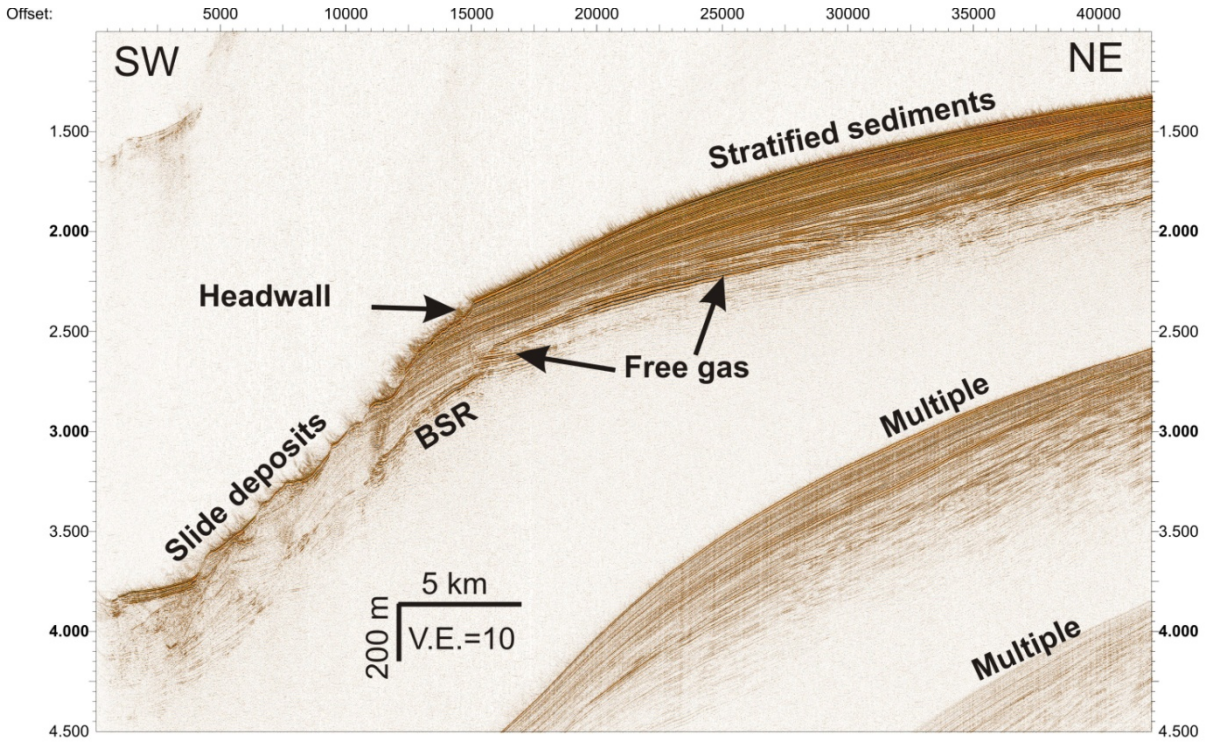

Fig. 5.1.4 Migrated brute stacks of seismic profile P500 crossing the slide area in the northern most working area. See Fig. 5.1.6 for location of profile.

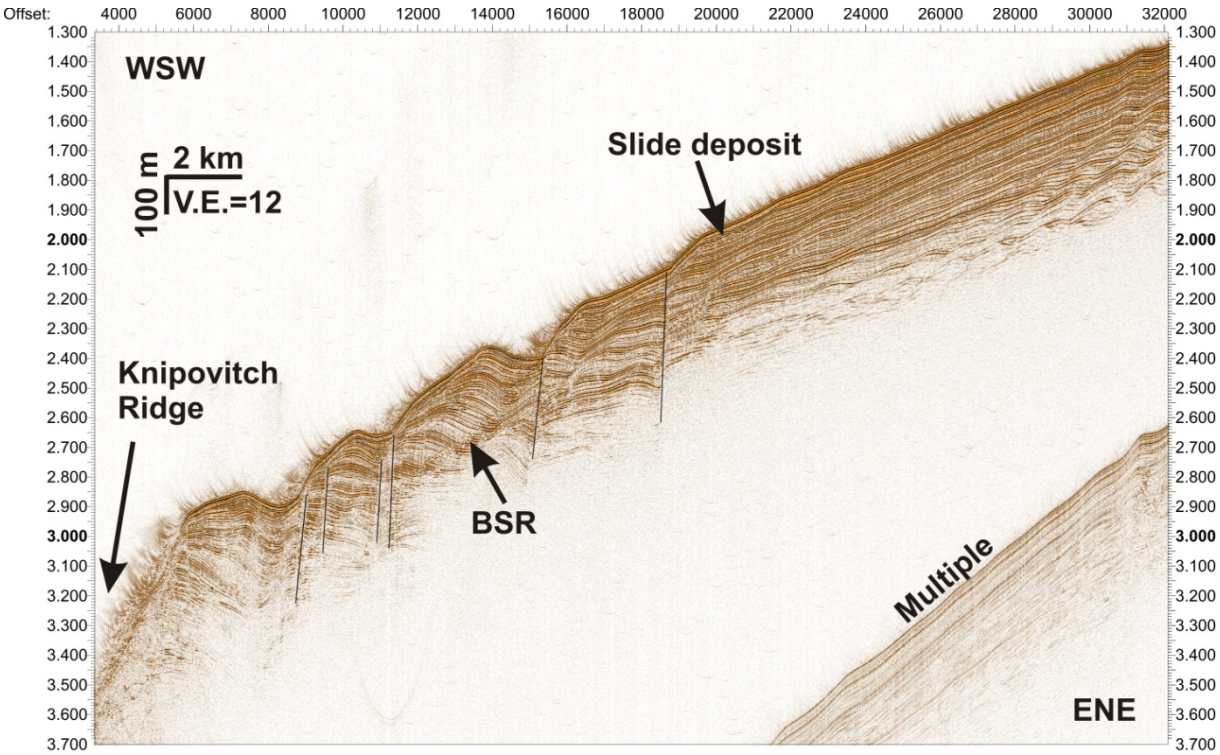

Fig. 5.1.5 Migrated brute stack of seismic profile P102. Thin black lines show locations of faults. See Fig. 5.1.3 for location of profile.

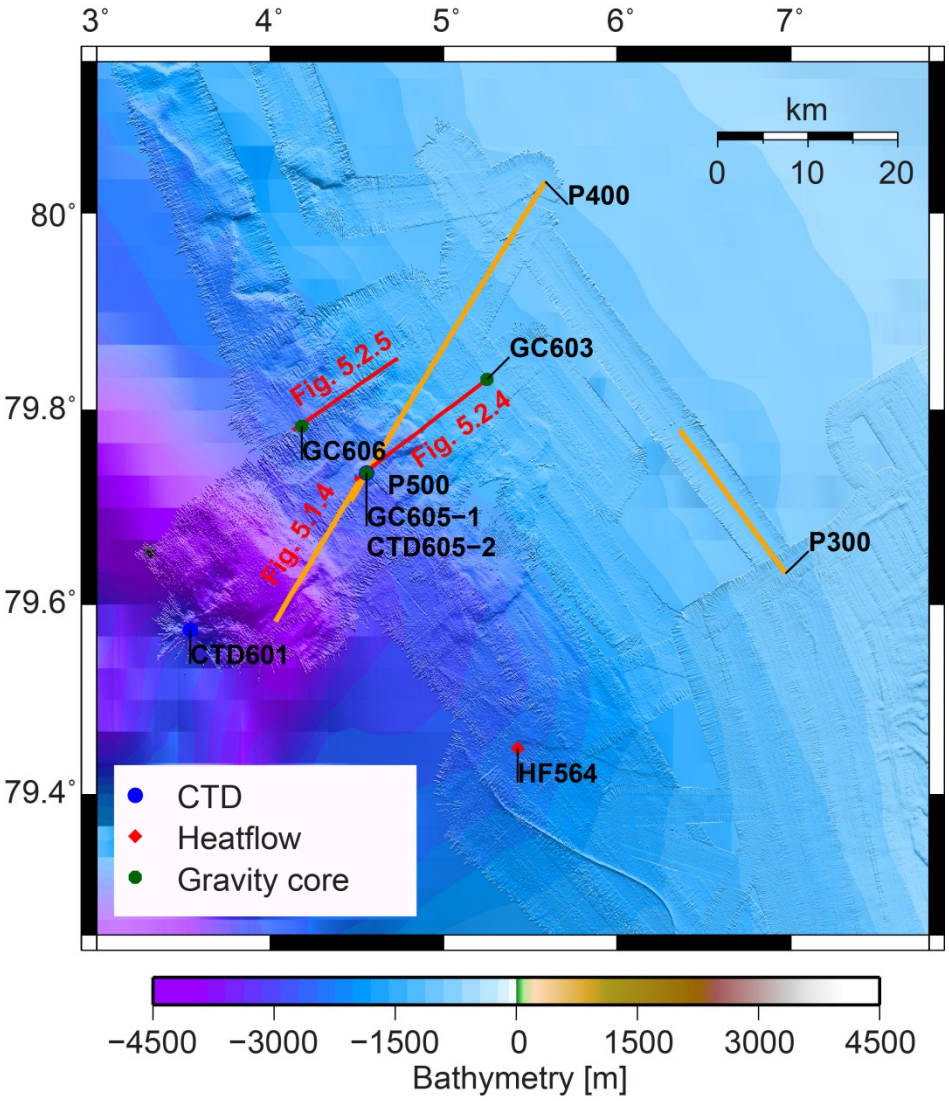

Fig. 5.1.6 Bathymetry map (IBCAO 2 and multibeam bathymetry compilation from various cruises) showing stations and seismic profiles (orange) in the Northern working area.

Fig 5.1.5 shows a profile crossing the continental slope off Svalbard down to the Knipovich Ridge, which is the slowly- and obliquely-spreading northernmost extension of the Mid-Atlantic Ridge system (Thiede and Myhre, 1996). Especially the lower part of profile shows prominent wavy sediment patterns; some wavy patterns are also found in the lower part of the sedimentary succession further upslope. This pattern reflects turbiditic, glaciomarine and hemipelagic sediments, significantly reworked by contour currents. Faults are imaged in the lower part of the profile close to the Knipovich Ridge. A BSR is found at some parts of the profiles. A BSR along this profile extends the previously mapped area of a BSR off Svalbard. The seismic data show some small landslide deposits, which are covered by undisturbed sediments.

Parts of profile P700 (Fig. 5.1.7) were collected on a bathymetric high west of the Knipovich Ridge. Several of these highs are found in this region; it is controversially debated whether they are oceanic or continental blocks. The seismic data (Fig. 5.1.7) show a relatively thick (at least 500 m) sedimentary succession, which contradicts a young oceanic origin. A BSR is also clearly imaged on this profile.

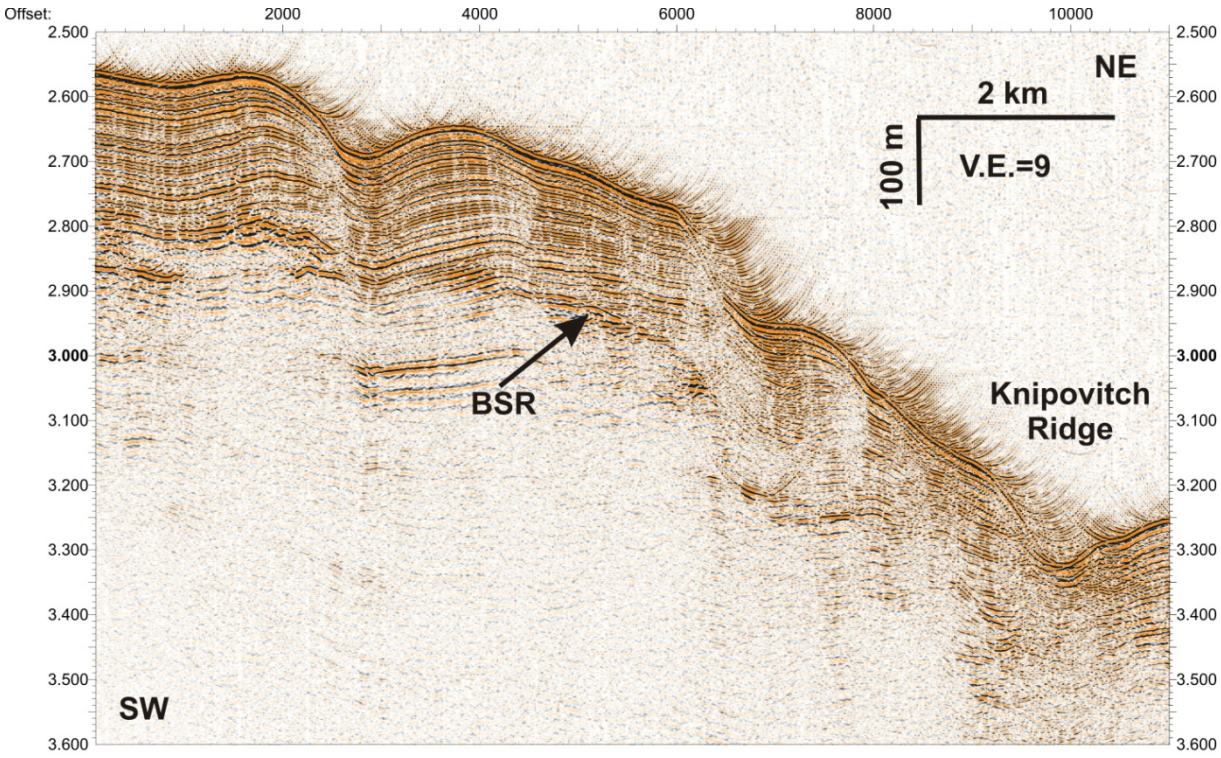

Fig. 5.1.7 Part of seismic profile P700 collected on a bathymetric high west of the Knipovich Ridge. See Fig. 5.1.3 for location of profile.

5.2 PARASOUND acquisition

(Sebastian Krastel, Felix Gross)

5.2.1 System description

The hull-mounted parametric sub-bottom profiler PARASOUND DS3 (Atlas Hydrographic) was operated on a 24-hour schedule for flare imaging and to provide high-resolution information on the uppermost 50-100 m of sediment. PARASOUND DS3 works as a narrow beam sediment echo sounder, providing primary frequencies of 18 (PHF) and adjustable 18.5 – 28 kHz, thus generating parametric secondary frequencies in the range of 0.5 – 10 kHz (SLF) and 36.5 – 48 kHz (SHF) respectively. The secondary frequencies develop through nonlinear acoustic interaction of the primary waves at high signal amplitudes. This interaction occurs in the emission cone of the high-frequency primary signals which is limited to an aperture angle of 4° for the PARASOUND DS3. This narrow aperture angles is achieved by using an array of 128 transducers on a rectangular plate of approximately 1 m² surface area. Therefore the footprint size is 7% of the water depth and vertical and lateral resolution is significantly improved compared to conventional 3.5 kHz echo sounder systems. The PARASOUND DS3 is an improvement of the former PARASOUND DS2 (Atlas Elektronik) and is installed on RV Maria S Merian since 2005. The system provides features like recording of the 18 kHz primary signal and both secondary frequencies, continuous recording of the whole water column, beam steering, different types of source signals (continuous wave, chirp, barker coded) and signal shaping. Digitization takes place at 96 kHz to provide sufficient sampling rates for the high secondary frequency. A down-mixing algorithm in the frequency domain is used to reduce the amount of data and allow data distribution over Ethernet.

For the standard operation a parametric frequency of 4 kHz and a sinusoidal source wavelet of 2 periods were chosen to provide a good balance between signal penetration and

vertical resolution. The 18 kHz signal was also recorded permanently. If the system was mainly used for flare imaging, it was operated in a single pulse mode. This was changed to the quasi-equidistant mode in deeper water, when the uppermost sediments had to be imaged.

Unfortunately, technical problems which could only partly be solved during the cruise resulted in frequent loss of data due to software malfunctioning. Several parts of the system were replaced but frequent program crashes (at least one a day) occurred until the end of the cruise. However, these data gaps rarely exceeded some minutes and the overall data quality is very good.

All raw data were stored in the ASD data format (Atlas Hydrographic), which contains the data of the full water column of each ping as well as the full set of system parameters. Additionally a 400 m-long reception window centered on the seafloor was recorded in the compressed PS3 data format after mixing the signal back to a final sampling rate of 24 kHz. This format is in wide usage in the PARASOUND user community and the limited reception window provides a detailed view on the subbottom structures. When the system was used for flare imaging, the full water column above the sea floor (usually 500 m) was recorded in PS3 format.

All data were converted to SEG-Y format during the cruise using the software package ps22sgy (Hanno Keil, Uni Bremen). The software allows generation of one SEG-Y file for longer time periods. If seismic data were collected simultaneously, one SEG-Y file was created for the length of each seismic profile. In all other cases 2h-long pieces were generated (e.g. during transit). All data were loaded to the seismic interpretation software HIS Kingdom. This approach allowed us to obtain a first impression of sea floor morphology variations, sediment coverage and sedimentation patterns along the ship's track. In addition the exact locations of the abundant flares could be determined, which was important for selecting locations for JAGO-dives, sediment coring, and water sampling.

5.2.2 Preliminary Results

The PARASOUND-system was used for sediment echo sounding and flare imaging. PARASOUND data were collected during all profiles and transits. It was also operated on most station in order to estimate the rising velocity of gas bubbles.

Several dense grids of PARASOUND profiles for flare imaging were collected during breaks between JAGO-dives. Profile distance was in the range of 40 m. Given a 40 m foot print of the PARASOUND system at 390 m water depth (typical depth of flares) this allowed us to obtain complete coverage of the flare locations within this area. Flares are clustered at a water depth around 390 m, which corresponds to the boundary between stable gas hydrates below and free gas occurrences in shallower water depth. No flares were found in water depth deeper than 400 m. A typical example of flares located in water depths shallower than 400 m is shown on Fig. 5.2.1. The profile crosses the site of the MASOX observatory. A strong flare is clearly visible at this site. Some additional flares are found along this profile as well. This profile was also chosen as location for a joint heat flow / CTD transect. Locations of the individual measurements are marked on the profile (Fig. 5.2.1). Most of the flares seem to be relatively small with heights less than 50 m. The flares, however, are deflected by strong currents. The dip direction seems to be more or less perpendicular to the profile orientation. This is clearly indicated by the accumulation of free gas bubbles in the water column, which do not have a connection to the sea floor on this profile, as the origin of these flares is out of the plane shown here.

The variation of the dip of the flares over time is clearly shown by the images shown on Fig. 5.2.2. The two images are collected almost along the same profile on different days; they do show similarities and differences. The flares are mostly active at the same locations suggesting constant activity. The upper image shows a large dip (~30°) of the flares while the

flares are almost vertical in the lower image. This corresponds well with observations made during JAGO dives, where a current velocity of 0.4 kts was estimated for August 18th, while the current almost stalled during dives on August 22nd. Flare heights are in the range of 200 m.

Fig. 5.2.3 shows an 18 kHz PARASOUND image while being on station. Rising gas causes the pronounced inclined reflections. Such an image can be used to estimate the velocity of rising bubbles. The image shows slight variation for individual gas flares; the average velocity is 0.2 m/s. Variations in velocity are probably caused by varying bubble sizes.

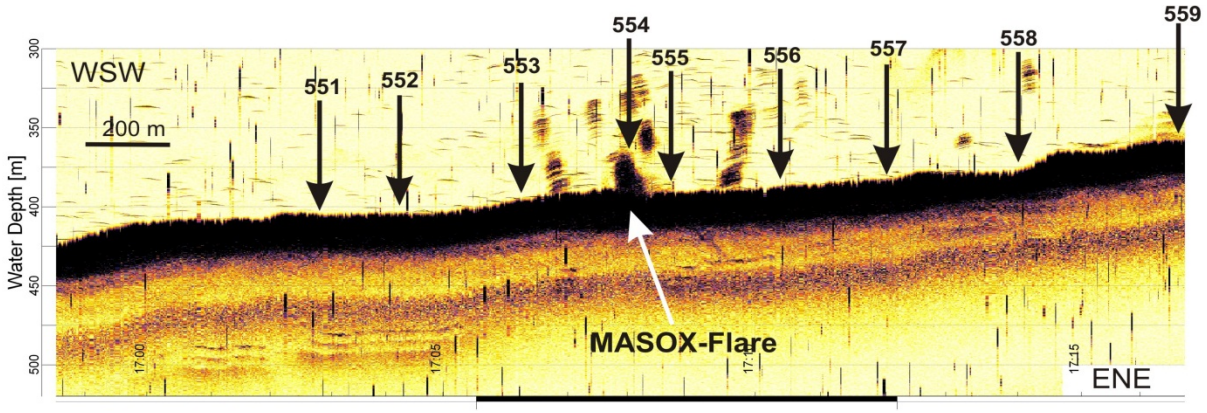

Fig. 5.2.1 Flares observed around the MASOX observatory site. The arrows indicate the locations of a combined heat flow / CTD-transect.

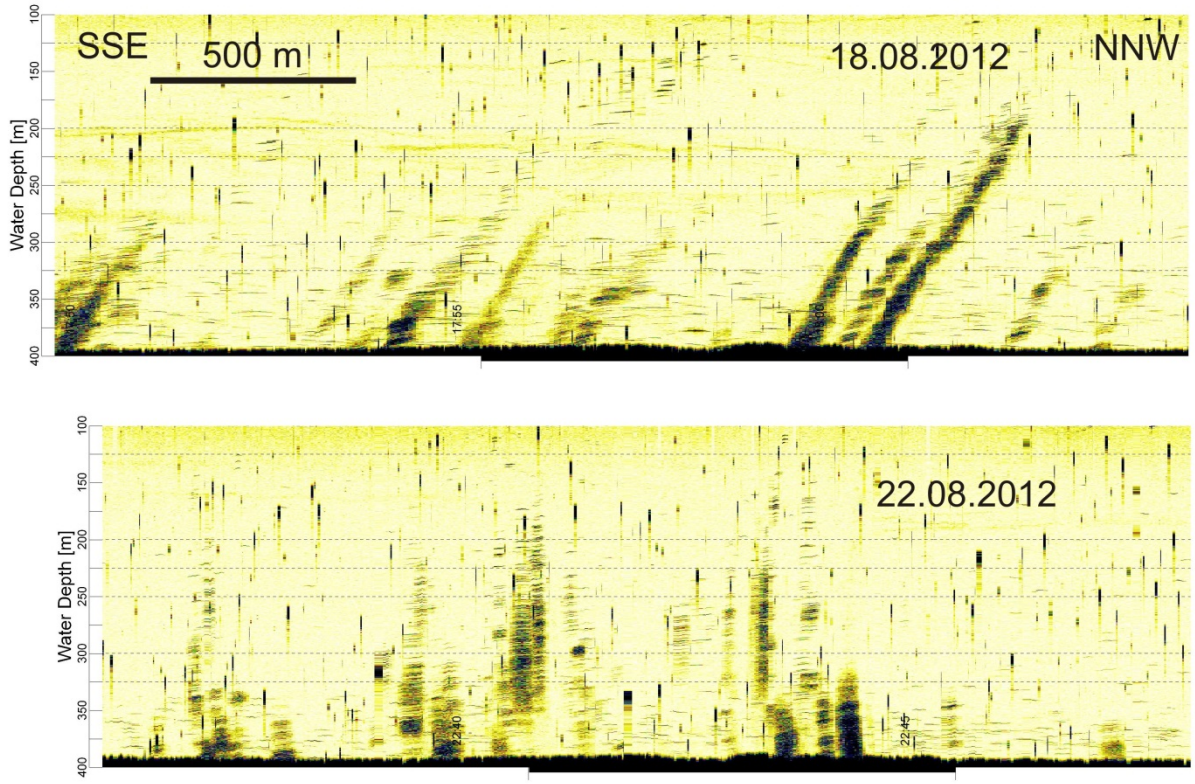

Fig. 5.2.2 Comparison of flares observed along the same profile on two different dates. Flares show a dip of ~30° on August 18th as a result of strong currents; in contrast flares rose close to vertical on August 22nd.

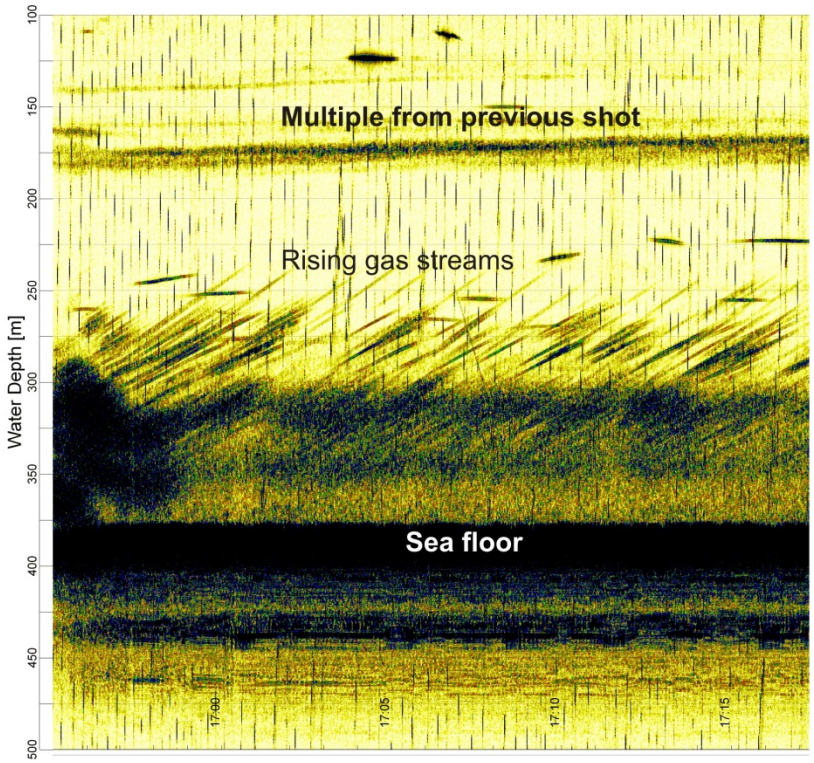

Fig. 5.2.3 18 kHz-PARASOUND image collected while being stationary (78°36.68'N, 009°25.50'E, Hybis Site). The inclined reflections are caused by rising gas streams.

The PARASOUND echo sounder was also used in a conventional way for imaging the uppermost sediments, e.g. for selecting coring locations at the newly discovered landslide in the northern most working area (see previous chapter). Fig. 5.2.4 shows a profile crossing gravity cores 603 and 605. Core 603 is taken in undisturbed background sediments. A first significant increase in slope angle is found in about 1500 m water depth. Bathymetric data reveal a headwall in this area. The PARASOUND data, however, show a smooth surface and no sharp step. No slide deposits are found beneath the increase in slope angle. Hence this headwall seems to be old and already covered by sediments. A very prominent stepped pattern is found between 1950 m and 2100 m water depth. These steps clearly cut stratified sediments. A hummocky surface is found beneath these steps. This feature is interpreted as a young landslide as no undisturbed sediments are imaged above the slide deposits though we like to point out that drapes thinner than ~1 m are not detectable with the system. Core 605 was taken from a small transparent body, which is also interpreted as a slide deposits. Fig. 5.2.5 shows a parallel profile crossing core 606. No obvious headwalls are found along this profile but the transparent body at the location of station 606 most likely represents slide deposits. The cores taken in this area were not opened while being at sea.

Fig. 5.2.6 illustrates a 4 kHz-PARASOUND profile perpendicular to the slope, starting at the MASOX site. The lower slope is covered by well-stratified sediments. Some incisions were found between offset 6500 m to 13000 m. Penetration is significantly reduced at the upper slope.

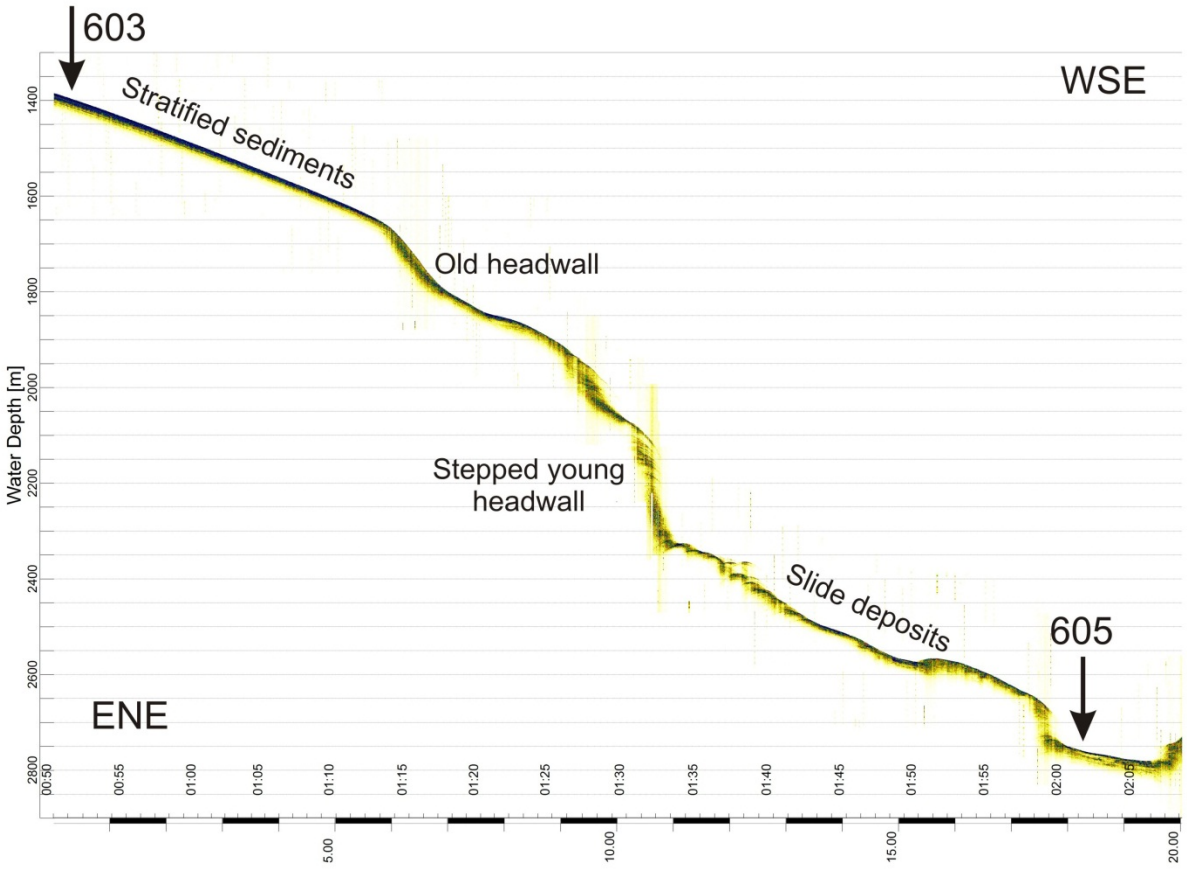

Fig. 5.2.4 PARASOUND profile crossing the locations of gravity cores 603 and 605. See Fig. 5.1.6 for location of profile.

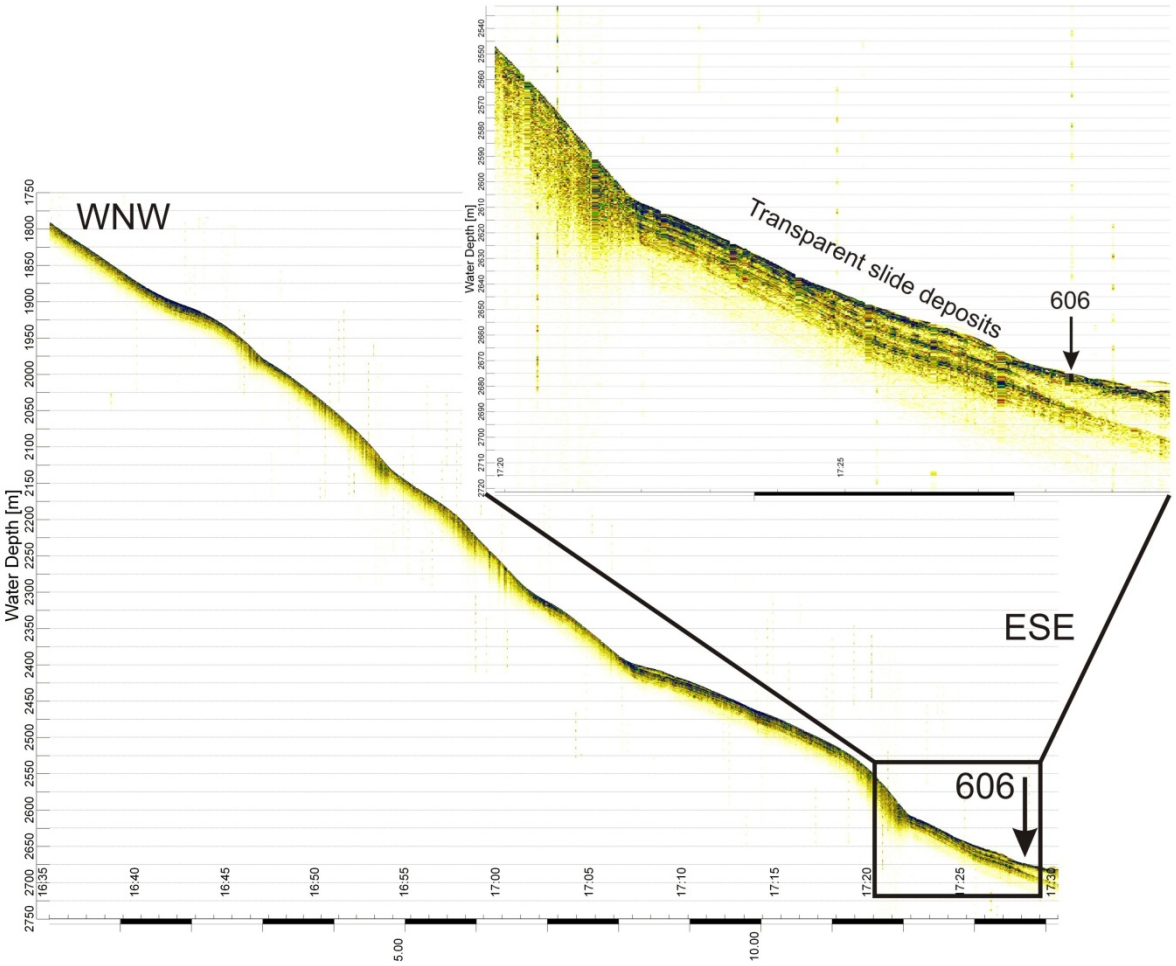

Fig. 5.2.5 PARASOUND profile crossing the location of gravity core 606. See Fig. 5.1.6 for location of profile.

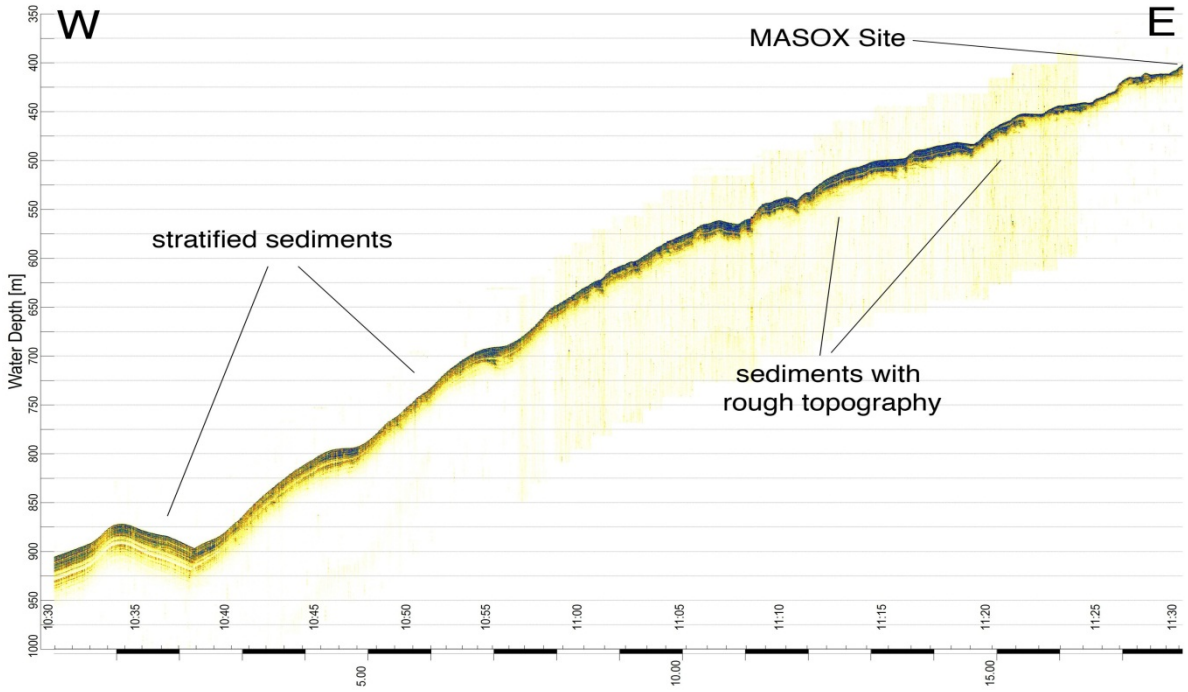

Fig. 5.2.6 West to east running PARASOUND profile starting at the MASOX site. See Fig. 5.1.3 for location of profile.

5.3 EM120 Multibeam echosounder

(Kathrin Lieser)

5.3.1 System description

During Cruise MSM21/4 the hull-mounted Kongsberg Simrad system EM120 was used for bathymetric mapping continuously while we were in the Svalbard study area. The EM120 system allows accurate bathymetric mapping up to full ocean depth. Basic components of the system are two linear transducer arrays in a Mills cross configuration with separate units for transmitting and receiving. The nominal sonar frequency is 12 kHz with an angular coverage sector of up to 150° and 191 beams per ping. The emission angle is up to 150° wide across track, and 1° along track direction. The reception is obtained by beam forming of 191 beams, with widths of 2° across track and 20° along track. Thus, the actual footprint of a single beam has a dimension of 1° by 2°. The achievable swath width on a flat bottom will normally be up to six times the water depth dependent on the character of the seafloor and the selected opening angle. The angular coverage sector and beam pointing angles may be set to vary automatically with depth according to achievable coverage. This maximizes the number of usable beams. In areas where we collected a dense net of PARASOUND profiles with a profile distance of less than 100 m, the swath width was manually reduced in order to increase data density and quality. The beam spacing is normally equidistant, but equiangular is also available. For depth measurements, 191 isolated depth values were obtained perpendicular to the track for each ping. Using the 2-way-travel-time and the beam angle known for each beam, and taking into account the ray bending due to refraction in the water column by sound speed variations, depth is calculated for each beam. CTDs for collecting an accurate sound velocity profile were taken at several sites. A combination of amplitude (for the central beams) and phase (slant beams) is used to provide a measurement accuracy practically independent of the beam pointing angle. Beside the depth values, the EM120 provides also backscatter values and pseudo-sidescan images.

In general the system worked reliably and only minor data gaps exist. However, the outer beams exceeding 60° have a hardware-related azimuth error, which may limit the usable swath width. Onboard processing was not able to correct this error.

5.3.2 Preliminarily results

For onboard processing and display of the data for cruise planning purposes, Kongsberg's Neptune software was used. The processing of the data set included flagging of outer beams, applying a noise limit of 3 %, and generating a grid with a spacing of 100 m. Wrong values such as multiples were removed manually. The free software Generic Mapping Tool (GMT) was used for plotting maps.

Fig. 5.3.1 shows a coverage map of all bathymetric data recorded during the cruise. Fig. 5.3.2 shows an enlargement of the northernmost working area. This map shows a complex landslide with multiple headwalls of varying height. Maximum headwall height is up to 150 m. The width of the landslide complex is at least 35 km. The presence of headwalls at different depth levels indicates either retrogressive failure or multiple landslide events in the same area.

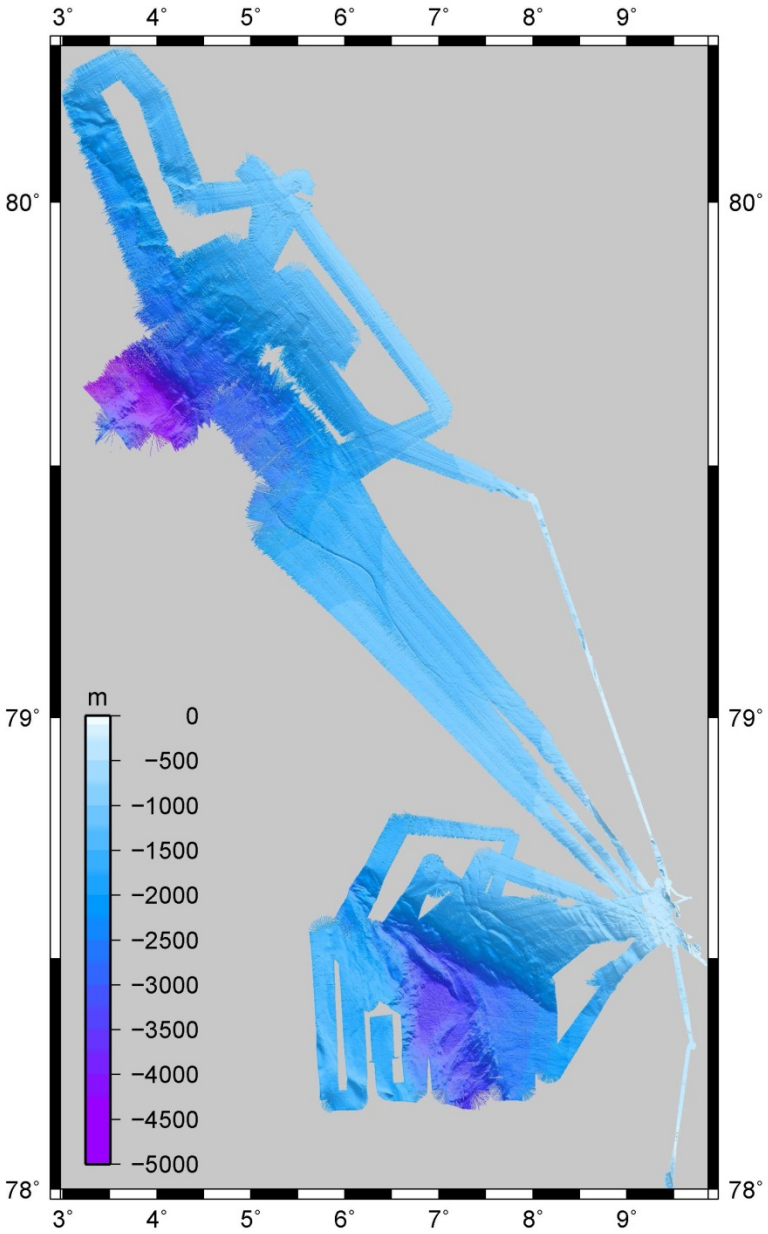

Fig. 5.3.1 Multibeam bathymetry coverage for the study area of Svalbard.

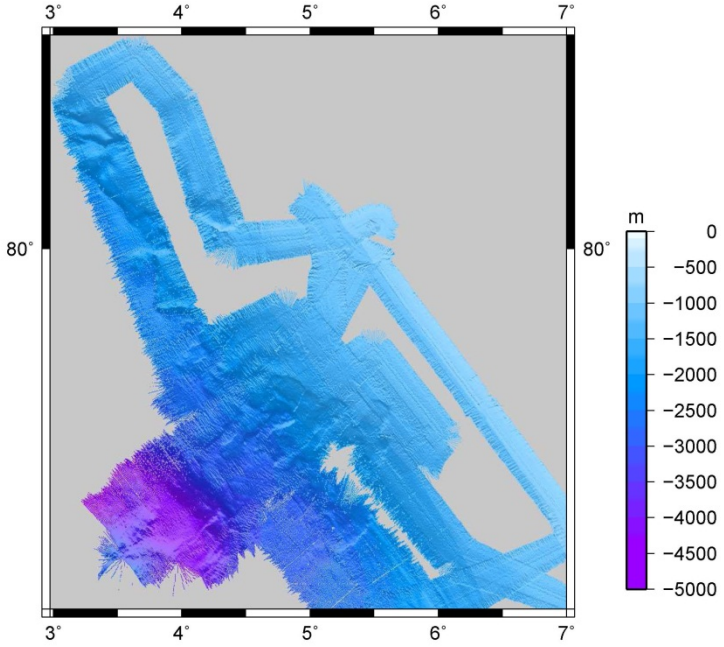

Fig. 5.3.2 Enlargement for the northern study area showing the headwalls of the newly discovered landslide.

5.4 Submersible JAGO operations

(Karen Hissmann)

The manned submersible „JAGO“ (Fig. 5.4.1), operated by GEOMAR in Kiel, was used during MSM 21/4 for in situ video documentation of the seep sites, for sampling sediments and bacteria mats with push cores and for collecting near-bottom water, gas, rocks, carbonate crusts and biological samples. The first dive was dedicated to the recovery of the MASOX observatory.

The submersible has a maximum operating depth of 400 m and is therefore an ideal tool for working at the upper limit of the gas hydrate stability zone at the Spitsbergen shelf break. JAGO can accommodate two persons, the pilot and a scientist/observer. The highly manoeuvrable vehicle has two large acrylic dome ports, one at the front (diameter 70 cm) and one at the top (45 cm). It is electrically driven and moves autonomously within the reach of the navigation and communication systems on board the support vessel. JAGO is equipped with USBL underwater positioning system, electronic compass, vertical and horizontal sonar, underwater telephone for communication, digital video (HDV) and digital still cameras, CTD and a manipulator arm for collecting and handling sampling devices. The compact size of the submersible (3 x 2 x 2.5 m LWH) and its relatively small weight of 3 tons allow a launch and recovery from a wide variety of ships with sufficient crane capacity (min. 5 tons SWL). The entire equipment including the submersible fits into a single 20’ ISO container. The JAGO team consists of three staff members: the chief pilot / senior technician, the operational manager in charge of the communication and navigation on board the support vessel, and a technician assistant / swimmer for support during launch and recovery.

The submersible operates worldwide and is regularly used from the German research vessels among which R/V M.S.MERIAN is one of the most suitable for JAGO. The vessel behaves extremely stable at station, is dynamically positioned, has a large working deck, and possesses three deck cranes with sufficient lifting capacity and outreach for save handling of the manned underwater vehicle.

During MSM 21/4 JAGO was lashed on deck amidships at container storage position #23, the 20’ transport and storage container lengthwise at position #29/30 with the doors opening

towards the ship's bow. JAGO was launched and recovered with deck crane #3 at the starboard aft deck (fully-hydraulic knuckle boom crane). The boatswain who was familiar with the handling procedure from previous JAGO operations from on board the M.S.MERIAN operated the crane. The DSB work boat (6 m TL inflatable with aluminium hull and 60 HP Yamaha outboard engine), steered in shifts by the first and second navigation officer, was used to tow JAGO away from the ship's side after deployment and back under crane position for recovery. Initially designed for the recovery of the MASOX observatory, a new descent and positioning procedure was used regularly to minimize the descending time and to reduce the time needed for approaching the target sites at the sea floor. The steel cable of the large starboard sliding beam (hydraulically-extendable jib crane), to which a steel weight of 300 kg was attached, was used as a guiding line to the target site. First the weight was lowered to approximately 5 m above the seabed. Afterwards the submersible was launched to the water surface. The ship's bow was kept at an angle of maximum 45° to the wind direction during the entire procedure. This provided a large relatively calm area at the starboard side for JAGO and the crane cable. The JAGO pilot approached the cable while the submersible was still afloat at the surface, submerged close to it and then hooked the cable into an open steel hook attached to the upper lamp bar above JAGO's bow window. Small-radius movements of the ship assisted the exact positioning of the sub. When attached to the cable in close distance to the ship's side, JAGO started to descent down the cable while being slowly towed by the vessel towards the target site. A few metres above the 300 kg weight the pilot released JAGO from the crane cable and approached the bottom in save distance while the weight was lifted. The entire procedure was carefully monitored, guided and controlled by DP, USBL positioning, VHF and underwater communication (see below). It effectively reduced searching and approaching times at the sea floor and current induced displacement from the main target site while descending. The procedure was successfully applied during all dives.

While submerged, JAGO was tracked and guided by POSIDONIA 6000 (USBL underwater positioning system from IXSEA France), part of the ship's equipment. The POSIDONIA mini-transponder MT 861S-HD-R was mounted on top of the submersible and connected to JAGO's power supply system. The position data (ship and sub) were integrated into ABYSS navigation software (IXSEA) to display and follow both JAGO and MERIAN tracks geographically and in real time on a computer monitor. The initial plan to use the OFOP software (http://ofop.texel.com) to display the position data upon GIS based bathymetric maps had to be skipped. It was not possible to send an adequate NMEA telegram with compiled ship position strings from the DShip database to the OFOP PC due to a server problem. The vessel's electronics engineer finally managed to provide the required telegram by using the terminal server of the SatTV system which was not in use. Thanks to his support the OFOP software could be tested at least once and in parallel with ABYSS during the last JAGO dive. This problem with the database urgently needs fixing. The tracking accuracy was generally good. Transducer signals could be detected by the acoustic array from ca. 60 m water depth downwards during descents and up to 20 m water depth during ascents within a horizontal distance of up to 100 m around the ship. All position data were logged on the POSIDONIA PC in the data centre and later extracted as column-based ASCII files from the DShip database. All JAGO dive tracks and sampling sites are available to be plotted on the multibeam maps combined with the individual dive logs, video sea floor observations and CTD records. Time codes were all set and synchronised to GMT.

Communication between JAGO and MERIAN during dives was maintained by acoustic underwater telephone (ORCATRON) and a hydrophone/transducer that was lowered over the ship's starboard side to ca. 2 m water depth below the ship's keel. The MERIAN transducer which is permanently installed on an extendable pole inside the vessel's bow could not be used due to strong acoustic interferences while the pump jet was running. Installation of the

hydrophone below the equipment platform inside the hydrographic pool, situated amidships about 6 m aft of the pump jet, did not improve the acoustic quality. The deck unit of the underwater telephone was established in the data centre next to the POSIDONIA control unit.

During MSM 21/4, JAGO performed a total of 10 dives to bottom depths between 245 and 396 m at three different target sites. The total dive time was 34 hours 20 minutes. Nine different scientists participated in the dives. Most of them entered a manned submersible for the first time.

Prior to each dive, gas seepage at the selected sites was verified by PARASOUND and multi-beam bathymetry. Flare positions and positions of deployed devices were loaded as waypoints into the ABYSS navigation system and displayed on the navigation grid chart. To find and relocate these particular spots at the sea floor was no problem. Most dives focussed on the seeps at the shelf break at the upper limit of the gas hydrate stability zone (385-392 m). One dive took place on the shallower shelf plateau in 245-247 m water depth, and the first dive of the cruise was dedicated to the recovery of the MASOX bottom observatory (section 5.5) at 392 m water depth. During most of the dives, bottom currents were moderate.

The habitat and activities at the seafloor were continuously video-documented with a SONY HDV Camcorder HVR-V1E mounted in the centre of JAGO's large bow viewport. After each dive, post-processing of the original HDV video footages provided digitized .mov and .mpg4 copies of the video material with overlaid GMT time code for evaluation by the science party. Video still images were captured by video-grabbing after each dive. A dive protocol was produced by each of the dive participants inside JAGO to log observations and activities.

Sediment, sediment in-fauna and bacteria mats were collected with 2 types of push corers. The larger corers have an inner length of 255 mm and an inner diameter of 72 mm. Maximum six push corers per dive were stored in the sampling basket attached to the instrument porch at the lower front of the submersible. At most of the sampling sites it was extremely difficult to push the corers into the substrate. Gravel and stones embedded in the upper sediment layers prevented a deeper penetration. The manipulator arm and an additional drop-weight of 3.5 kg were used as a hammer to force the core liner into the substrate (Fig. 5.4.3). Retrieved sediment cores had a length of ca. 15 cm. The smaller corers, named mini-push corers, had an inner length of 300 mm and an inner diameter of 26 mm. Six of them per dive were stored in a specially designed rack (32 x 20 x 41 cm LWH) before and after sampling. The mini-push corers penetrated a bit easier into the sediment than the larger corers due to the smaller diameter of their liners. Retrieved cores had a length of up to 12 cm. Push coring took place on or in close vicinity to bacteria mats, seeps and pogonophoran field (Fig. 5.4.8 and 5.4.10).

Peepers are devices for collecting pore water from seep site sediments. They were specially designed and constructed for this cruise to be handled by JAGO’s manipulator arm (Fig. 5.4.3 to 5.4.7). They consist of an outer and inner tube of 50 cm length and 2 cm diameter. The inner tube has 8 sample cells that contain “dialysis bags” filled with sterilized bottom seawater. While sticking inside the sediment, the seawater is replaced by surrounding pore water through equilibration. For transport to and from the sampling site in a depth of 395 meter, six peepers were inserted into a rack (62 x 11 x 58 cm) mounted on JAGO’s instrument porch. The peepers were recollected after 11 days.

A temperature probe (T-Stick) of 40 cm length was inserted into the sediment at the same site as the peepers (Fig. 5.4.7). It was recovered together with the peepers after 11 days.

Near-bottom water samples were taken with a 2.5 L NISKIN bottle attached to the port bow of the submersible. Gas bubbles were collected with a funnel hold directly above the seeps (Fig. 5.4.9). They rose inside a flexible hose into a pressurized gas sampling device of 1 ltr volume. Carbonate and rock samples were transferred into the sampling basket, or, if too large, on top of the porch beside the basket. Benthic macrofauna like single specimens of brittle and sea stars, sea anemones, ascidians, bryozoans, tube worms, molluscs and sponges

(Fig. 5.4.14) were selectively collected and transferred into a closable sampling tube. Main sampling sites were marked with labelled site markers. A CTD (SAIV A/S SD204 Norway) at the stern of the submersible continuously recorded depth, temperature, salinity and density during de- and ascents and while "flying" close over the seafloor. All CTD data were made available on board as ASCII files.

Handling of the submersible from on board the MERIAN went extremely smooth even under less calm sea conditions thanks to the professional support from the entire ships crew on bridge, deck and work boat. The M.S.MERIAN is an excellent support ship for JAGO operations.

Fig. 5.4.1 Submersible JAGO equipped with sampling devices (on porch sampling basket, push corer, tube for biosamples, marker; on vertical pole gas and water sampler) on board of M.S.MERIAN during MSM21/4 (left) and during launching (top) off Prins Karls Foreland / Spitsbergen

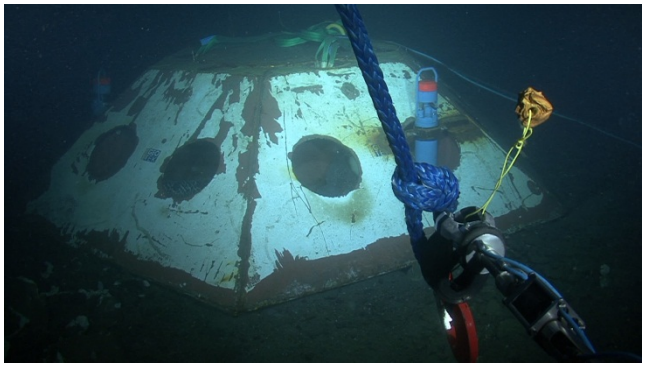

Fig. 5.4.2 Recovery of MASOX observatory at 394 m depth

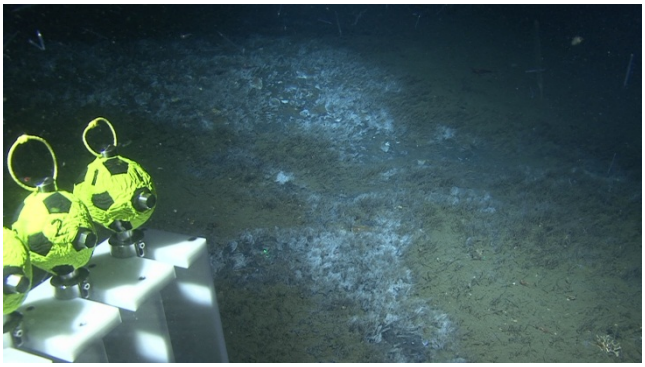

Fig. 5.4.3 Sulfur bacteria mats and pogonophoran field at 395 m depth, left: peeper inside rack

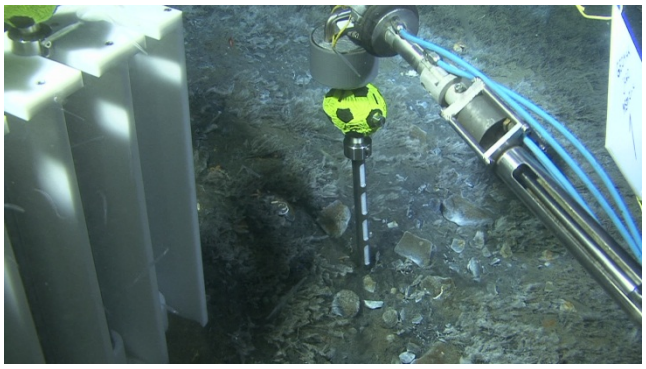

Fig. 5.4.5 Peeper deployment into bacteria mat at 395 m depth with JAGO's manipulator arm

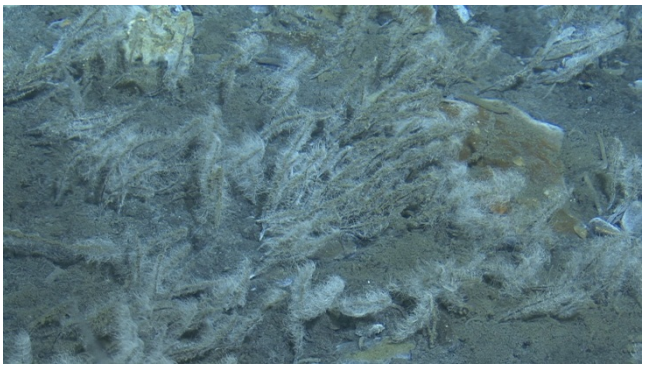

Fig. 5.4.6 Sulfur bacteria attached to pogonophoran tubes

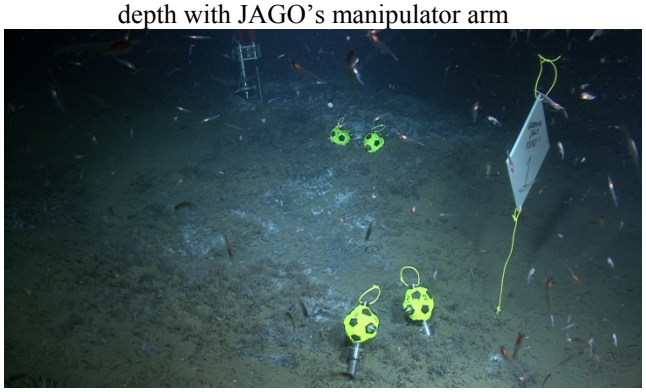

Fig. 5.4.7 Peeper, temperature probe (background) and marker deployed at seep site

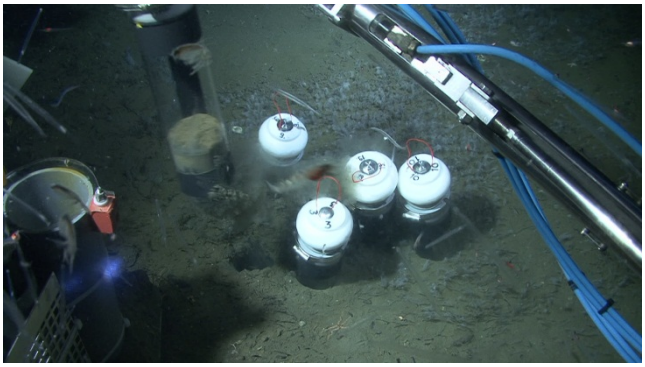

Fig. 5.4.8 Pulling large push corers out of sediment

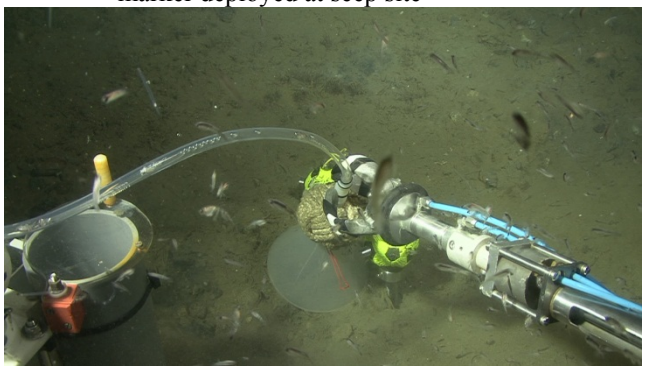

Fig. 5.4.9 Gas sampling at peeper site

Fig. 5.4.10 Six mini- and two large push corers deployed into sediment at 395 m water depth

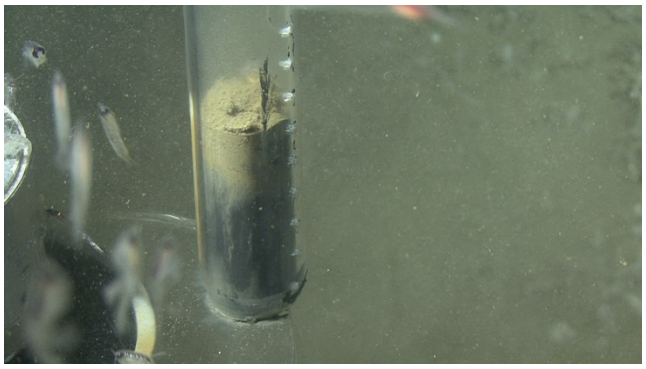

Fig. 5.4.11 Retrieved mini core

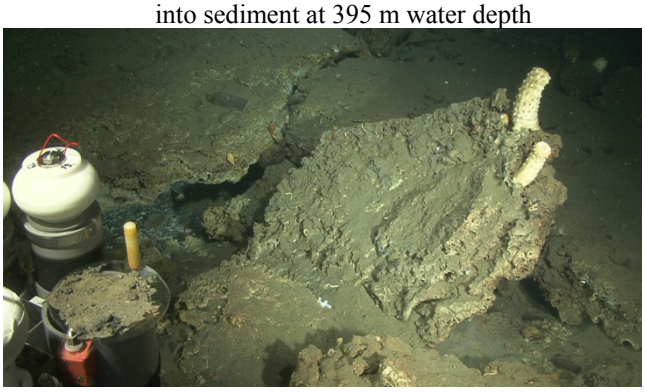

Fig. 5.4.12 Massive carbonate capping at 382 m

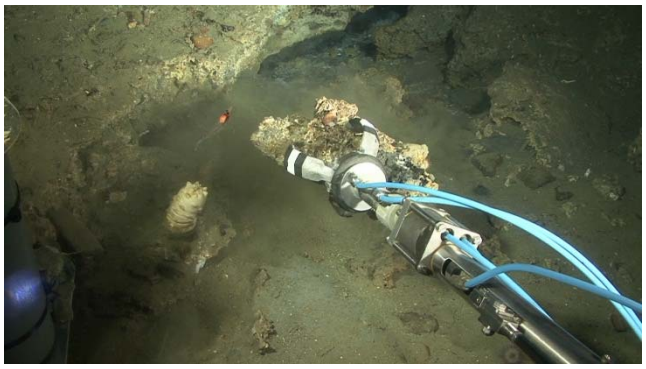

Fig. 5.4.13 Carbonate sampling at 382 m depth

Fig. 5.4.14 Spotted wolffish *Anarhichas minor* in cave below massive carbonate crust, 333 m

Fig. 5.4.15 Collection of a sponge at 345 m water depth

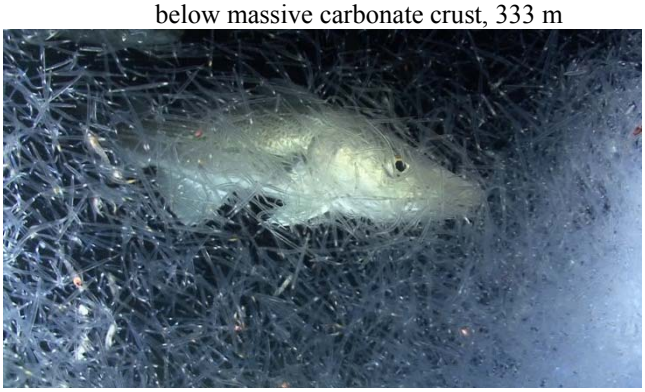

Fig. 5.4.16 Cod hunting zooplankton (arrow worms, shrimps, copepods) attracted by JAGO's lights

5.5 MASOX observatory

(Veit Hühnerbach)

5.5.1 Instrument design

The MASOX seabed observatory consists of six 500 kg steel segments that assemble to a hexagonal bottom mount structure of 4 m diameter and 1.5 m height (Fig. 5.5.1).

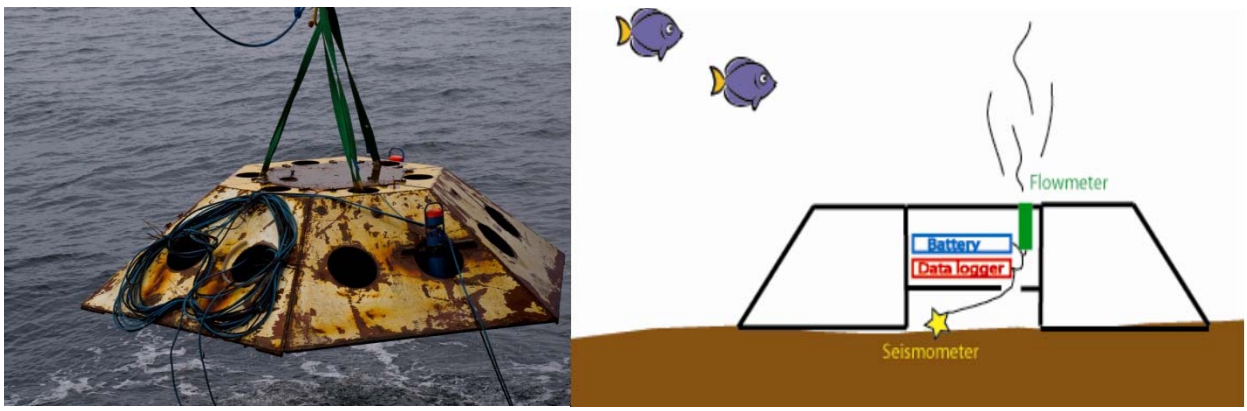

Fig. 5.5.1 Left: MASOX seabed observatory recovered. Clearly visible are the two Seaguard RCMs and the thermistor chain. Right: Schematic drawing of the observatory and its instruments.

Its design is meant to shelter a stainless steel cage from bottom trawling. This cage of approximately 1 m diameter sits inside the structure and houses the scientific instruments (Fig. 5.5.1).

A second function of the design is to amplify any fluid/gas flow; the volume inside the bottom mount is around 9000 cm^3 but any fluids and/or gas can only exit this space via a small inverted funnel with 13 cm diameter as they pass the flow meter. The instrument suite inside the observatory consists of a seismometer (4.5-200 Hz geophone), a hydrophone, and a titanium pressure cylinder with the SEND data logger and Lithium battery packs as power source. Sampling rate for the seismometer and the hydrophone is 50 Hz, 19 bits. Data storage is on flash cards with a total capacity of 24 GByte.

In addition, a highly sensitive flow meter, two titanium pressure cylinders with an additional SEND data logger and battery packs (276 Li-cells; enough for about 1 year) for the flow meter. Sampling rate for the flow meter is 50 Hz, 19 bits. Data storage is on flash cards with a total of 14 GByte.

In addition, there are 2 Seaguard RCM current meters mounted to the outside of the hexagonal bottom structure. They contain temperature, conductivity, turbidity sensors and oxygen optodes.

The MASOX observatory, first deployed in October 2010, was placed in the flare cluster B (see RV JAN MAYEN cruise report, Mienert et al 2010). It was serviced in August 2011 during RRS JAMES CLARK ROSS voyage 211 including a data download, data logger hardware update and replacement of battery packs. During JR211, a thermistor chain of 100 m length with 6 temperature sensors was attached to the observatory. The temperatures on the seabed were logged every 60 mins and stored on a 1 GB MicroSD card. About 50 m of the chain could be laid out on the seabed.

In August 2012, it was recovered during RV MARIA S. MERIAN using the manned JAGO submersible. Upon recovery, it was noted that the data logger for the flow meter had switched off about two months earlier due to the lack of power. This was probably caused by low temperatures on the seabed. The seismometer and hydrophone assembly worked well, despite seawater ingress into the pressure cylinder causing 5 Li-cells to corrode, fortunately without causing any damage to the logging equipment.

The thermistor chain worked also throughout the entire duration of the deployment, although on first inspection of the data, it seems that the temperature values are too high compared to the actual CTD casts run in the vicinity of the observatory prior its recovery. It may be necessary to calibrate the thermistor chain again to establish any drift of the instrument.

Toward the end of the voyage the seabed observatory was re-deployed in the Sleipner gas field in 85 m depth. The exact position is 58° 35.760’ N and 002° 05.341’ E. The aim is to monitor potential gas leakage from the geological formation into which gas from the production site is pumped continuously for the last 14 years. The instruments contain the flow meter, seismometer and their logger/battery cylinders and two Seaguard RCMs. The battery voltages for the flow meter/ seismometer set are both 14.74 V, for the RCMs 9.7 V (alkaline) and 7.36 V (lithium) respectively.

5.5.2 Preliminary results

Seaguard RCMs: data from both current meters could be retrieved although one unit ran out of power during the deployment prior to its recovery. It is not possible to establish the exact date when this happened because the Seaguard Studio software to read out the data was not aboard, but this will be done back in the office.

Seismometer: all data was retrieved from the logger, converted and tested. Data was logged throughout the entire period.

Flowmeter: power problems due to the low seabed temperature and a different, less powerful, type of batteries meant that the logger did not record until August 2012. It also did not set an

end of file mark, making synchronisation very difficult. First inspection of the raw data shows a week-long flowmeter sequence from November 2011 (Fig 5.5.2). The data shows that most of the time flow was out of the observatory (positive). Further analysis will be needed to establish how tidal cycles etc have impacted the dataset.

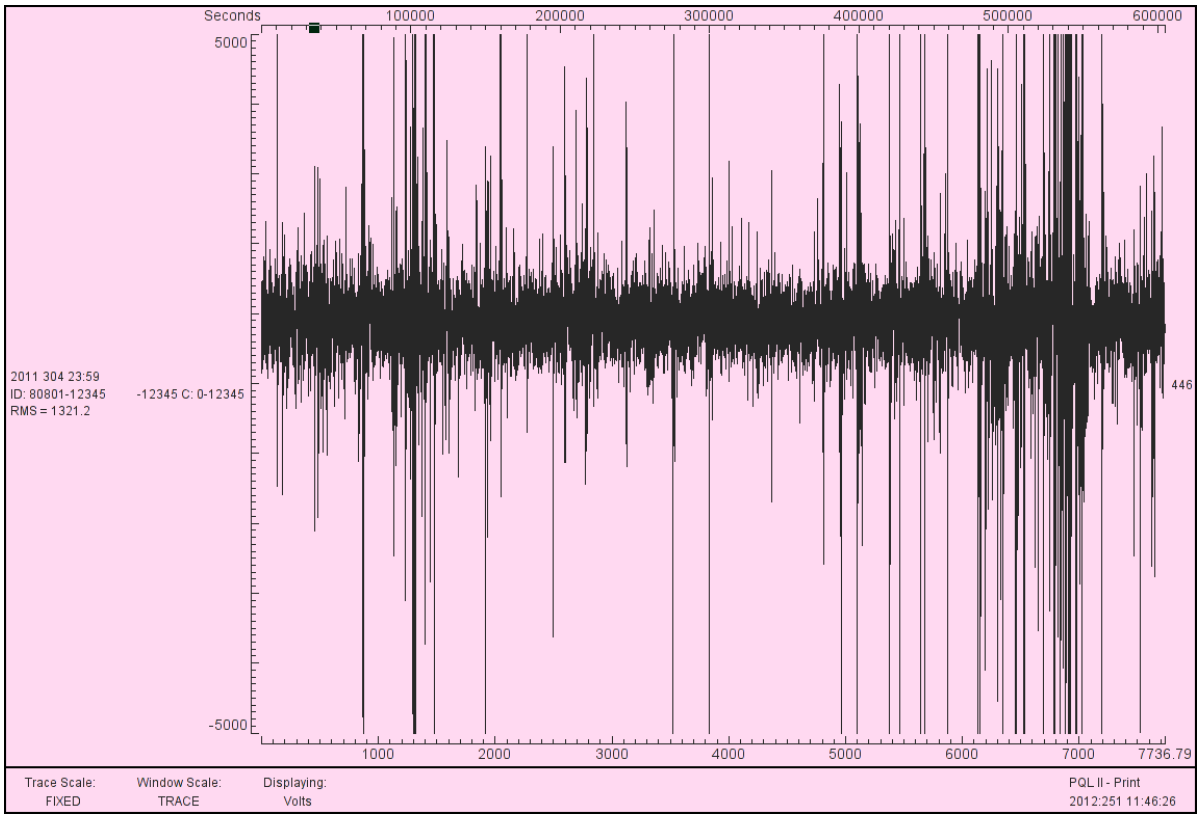

Fig. 5.5.2 Flowmeter raw data example covering one week in November 2011.

Thermistor chain: all 6 temperature nodes within the ~100 m of chain deployed worked throughout the entire one year-long deployment (Fig. 5.5.3). However, comparing the data to the JAGO-mounted CTD during recovery there seems to be an offset of approximately +0.5 °C for all the nodes. Individual measurements were recorded every hour.

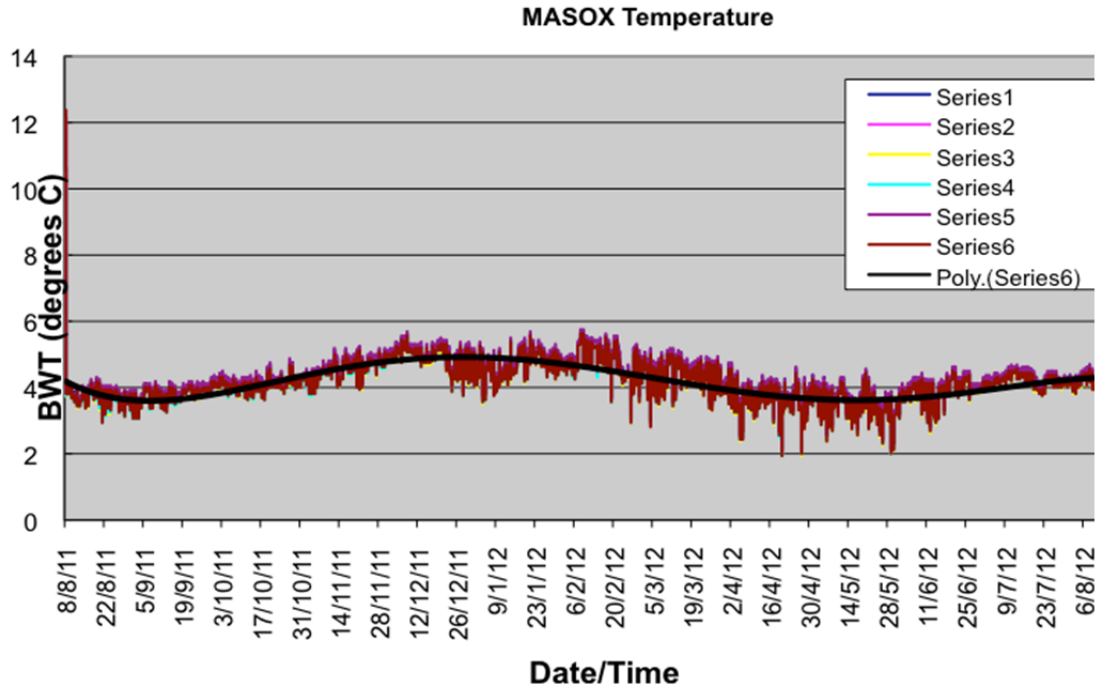

Fig. 5.5.3 Bottom water temperature variations for the second year deployment of the MASOX observatory. While the temperature values are very consistent for the six different sensors, comparison with the JAGO CTD indicates that they are all 0.5 degrees too high.

5.6 Gravity cores

(Ines Dumke)

Gravity cores were collected using RV Meteor's piston corer. At the HyBIS site, MASOX site and at the Knipovich Ridge, as well as in the Northern survey area, the piston corer was deployed with a 6 m long PVC core liner, while on the Vøring Plateau a 12 m long liner made up of two 6 m liners was used to enable the recovery of longer gravity cores. A list of collected gravity cores is given in Table 5.6.1. Locations of coring stations are shown in Fig. 5.6.1 for the HyBIS and MASOX sites, and in Fig. 5.1.3 and 5.1.6 for the Knipovich and Northern area, respectively.

Cores taken at the HyBIS site, MASOX site and Knipovich Ridge were collected using plastic bags instead of PVC liners to facilitate sub-sampling. The cores were sub-sampled immediately after recovery as described in section 5.7. These cores were not archived; after extraction of samples, the remaining sediment was disposed of.

Cores taken at the Fram Slide in the Northern survey area and on the Vøring Plateau were sealed immediately after recovery in order to be transported back to the lab to be opened, described, sampled and archived at a later stage. The only sampling performed on board consisted of sediment and porewater samples extracted through openings (11-13 per core) cut into the PVC liner for cores 603, 605 and 606 (Northern area), 660 and 661 (Gjallar Ridge on Vøring Plateau).

Table 5.6.1 Overview of gravity cores taken during MSM21-4

Station no.	latitude	longitude	depth	deployment		recovery		length [cm]
				date	time	date	time	
561-1	78° 33.28' N	9° 28.00' E	396.1	19/08/2012	14:33	19/08/2012	14:54	/
561-2	78° 33.28' N	9° 28.00' E	396.5	19/08/2012	15:18	19/08/2012	15:37	120
563	78° 33.29' N	9° 28.54' E	389.4	20/08/2012	11:51	20/08/2012	12:11	100
567	78° 33.32' N	9° 28.41' E	389.8	21/08/2012	23:27	21/08/2012	23:47	130
603	79° 49.87' N	5° 14.98' E	1355.4	26/08/2012	23:50	27/08/2012	0:32	351
605-1	79° 44.14' N	4° 33.25' E	2706.1	27/08/2012	2:24	27/08/2012	3:35	362
606	79° 47.02' N	4° 10.92' E	2622.7	27/08/2012	5:24	27/08/2012	6:33	387
626-1	78° 33.54' N	9° 27.86' E	392.6	30/08/2012	11:01	30/08/2012	11:19	/
626-2	78° 33.54' N	9° 27.86' E	391.9	30/08/2012	12:55	30/08/2012	13:38	/
627	78° 33.52' N	9° 27.89' E	393.3	30/08/2012	14:02	30/08/2012	14:18	/
628	78° 33.48' N	9° 28.13' E	391.2	30/08/2012	14:45	30/08/2012	15:02	/
629	78° 33.45' N	9° 27.97' E	393.0	30/08/2012	15:35	30/08/2012	15:53	130
630	78° 33.41' N	9° 28.20' E	392.0	30/08/2012	16:23	30/08/2012	16:43	/
631	78° 33.42' N	9° 27.11' E	401.2	30/08/2012	17:30	30/08/2012	17:49	/
643	78° 37.03' N	9° 19.02' E	437.2	31/08/2012	10:11	31/08/2012	10:44	/
644-1	78° 37.01' N	9° 19.06' E	436.2	31/08/2012	11:08	31/08/2012	11:56	/
644-2	78° 37.01' N	9° 19.08' E	435.5	31/08/2012	13:29	31/08/2012	14:12	/
648-2	78° 33.34' N	9° 28.46' E	386.9	2/09/2012	19:11	2/09/2012	19:48	/
648-3	78° 33.34' N	9° 28.47' E	385.0	2/09/2012	20:08	2/09/2012	20:42	/
652	78° 40.84' N	6° 57.50' E	1450.6	3/09/2012	18:06	3/09/2012	18:48	/
653-1	78° 33.31' N	7° 51.95' E	1490.0	3/09/2012	20:30	3/09/2012	21:25	/
657	78° 33.34' N	9° 28.38' E	388.4	4/09/2012	04:33	4/09/2012	05:00	210
660	67° 6.68' N	4° 41.74' E	1348.0	6/09/2012	18:24	6/09/2012	19:19	540
661	67° 6.64' N	4° 41.64' E	1344.0	6/09/2012	19:59	6/09/2012	20:57	573
662	64° 42.31' N	4° 58.38' E	798.4	7/09/2012	11:15	7/09/2012	11:49	734
663	64° 35.12' N	4° 45.76' E	1143.9	7/09/2012	13:36	7/09/2012	14:13	878

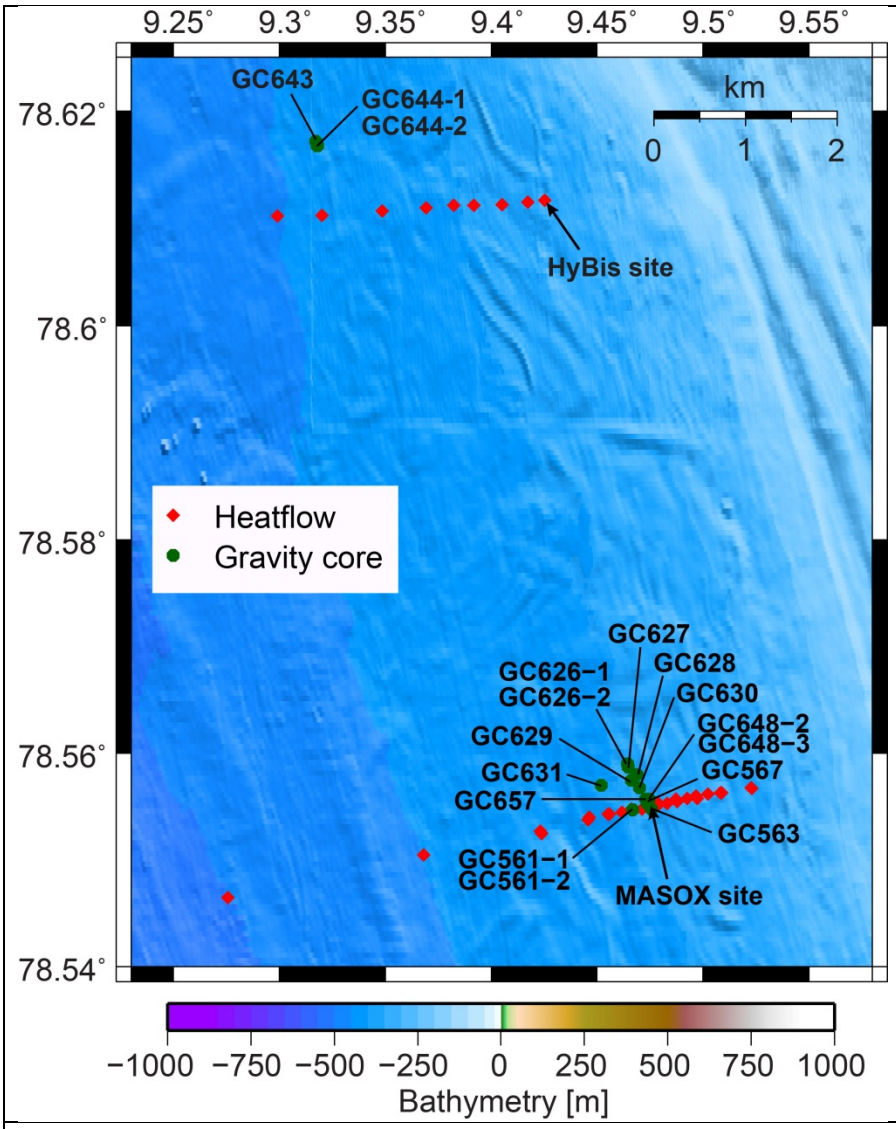

Fig. 5.6.1 Bathymetric map (EM120 data) showing gravity core locations and heatflow stations at the HyBIS and MASOX sites. Map location shown in Figs. 3.1 and 5.1.3.

5.7 Sediment biogeochemistry

(Tina Treude, Stefan Krause)

5.7.1 Instrument design and methods

Biogeochemical investigations of methane seeps focussed on the area around the Polarstern Site, the Hybis Site and the MASOX Site. Surface sediments of seeps were sampled either with JAGO push cores (large and small, see section 5.4) or with 6 m gravity cores. Push cores were placed into sediments, which featured clear indications of methane seepage at the surface, i.e., gas vents or chemoautotrophic communities (sulphur bacteria mats, pogonophoran fields). Gravity cores were processes only if they revealed foaming or sulphidic smell as indicator for high methane concentration and anaerobic oxidation of methane, respectively. So-called Peepers (max sampling depth 41 cm) were used to extract porewater from a seepage site (MASOX area), which could not be sampled with push cores due to the presence of gravels and stones (see section 5.4). Two replicate Peepers were placed into a sulphur bacteria mat, a pogonophoran field and around a gas vent, respectively. The three habitats were in close proximity to each other (~5 m).

All samples (push cores, gravity cores, and peepers) were analyzed for geochemical parameters in the porewater including, e.g., total alkalinity (TA), sulphide, ammonium, sulphate, chloride, nitrate, nitrite, dissolved inorganic carbon (DIC), $d^{18}O$, trace elements. The amount of parameters measured was depended on the extractable porewater volume. Labile parameters (TA, sulphide, ammonium, nitrite) were processed immediately on board, whereas other parameters were preserved and will be processed at home.

Sediments of push cores and gravity cores were additionally sub-sampled for methane (and higher hydrocarbons), porosity, anaerobic oxidation of methane (^{14}C-methane incubations), sulphate reduction (^{35}S-sulfate incubations), microbial abundance (via Catalysed Reporter Deposition Fluorescence In Situ Hybdridization = CARD-FISH), microbial diversity (via DNA/RNA analyses), lipid biomarker (composition and $d^{13}C$), carbonates (composition, U/Th dating, and $d^{13}C$) and macrofauna ($d^{13}C$). Bacterial nitrogen fixation was measured at some selected sites.

Besides sediments, also massive carbonates and animals (e.g. brittle stars, sponges, ascidians, clams, snails, and shrimps) were collected from seep sites by JAGO and preserved for analyses. Specifically carbonates were of major interest to estimate the age of seeps via U/Th dating. Animals will be analysed to test whether methane-derived carbon enters the food chain via methanotrophic biomass.

Table 5.7.1 Overview of benthic biogeochemical sampling

Station	Geochemistry	Methane oxidation / sulfate reduction	Nitrogen fixation	CARD-FISH	Biomarker	RNA/DNA	Anocix sediment	Carbonates	Animals
549-1									x
561-2	x	x		x	x	x			x
563-1	x	x	x	x	x	x		x	x
567-1	x	x		x	x	x			x
579-1	x			x					
585-1	x		x	x	x	x		x	x
587-1		x						x	
597-1	x	x		x	x	x		x	x
599-1		x	x					x	x
603-1	x								
605-1	x								
606-1	x								
611-1	x	x	x	x	x	x		x	x
620-1		x						x	x
629-1	x								
647-1	x			x	x	x			
648-3							x		
652-1	x								
657-1	x	x	x	x	x	x	x	x	
660-1	x								
661-1	x								

5.7.2 Preliminary results

Polarstern Site

The Polarstern Site was characterized by seeps with active gas bubble seepage featuring massive carbonate plates on the seafloor (Fig. 5.7.2). Carbonate plates appeared partly eroded, i.e. sediment was probably removed from the surface and below by currents thereby

sometimes creating a refuge for animals such as large fish and brittle stars. Sessile animals (e.g., clams, ascidians, and sponges) used carbonates as a hard substrates for settlement. Sediment sampling via push cores was impossible in this area due to the hard underground. Carbonates were sampled by JAGO for geochemical and biomarker analyses.

Fig. 5.7.2. Station 620-1. Top: Carbonate landscape of a gas seep at the Polarstern Site (Foto: JAGO). Bottom left: Carbonate sampled from the station. Bottom right: The same carbonate from a different perspective showing a large (gas?) channel that is penetrating the carbonate.

Hybis Site

The Hybis Site featured both eroded carbonate plates (Fig. 5.7.3) and sediments covered with chemoautotrophic communities (sulphur bacteria mats and pogonophoran fields, Fig. 5.7.3). Carbonate samples appeared rather porous and fragile compared to the massive carbonates from the Polarstern Site. Push cores taken at a field featuring both sulphur bacteria mats and pogonophorans revealed saturated methane concentrations (up to 1.3 mM), high sulphide concentrations (max. 5 mM) and an elevated TA profile (17 mEq L^{-1}) in the top 10 cm of the sediment.

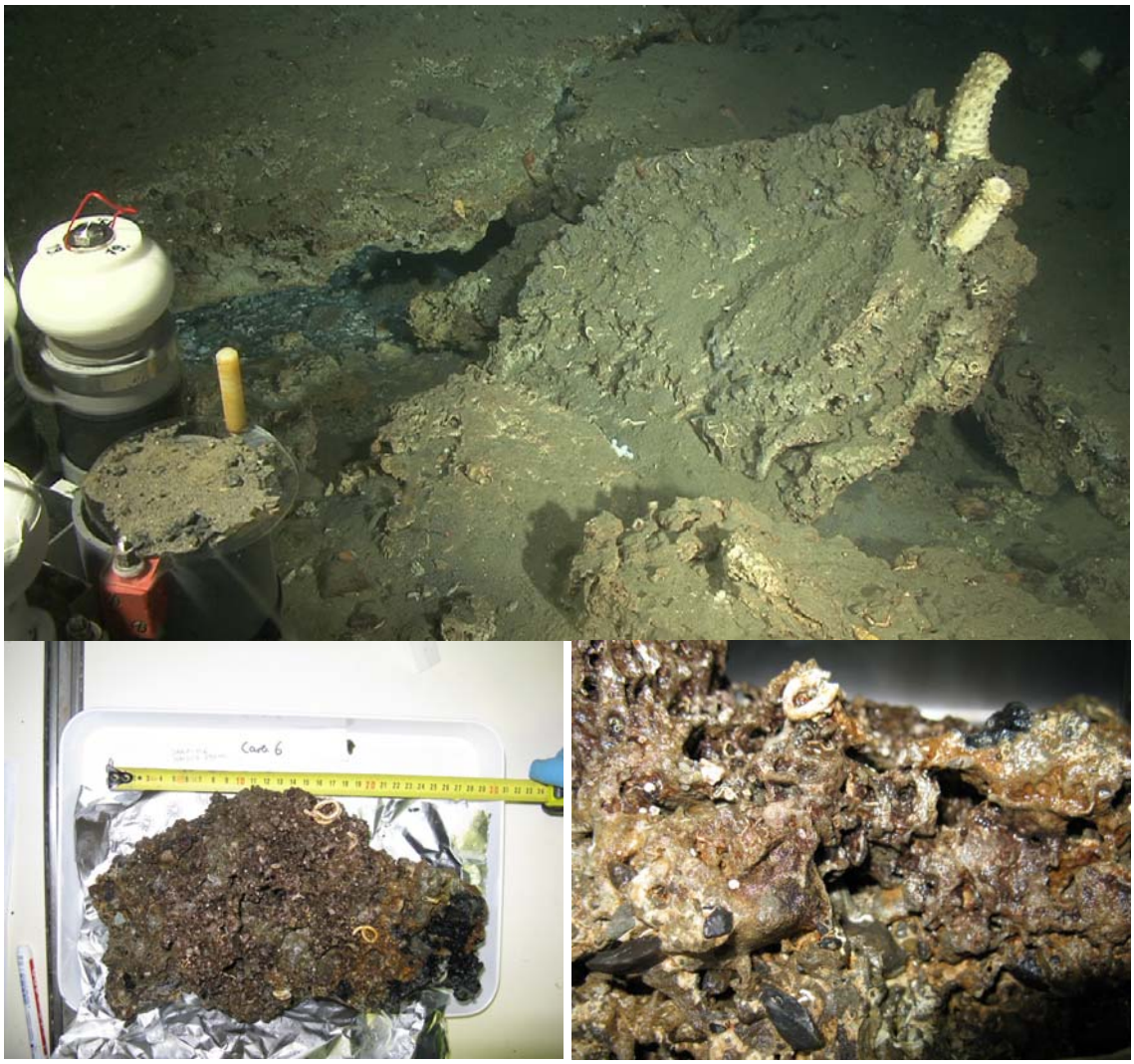

Fig. 5.7.3 Station 597-1. Top: Carbonate landscape of a gas seep at the Hybis Site (Foto: JAGO). Bottom left: Carbonate sampled from the station. Bottom right: Close-up of the carbonate showing porous branches and embedded gravels.

MASOX Site

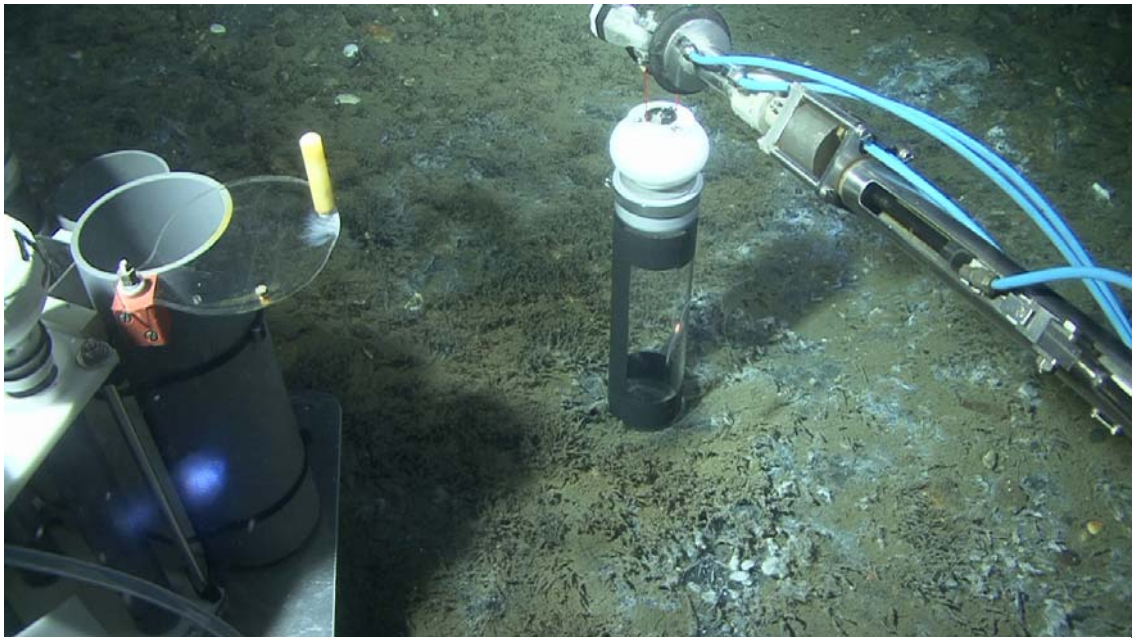

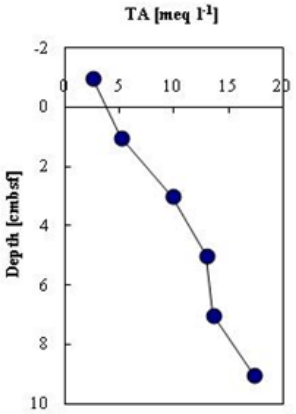

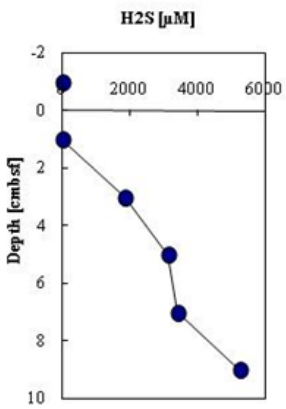

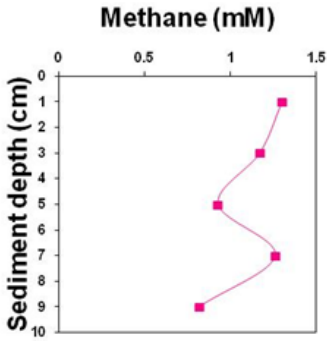

Fig. 5.7.4 Station 597-1. Top: Sulfur bacteria mat / pogonophoran field mixture sampled by a JAGO push core (Foto: JAGO). Middle: Core sampled for porewater extraction. Displayed are results of total alkalinity (TA) and sulphide (H_2S) measurements. Bottom: Core sampled for sediment solid phases. Displayed is the result of the methane measurement.

At the MASOX Site, several JAGO surveys could not confirm the presence of massive, eroded carbonate plates. Instead sediments were covered with patches of chemoautotrophic communities (sulphur bacteria mats, pogonophoran fields, and mixtures of both). Carbonates

were found only inside the sediment in the form of small nuggets or as a thin film covering gravels. Very interesting was the finding that filamentous sulphur bacteria often attached to pogonophoran tubes instead of covering sediment surfaces (Fig. 5.7.4). Porewater profiles did not reveal higher concentrations of sulphide in the top 10 cm. One possible explanation is that pogonophoran tubes channel sulphide from a deeper source to the sediment surface, where it can be utilized around the tube wall by the sulphur bacteria.

The deployment of the Peeper proto-types (re-build of a development by S. Dattagupta and co-workers) at the MASOX site was very successful. Eleven days deployment time appeared to be enough to equilibrate the seawater in the bags with the ambient sediment porewater. Geochemical data (here shown: sulphide) showed distinct differences from the seawater level (up to 11 mM compared to zero, Fig. 5.7.5). Replicates were very similar and profiles were consistent. Between habitats, a gradient was observed revealing decreasing sulphide (and TA; data not shown) levels from the sulphur bacteria mat to the pogonophoran field and to the gas vent (Fig. 5.6.6). Probably the gas vent was a younger seepage area compared to the other two habitats, since no chemoautotrophic communities were visible on the surface. Upon Peeper recovery new gas vents were created pointing to the accumulation of gas below the sediment surface.

After Peepers were removed, a gravity corer was deployed at the same site using the shipboard POSIDONIA system. A 210 cm long core was retrieved, which had a strong sulphide smell throughout the core. The core surface featured pogonophoran tubes. The top 60 cm of the core was very foamy (gassy) and crunchy (small carbonate nuggets). When sampling this section with syringes, the sediment released small bubbles. Preliminary analyses show a strong peak in methane (~2.5 mM) between 50-70 cm. Slightly above the methane peaking a peak in sulphide (11 mM) and TA (30 mEq L^{-1}) was detected. Interestingly, TA and sulphide increased again below ca. 100 cm. Methane concentration increased again slightly towards the end of the core (at 210 cm). The geochemical profiles suggest that the system at the core site was not in equilibrium. The cause of this disequilibrium is still a matter of debate, but seasonality of gas hydrate formation or a sudden increase in methane flux are possible explanations. Carbonate samples were collected over different depths of the core. In most layers carbonates were present in the form of small nuggets (Fig. 5.7.7). At the bottom of the core, carbonates acted like glue for empty snail shells, which were present in high abundance at this depth.

5.6.3 Summary and preliminary conclusions

- We were able to show that anaerobic oxidation of methane (AOM) is well established in the sediments of the shallow Svalbard methane seep area along and above the gas hydrate stability line and leads to sulphide accumulation and authigenic carbonate precipitation.
- We found that the methane seep area features chemoautotrophic communities (filamentous sulphur bacteria and pogonophoran) similar to deeper Arctic cold-seep systems (e.g. Haakon Mosby Mud Volcano, Vestnesa).
- We hypothesize from our preliminary observations that carbonates could be oldest at the Polarstern Site (245 m, massive eroded carbonate plates), followed by the Hybis Site (381 m, porous eroded carbonate plates), and youngest at the MASOX site (394 m, small nuggets of carbonates inside the sediment).
- From preliminary geochemical data we suggest that the MASOX site is currently out of equilibrium (double peaking in sulphide, alkalinity and methane), i.e. methane fluxes and the depth of the methane consumption zone must have changed dramatically in the past or are fluctuating. What caused this change is still unknown but will be further investigated at home (analyses of carbonates, pore water, and microbial activity).

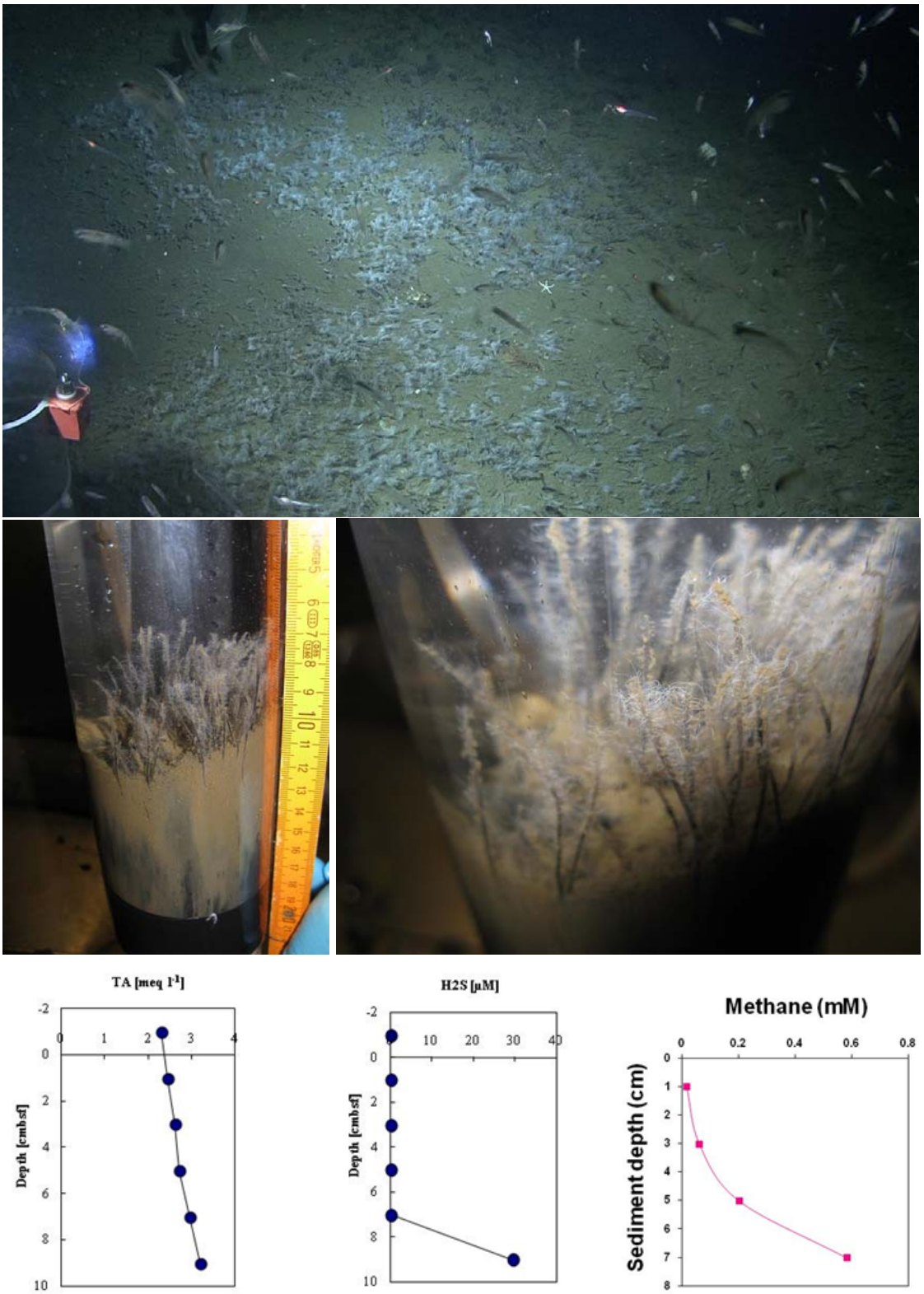

Fig. 5.7.5 Station 585-1. Top: Pogonophoran field with sulphur bacteria at the MASOX station. Middle: Core taken within the pogonophoran field and close-up showing sulphur bacteria attached to the pogonophoran tube walls. Bottom: Total alkalinity (TA), sulphide (H_2S) and methane profile from the pogonophoran field.

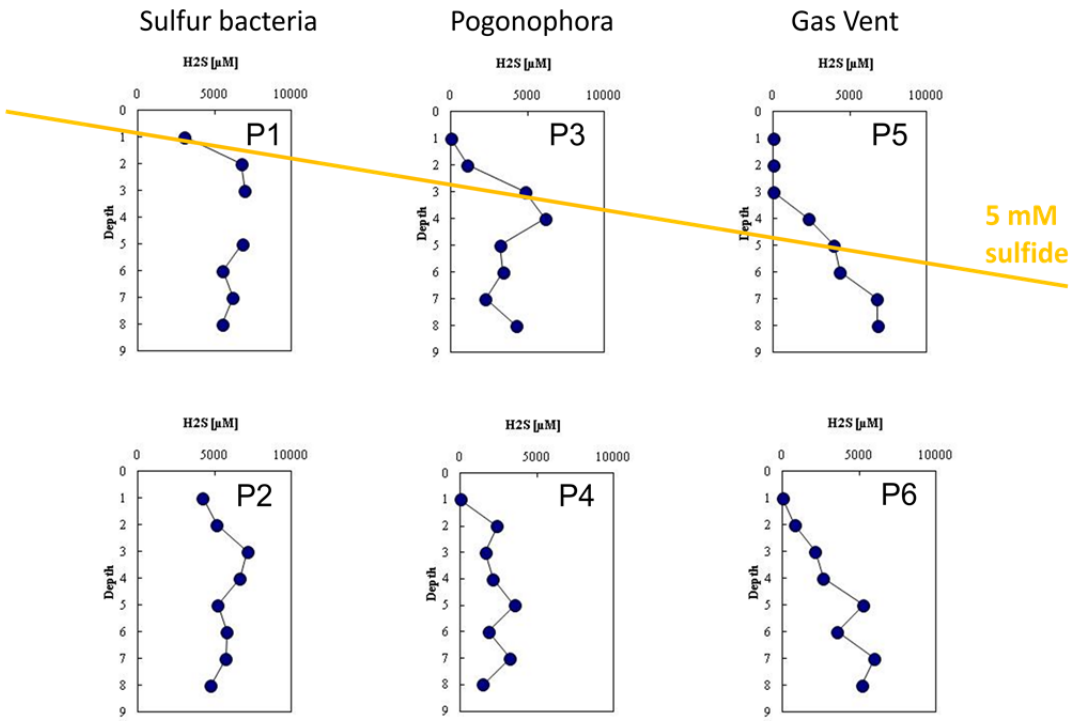

Fig. 5.7.6 Station 647-1. Sulfide profiles of Peeper 1-6. Peeper 1 and 2 were placed in a sulphur bacteria mat, Peeper 3 and 4 in a pogonophoran field, Peeper 5 and 6 in a gas vent. At the top profiles, a 5 mM line is drawn to illustrate the sulphide gradient between the three habitats.

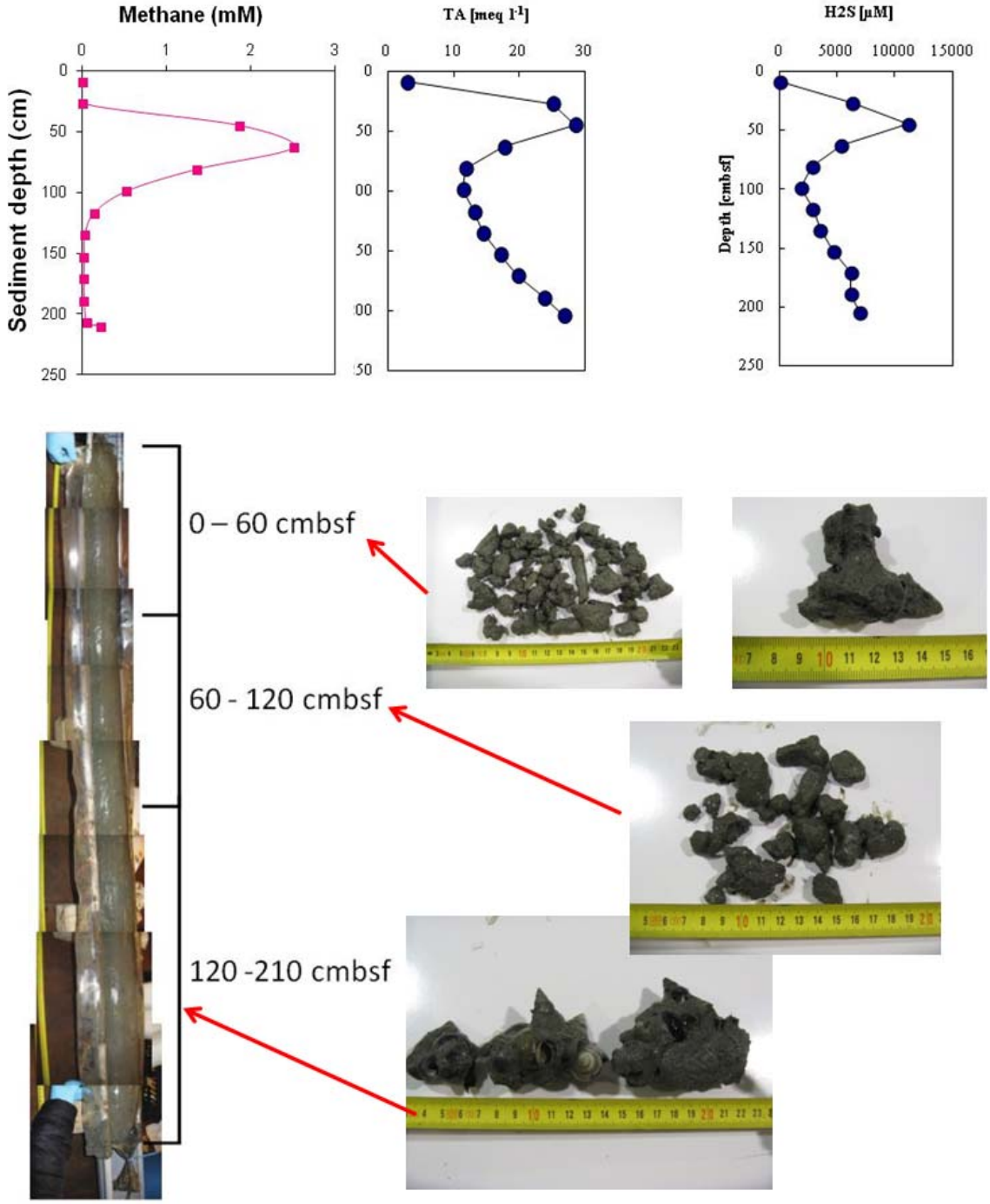

Fig. 5.7.7 Station 657-1. Gravity core from the Peeper site (MASOX area). Top: Profiles of methane, total alkalinity (TA) and sulphide (H_2S). Bottom: Carbonates collected from different depths of the core.

5.8 Water column biogeochemistry

(Helge Niemann)

5.8.1 Introduction

Large quantities of the greenhouse gas methane (CH4) are stored in sediments of continental margins, most importantly in the form of clathrate hydrate, which forms naturally when CH4 and water are subjected to low temperature (T) and high pressure (P). Typically, these conditions are met below 300 to 600 m water depth. An increase in bottom water T thus shifts the upper P/T boundary at which CH4 hydrates are stable towards greater water depth. Consequently, hydrate layers could then be exposed to P/T conditions where they become unstable. This leads to a liberation of CH4 into surface sediments, the overlying water column and, potentially, into the atmosphere where it further contributes to global warming. However, microbial CH4 oxidation may counteract this development. At present, most methane is retained in anoxic ocean sediments because it is oxidised by specialised archaea in consortium with sulphate reducing bacteria (Knittel and Boetius, 2009). In addition, aerobic bacteria in the water column have the potential to consume CH4 that has bypassed the benthic, microbial filter (Reeburgh 2007). However methane cycling in (aerobic) marine waters is not well constrained. Typically, the identity and distribution of methanotrophic communities within the water column have not been investigated in depth. Similarly, further research is needed to understand key physical, chemical and biological factors controlling the magnitude of microbial activity and CH4 transport to constrain CH4 budgets at cold seeps.

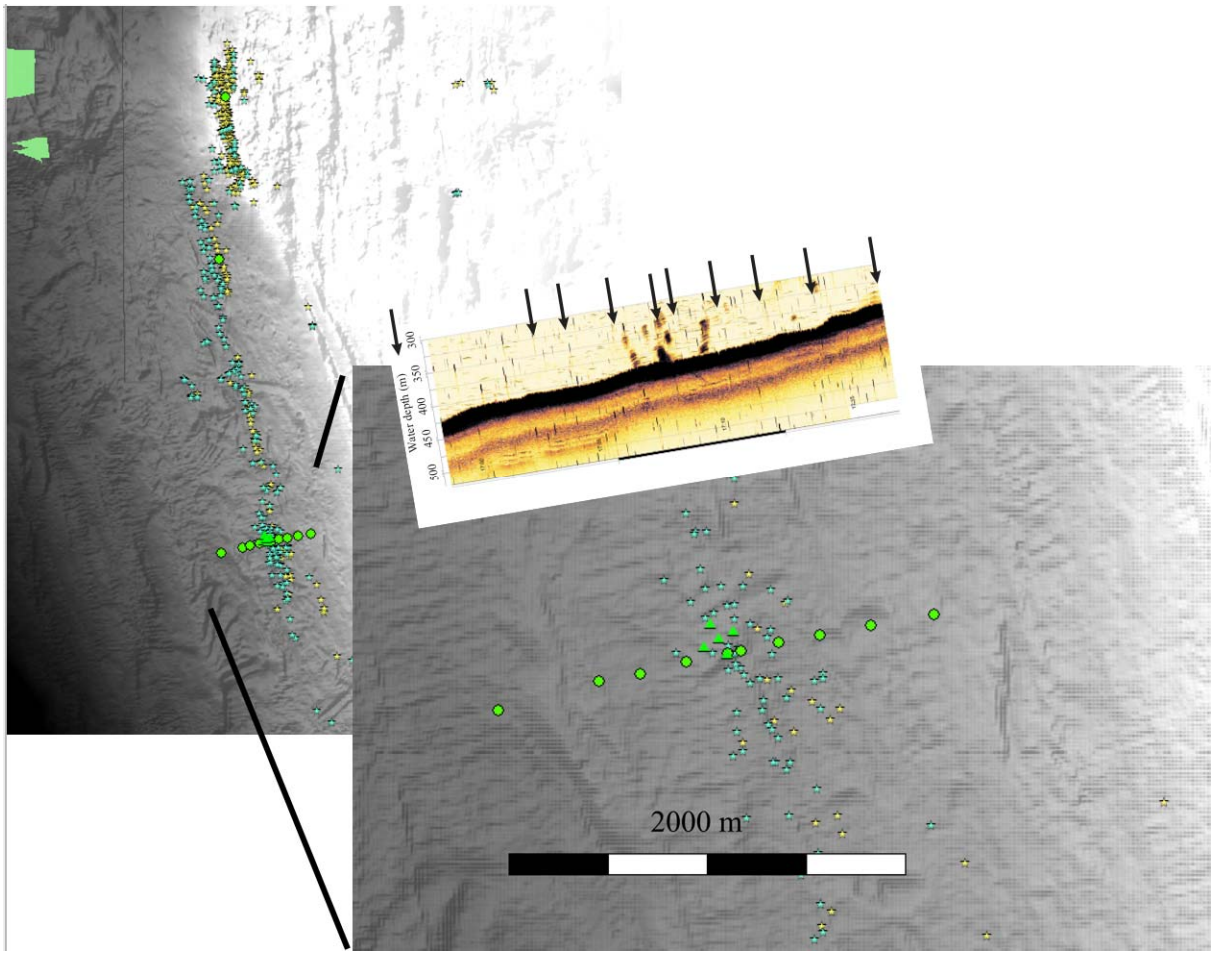

Fig. 5.8.1 Location of CTD casts (green dots and triangles) sampled during cruise MSM/21-4. Flare locations are highlighted as cyan and yellow stars. The sectional enlargement shows the position of the transect crossing the flare 'line'. Flares were imaged before transecting using PARASOUND.

The recently discovered efflux of CH4 from sedimentary sources, possibly destabilising gas hydrates, into the water column at the West Spitsbergen continental margin (Westbrook et al. 2009) provides a natural laboratory for studying water column methane cycling above relatively shallow CH4 sources (~ 300-400 m water depth), i.e. systems that can be expected to contribute to the atmospheric CH4 budget.

Our aims during cruise MSM/21-4 were to investigate water column methane cycling applying a combined biogeochemical-microbiological approach to determine magnitudes and controlling factors of CH4 fluxes and MOx activity.

5.8.2 Material and Methods

Analytical approach: We measured physical and chemical properties of sea water (conductivity, T, O2 content, fluorescence and backscatter) continuously using a CTD-device (Seabird SBE 9). The CTD was combined with a rosette sampler (24 × 10 l), which was used to collect seawater samples from discrete water depths. Water samples were analysed directly on board for hydrocarbon concentrations (gas chromatography with flame ionisation detection) and MOx activity (ex situ incubations with trace amounts of C3H4). Parallel incubations with 14CH4 were conducted, but these need further analysis in our home laboratories. Similarly, we also collected samples for determining stable isotope composition of hydrocarbons, concentrations of dissolved inorganic carbon (DIC) and macro nutrients (NO3-/NO2-, PO4-, SiO2) as well as for staining of microbial communities (fluorescence in situ hybridisation - FISH) and for lipid biomarker concentration and stable isotope composition measurements.

Sampling approach: To account for a potential spatio-temporal heterogeneity of the above described parameters, we sampled the water column at 10 cast stations along a transect crossing the the SE-NW ‘line’ of flares (Fig. 5.8.1) during two nights (Aug. 18th/19th and 30th/31st). We chose to sample the central part of the transect, i.e. at flare locations, more closely and increased the distance between cast stations towards the beginning and the end of the transect in order to maximise our chances for sampling hot spots of water column CH4 cycling. In addition to the entire transect, we also sampled the central station of the transect during two single casts (Aug. 28th and Sept. 4th) and as part of 5 casts closely spaced together in the vicinity of the central part of the transect (Aug. 23rd/24th; Fig. 5.8.1). Finally, we also sampled two other locations further NW of the transect on Sept 4th, one in the central part of the ‘line of flares at the edge of the hydrate stability zone and the second in comparably shallow waters on a plateau (Fig. 5.8.1). A reference station was sampled ~20 nm NE of the flare locations. However, high CH4 concentrations and MOx activity indicate seepage at this location, thus invalidating it as a reference site.

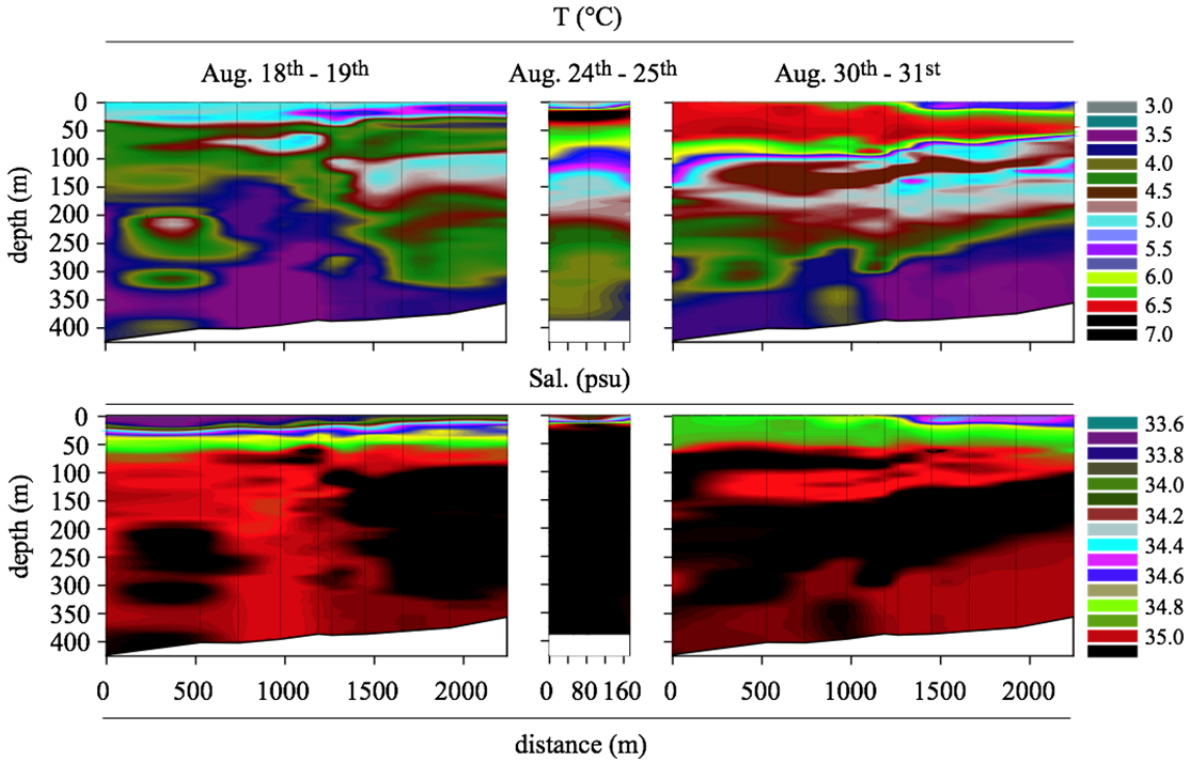

Fig. 5.8.2 2D-distribution of T and Sal. during the transect sampling campaigns (left and right pannels) and while sampling the central part of the transsect (middle panel; here cast stations corespond to the W-E aligned triangles in Fig. 5.8.1).

5.7.3 Preliminary results

CH_4 concentrations: highest CH_4 concentrations were typically found in the lowest ~100 m of the water column with maximum concentrations of about 500 nM, but more commonly ranging at ~100 nM (data not shown). During the time of our investigation, we could not find any obvious temporal variation in seep activity.

MOx activity: highest rates of MOx (~2 nM d-1) were found close to the sea floor (data not shown), similarly to methane concentrations. Yet, it appeared that the maximum of microbial activity was ~ 20 - 50 m above sea floor. Interestingly, we could find a very high spatiotemporal variation in microbial activity. While rates were high during one of sampling time periods, they seemed rather low during another. While this was independent of the CH_4 concentration, we believe that microbial activity was controlled by oceanographic effects, possibly related to the meandering of the West Spitsbergen current leading to the presence/absence of relative cold water masses.

Properties of sea water: Typically, water masses showed a strong spatiotemporal heterogeneity (Fig. 5.8.2). For instance, during the first transect sampling campaign, comparably cold water masses (<4°C) prevailed at the sea floor overlaid by warmer water masses (4-5°C). In contrast, when we sampled the middle of the transect again a few days later, bottom waters were up to 1°C- and surface water up to 2°C warmer indicating a stronger influence of the West Spitsbergen current during this time period. The second cast sampling campaign was again different with returned colder bottom waters but still relatively warm surface waters. Similar variations could be found for salinity (Fig. 5.8.2), O_2 contents and backscatter, while fluorescence was rather stable with a maximum at ~20 m water depth indicating a phytoplankton maximum at this water depth (data not shown).

5.9 Air Sampling for Methane Isotopic Analysis

(Carolyn Graves)

In the vicinity of the study area offshore western Svalbard, plumes of gas have been observed rising from the seabed, which lead to extremely high methane concentrations in bottom waters and super saturation of surface waters with respect to atmospheric equilibrium. Determining local atmospheric methane concentrations and further characterizing atmospheric methane by isotopic analysis represents the final stages of tracing the methane upwards from the sediments (e.g. Fisher et al, 2011). As atmospheric methane contributes to the greenhouse warming effect it is important to link concentration anomalies and isotopic signatures in sediments and seawater to atmospheric samples.

On behalf of Euan Nisbet (Royal Holloway University of London) we collected air samples from outside the bridge of the RV Merian daily, both at the study site and in transit from Iceland and into Germany. Samples were collected from the oncoming wind only when the ship was moving to avoid capturing ship emissions with samples. The samples will be analysed for methane concentration and carbon isotopic signature at Royal Holloway University of London by gas chromatography isotope ratio mass spectrometry.

5.10 Heat flow measurements

(Tomas Feseker)

5.10.1 System overview and deployments

In-situ measurements of sediment temperature and thermal conductivity were obtained using a standard violin-bow type heat flow probe, manufactured by FIELAX GmbH, Bremerhaven. The instrument is equipped with 22 temperature sensors distributed equally over an active length of 5.46 m. Measuring at a resolution of 0.0006 °C the sensors were calibrated to a precision of 0.002 °C. Additional sensors for acceleration, tilt, and water temperature help to control the measurements. All data can be transmitted from the probe to the winch control room in real time when using the ship's coax cable. Alternatively, the probe can also be operated in an autonomous mode when using a standard wire.

At each station, the sediment temperature profile was measured during the first 7 minutes after penetration. The equilibrium temperatures were obtained by extrapolation from the recorded time series (Villinger and Davis 1987). At selected stations, the thermal conductivity of the sediments was determined by measuring the decay of a heat pulse emitted from a heater wire along the entire active length of the probe following the initial temperature measurement. The sensor strings were calibrated at water depth greater than 1000 m.

Four heat flow measurements were obtained from stations at and near the Knipovich ridge. Within the working area on the upper slope of the western Svalbard margin, heat flow measurements were conducted along two transect lines across the upper limit of the gas hydrate stability zone (GHSZ) at the seafloor. The first transect line crosses the site of the MASOX lander that was recovered at the beginning of this cruise. Heat flow measurements were conducted at ten stations along the transect line at water depths of between 428 and 360 m, in alternation with CTD casts. These measurements were repeated at the exact same locations 12 days later. Seven additional measurements completed the transect down to 500 m water depth and filled gaps in between the ten main stations. The second transect line crosses the location of a flare site that was observed using HyBis during the JR253 cruise. This transect consists of seven stations at water depths of between 452 and 387 m.

In addition to the measurements using the winch-operated heat flow probe, a short temperature probe was operated by the submersible JAGO. The "T-Stick" consists of a lance

with 8 temperature sensors distributed equally over a length of 0.6 m and a data logger, which is attached to the upper part of the lance (Feseker et al. 2012). Resolution and precision of the temperature sensors are the same as for the heat flow probe. The T-Stick was deployed during JAGO dive deployed during dive 1184 and remained in the sediment next to geochemical probes (Peeper) in a bacterial mat for 10 days and recorded temperature readings from all eight sensors at a time interval of 10 seconds. It was recovered during JAGO dive 1192.

5.10.2 Preliminary results

Geothermal gradient between Knipovich Ridge and the upper slope of the western Svalbard margin

The heat flow measurements conducted between Knipovich Ridge and the upper slope of the western Svalbard margin indicated a geothermal gradient or around 0.15 °C/m close to the ridge axis (Fig. 5.10.1). Away from the ridge, the geothermal gradient decreased rapidly to below 0.08 °C/m within 10 km. At station 625-1, around 20 km from the ridge axis, a geothermal gradient of nearly 0.09 °C/m pointed to upward fluid flow focussed at faults.

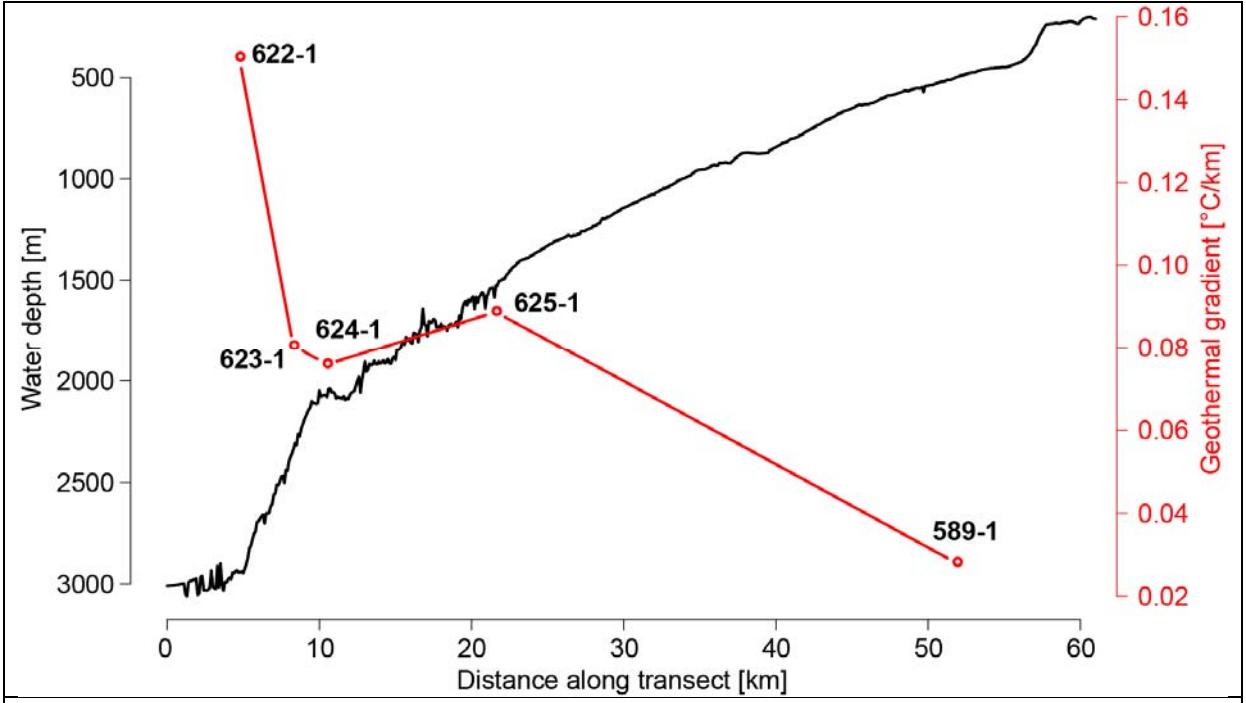

Fig. 5.10.1 Bathymetry and geothermal gradient between the Knipovich ridge and the upper slope of the western Svalbard margin. Labels indicate MSM-21 station numbers.

Sediment temperatures around the upper limit of the GHSZ at the seabed

The heat flow measurements conducted along the two transect lines on the upper slope of the western Svalbard margin all showed a strong influence of seasonal bottom water temperature changes (Fig. 5.10.2). Where sediment temperatures were near the dissociation temperature of pure methane hydrates (Tishchenko et al. 2005), the temperature profiles were non-linear with significant variations in temperature (Fig. 5.10.3). The differences between the results of repeated measurements at the same locations were significant. This unexpectedly high variability can be interpreted as the result of either strong heterogeneity over short distances, or as the result heat production and consumption by episodic hydrate formation and dissociation.

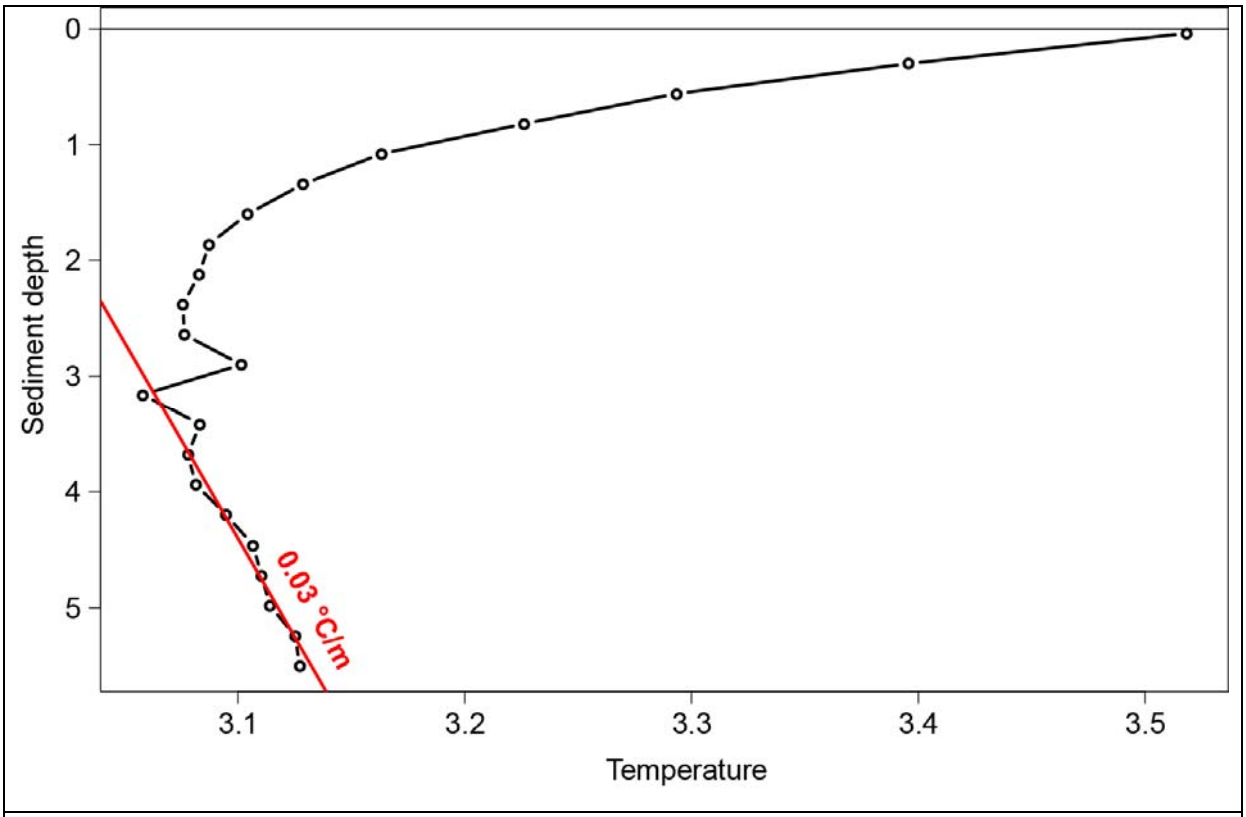

Fig. 5.10. In situ sediment temperature profile at station 589-1, located at 500 m water depth.

Bottom water and sediment temperature monitoring using the T-Stick

Placed on the edge of a bacterial mat near the position where the MASOX lander had been deployed, the T-Stick recorded bottom water and sediment temperatures for 10 days at an interval of 10 seconds. The T-Stick will be calibrated in the lab after the cruise, before the data can be interpreted.

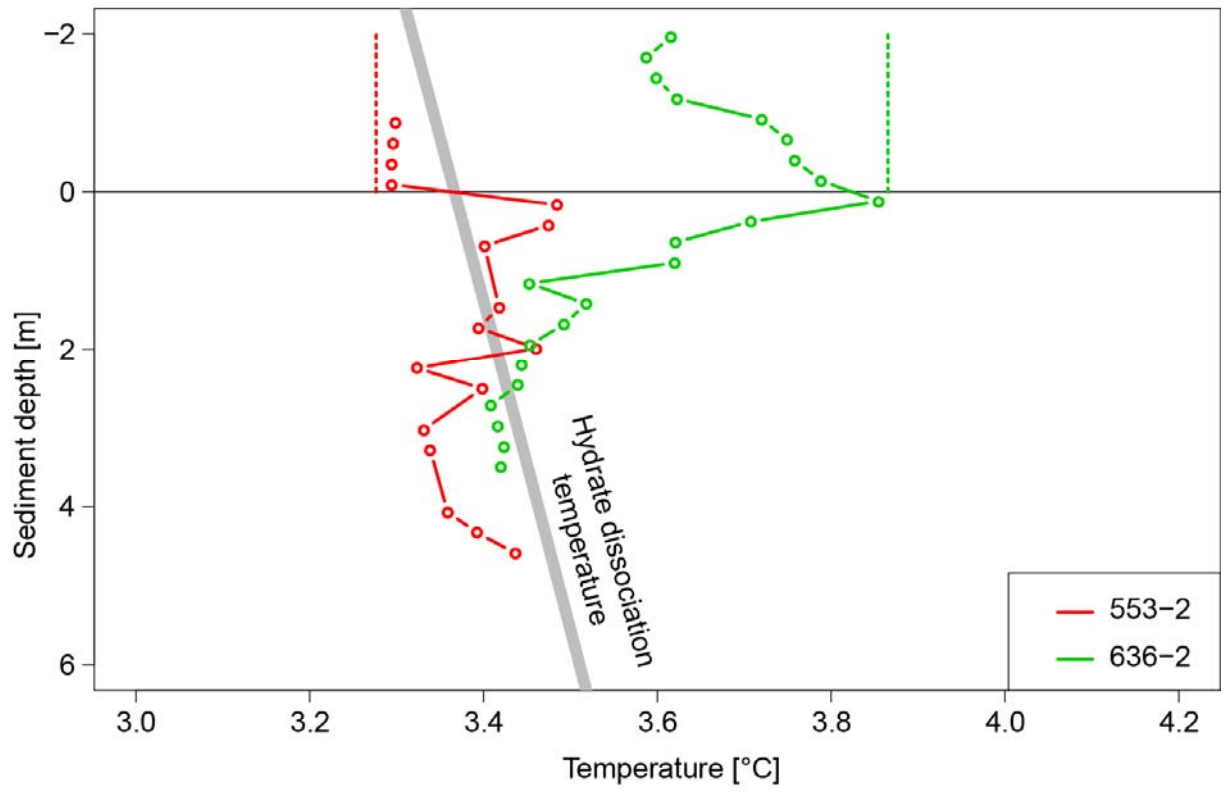

Fig. 5.10.3 In situ sediment temperature profiles at stations 553-2 and 636-2, located both at the same position at 402 m water depth, near the site of the MASOX lander. Dashed lines indicate bottom water temperature according the temperature sensor of in the head of the heat flow probe. Bottom water temperature changes episodically shift the sediment at this location into and out of the GHSZ.

6 Ship`s Meteorological Station

(Christian Berndt)

During the voyage the weather conditions were quite variable and worse than expected. While the transit from Iceland was made in calm weather, a low pressure system over the southern Barents Sea that slowly moved north controlled the weather during the entire time off Svalbard from 17.8. to 4.9. Thus, we were able to start the work program in calm seas and clear skies, while towards the beginning of September we continuously had more than Bf 5 often 7 with gusts up to 9. Fortunately, on September 3 the centre of the low pressure had moved right into the study area giving us a few hours of force 3-4. During this time we were able to carry out the last JAGO dive to retrieve the seafloor equipment. The transit back to Germany was characterized by a series of three low pressure systems (975-990 hPa) that caused high winds and hampered sediment coring on the Vøring Plateau. Temperatures off Svalbard were 0-7 degrees with frequent showers and snow.

7 Station List MSM21/4

Event label	Event	Time [UTC]	Latitude [N°]	Longitude [E°]	Water depth [mbsl]	Gear	Description	Remarks
MSM21/4-0544-1	HF 1	2012-08-17 04:37:00.0	78°37.00’	7°24.00’	1441.2	Heat Flow | HF	Heat Flow (calibration)	surface
MSM21/4-0544-1	HF 1	2012-08-17 04:45:00.0	78°37.00’	7°24.01’	1438	Heat Flow | HF	Heat Flow (calibration)	at 10 m
MSM21/4-0544-1	HF 1	2012-08-17 05:09:00.0	78°37.00’	7°24.00’	1439.5	Heat Flow | HF	Heat Flow (calibration)	at the bottom
MSM21/4-0544-1	HF 1	2012-08-17 05:45:00.0	78°37.00’	7°24.00’	1444	Heat Flow | HF	Heat Flow (calibration)	on deck
MSM21/4-0544-2	CTD 1	2012-08-17 05:56:00.0	78°37.00’	7°24.00’	1434.8	Conductivity Temperature Depth Probe with rosette watersampler | CTD/Ros	CTD/rosette water sampler	surface
MSM21/4-0544-2	CTD 1	2012-08-17 06:19:00.0	78°37.00’	7°24.01’	1438.8	Conductivity Temperature Depth Probe with rosette watersampler | CTD/Ros	CTD/rosette water sampler	at depth, SL max. 1300 m
MSM21/4-0544-2	CTD 1	2012-08-17 06:45:00.0	78°37.00’	7°24.01’	1439.6	Conductivity Temperature Depth Probe with rosette watersampler | CTD/Ros	CTD/rosette water sampler	on deck
MSM21/4-0545-1	Survey S01	2012-08-17 08:09:00.0	78°36.93’	7°26.60’	1389.6	Deep-Sea Multibeam Echosounder | EM120	Deep-Sea Multibeam Echosounder	start of survey
MSM21/4-0545-1	Survey S01	2012-08-17 10:40:00.0	78°33.33’	9°28.60’	3993.1	Deep-Sea Multibeam Echosounder | EM120	Deep-Sea Multibeam Echosounder	end of survey
MSM21/4-0546-1	CTD 2	2012-08-17 10:59:00.0	78°33.33’	9°28.62’	392.1	Conductivity Temperature Depth Probe with rosette watersampler | CTD/Ros	CTD/rosette water sampler	surface
MSM21/4-0546-1	CTD 2	2012-08-17 11:09:00.0	78°33.34’	9°28.62’	392.1	Conductivity Temperature Depth Probe with rosette watersampler | CTD/Ros	CTD/rosette water sampler	at depth, SL max. 360 m
MSM21/4-0546-1	CTD 2	2012-08-17 11:25:00.0	78°33.33’	9°28.62’	392	Conductivity Temperature Depth Probe with rosette watersampler | CTD/Ros	CTD/rosette water sampler	on deck
MSM21/4-0546-2	CTD 3	2012-08-17 12:22:00.0	78°33.31’	9°28.64’	392	Conductivity Temperature Depth Probe with rosette watersampler | CTD/Ros	CTD/rosette water sampler	surface
MSM21/4-0546-2	CTD 3	2012-08-17 12:26:00.0	78°33.31’	9°28.63’	389.6	Conductivity Temperature Depth Probe with rosette watersampler | CTD/Ros	CTD/rosette water sampler	at depth, SL max. 100 m
MSM21/4-0546-2	CTD 3	2012-08-17 14:22:00.0	78°33.31’	9°28.64’	390.8	Conductivity Temperature Depth Probe with rosette watersampler | CTD/Ros	CTD/rosette water sampler	on deck
MSM21/4-0547-1	JAGO test	2012-08-17 14:48:00.0	78°33.31’	9°28.64’	390.1	JAGO	JAGO Underwater Craft	JAGO to surface
MSM21/4-0547-1	JAGO test	2012-08-17 14:50:00.0	78°33.31’	9°28.64’	390.8	JAGO	JAGO Underwater Craft	towed by boat

Event label	Event	Time [UTC]	Latitude [N°]	Longitude [E°]	Water depth [mbsl]	Gear	Description	Remarks
MSM21/ 4-0547-1	JAGO test	2012-08-17 15:00:00.0	78°33.31’	9°28.63’	390.3	JAGO	JAGO Underwater Craft	connected to hook
MSM21/ 4-0547-1	JAGO test	2012-08-17 15:07:00.0	78°33.31’	9°28.63’	391.3	JAGO	JAGO Underwater Craft	JAGO back on board
MSM21/ 4-0548-1	Seismic profile P100	2012-08-17 19:32:00.0	78°31.19’	9°46.16’	365.5	2D-Multi-Channel-Seismic | 2D-MCS	Seismic reflection profile	end deployment
MSM21/ 4-0548-1	Seismic profile P100	2012-08-17 20:16:00.0	78°32.68’	9°40.92’	196.7	2D-Multi-Channel-Seismic | 2D-MCS	Seismic reflection profile	start of profile
MSM21/ 4-0548-1	Seismic profile P101	2012-08-18 01:55:00.0	78°42.39’	7°30.51’	1139.9	2D-Multi-Channel-Seismic | 2D-MCS	Seismic reflection profile	end of profile
MSM21/ 4-0548-1	Seismic profile P100	2012-08-18 01:55:00.0	78°42.39’	7°30.51’	1139.9	2D-Multi-Channel-Seismic | 2D-MCS	Seismic reflection profile	start of profile
MSM21/ 4-0548-1	Seismic profile P101	2012-08-18 04:30:00.0	78°30.78’	7°02.55’	2971.9	2D-Multi-Channel-Seismic | 2D-MCS	Seismic reflection profile	end of profile
MSM21/ 4-0548-1	Seismic profile P102	2012-08-18 04:30:00.0	78°30.78’	7°02.55’	2971.9	2D-Multi-Channel-Seismic | 2D-MCS	Seismic reflection profile	start of profile
MSM21/ 4-0548-1	Seismic profile P102	2012-08-18 08:15:00.0	78°35.64’	8°28.64’	909.8	2D-Multi-Channel-Seismic | 2D-MCS	Seismic reflection profile	end of profile
MSM21/ 4-0548-1	Survey S02	2012-08-18 08:15:00.0	78°35.64’	8°28.64’	907.3	Multibeam + Parasound | MB-PS	Multibeam and ParaSound	start of survey
MSM21/ 4-0548-1	Seismic profile P102	2012-08-18 08:35:00.0	78°36.14’	8°30.18’	882	2D-Multi-Channel-Seismic | 2D-MCS	Seismic reflection profile	end recovery
MSM21/ 4-0549-1	JAGO dive 01	2012-08-18 10:21:00.0	78°33.30’	9°28.58’		JAGO	JAGO Underwater Craft	recovery hook to water
MSM21/ 4-0549-1	JAGO dive 01	2012-08-18 11:18:00.0	78°33.30’	9°28.58’		JAGO	JAGO Underwater Craft	recovery hook at depth
MSM21/ 4-0548-1	Survey S02	2012-08-18 11:20:00.0	78°33.30’	9°28.58’		Multibeam + Parasound | MB-PS	Multibeam and ParaSound	end of survey
MSM21/ 4-0549-1	JAGO dive 01	2012-08-18 11:44:00.0	78°33.30’	9°28.58’		JAGO	JAGO Underwater Craft	JAGO to surface
MSM21/ 4-0549-1	JAGO dive 01	2012-08-18 12:00:00.0	78°33.30’	9°28.58’		JAGO	JAGO Underwater Craft	submerged
MSM21/ 4-0549-1	JAGO dive 01	2012-08-18 13:40:00.0	78°33.29’	9°28.61’		JAGO	JAGO Underwater Craft	hook connected to lander
MSM21/ 4-0549-1	JAGO dive 01	2012-08-18 14:04:00.0	78°33.29’	9°28.61’		JAGO	JAGO Underwater Craft	start hieving

Event label	Event	Time [UTC]	Latitude [N°]	Longitude [E°]	Water depth [mbsl]	Gear	Description	Remarks
MSM21/ 4-0549-1	JAGO dive 01	2012-08-18 15:45:00.0	78°33.30’	9°28.60’		JAGO	JAGO Underwater Craft	JAGO at surface
MSM21/ 4-0549-1	JAGO dive 01	2012-08-18 15:48:00.0	78°33.30’	9°28.60’		JAGO	JAGO Underwater Craft	connected to hook
MSM21/ 4-0549-1	JAGO dive 01	2012-08-18 15:58:00.0	78°33.30’	9°28.60’		JAGO	JAGO Underwater Craft	on deck
MSM21/ 4-0549-1	JAGO dive 01	2012-08-18 16:24:00.0	78°33.30’	9°28.60’		JAGO	JAGO Underwater Craft	Lander on deck
MSM21/ 4-0549-2	Survey S03	2012-08-18 16:56:00.0	78°33.16’	9°25.36’	424.7	Multibeam + Parasound | MB-PS	Multibeam and ParaSound	start of survey
MSM21/ 4-0549-2	Survey S03	2012-08-18 17:18:00.0	78°33.42’	9°31.74’	353.9	Multibeam + Parasound | MB-PS	Multibeam and ParaSound	profile break
MSM21/ 4-0549-2	Survey S03	2012-08-18 17:38:00.0	78°33.40’	9°32.02’	348.2	Multibeam + Parasound | MB-PS	Multibeam and ParaSound	alter course
MSM21/ 4-0549-2	Survey S03	2012-08-18 17:48:00.0	78°32.67’	9°29.91’	393.1	Multibeam + Parasound | MB-PS	Multibeam and ParaSound	continue survey
MSM21/ 4-0549-2	Survey S03	2012-08-18 18:08:00.0	78°33.85’	9°27.31’	397.7	Multibeam + Parasound | MB-PS	Multibeam and ParaSound	end of survey
MSM21/ 4-0550-1	CTD 4	2012-08-18 18:51:00.0	78°33.15’	9°25.41’	427.9	Conductivity Temperature Depth Probe with rosette watersampler | CTD/Ros	CTD/rosette water sampler	surface
MSM21/ 4-0550-1	CTD 4	2012-08-18 19:02:00.0	78°33.15’	9°25.42’	425.7	Conductivity Temperature Depth Probe with rosette watersampler | CTD/Ros	CTD/rosette water sampler	at depth, SL max. 423 m
MSM21/ 4-0550-1	CTD 4	2012-08-18 19:16:00.0	78°33.15’	9°25.42’	426	Conductivity Temperature Depth Probe with rosette watersampler | CTD/Ros	CTD/rosette water sampler	on deck
MSM21/ 4-0550-2	HF 2	2012-08-18 19:31:00.0	78°33.15’	9°25.42’	425.5	Heat Flow | HF	Heat Flow	surface
MSM21/ 4-0550-2	HF 2	2012-08-18 19:48:00.0	78°33.15’	9°25.42’	425.3	Heat Flow | HF	Heat Flow	at the bottom
MSM21/ 4-0550-2	HF 2	2012-08-18 20:30:00.0	78°33.15’	9°25.42’	425.2	Heat Flow | HF	Heat Flow	on deck
MSM21/ 4-0551-1	CTD 5	2012-08-18 21:05:00.0	78°33.24’	9°26.75’	404.6	Conductivity Temperature Depth Probe with rosette watersampler | CTD/Ros	CTD/rosette water sampler	surface
MSM21/ 4-0551-1	CTD 5	2012-08-18 21:14:00.0	78°33.24’	9°26.75’	404.1	Conductivity Temperature Depth Probe with rosette watersampler | CTD/Ros	CTD/rosette water sampler	at depth
MSM21/ 4-0551-1	CTD 5	2012-08-18 21:29:00.0	78°33.24’	9°26.75’	405.3	Conductivity Temperature Depth Probe with rosette watersampler | CTD/Ros	CTD/rosette water sampler	on deck

Event label	Event	Time [UTC]	Latitude [N°]	Longitude [E°]	Water depth [mbsl]	Gear	Description	Remarks
MSM21/ 4-0551-2	HF 3	2012-08-18 21:43:00.0	78°33.23’	9°26.75’	403.9	Heat Flow | HF	Heat Flow	surface
MSM21/ 4-0551-2	HF 3	2012-08-18 21:56:00.0	78°33.24’	9°26.75’	405	Heat Flow | HF	Heat Flow	at the bottom
MSM21/ 4-0551-2	HF 3	2012-08-18 22:23:00.0	78°33.24’	9°26.75’	404.5	Heat Flow | HF	Heat Flow	on deck
MSM21/ 4-0552-1	CTD 6	2012-08-18 22:41:00.0	78°33.26’	9°27.32’	404.2	Conductivity Temperature Depth Probe with rosette watersampler | CTD/Ros	CTD/rosette water sampler	surface
MSM21/ 4-0552-1	CTD 6	2012-08-18 22:52:00.0	78°33.26’	9°27.32’	404.6	Conductivity Temperature Depth Probe with rosette watersampler | CTD/Ros	CTD/rosette water sampler	at depth, SL max. 403 m
MSM21/ 4-0552-1	CTD 6	2012-08-18 23:03:00.0	78°33.26’	9°27.32’	404.5	Conductivity Temperature Depth Probe with rosette watersampler | CTD/Ros	CTD/rosette water sampler	on deck
MSM21/ 4-0552-2	HF 4	2012-08-18 23:08:00.0	78°33.26’	9°27.32’	404.5	Heat Flow | HF	Heat Flow	surface
MSM21/ 4-0552-2	HF 4	2012-08-18 23:15:00.0	78°33.26’	9°27.31’	404.5	Heat Flow | HF	Heat Flow	at the bottom
MSM21/ 4-0552-2	HF 4	2012-08-18 23:39:00.0	78°33.26’	9°27.32’	404.9	Heat Flow | HF	Heat Flow	on deck
MSM21/ 4-0553-1	CTD 7	2012-08-18 23:56:00.0	78°33.29’	9°27.94’	396.5	Conductivity Temperature Depth Probe with rosette watersampler | CTD/Ros	CTD/rosette water sampler	surface
MSM21/ 4-0553-1	CTD 7	2012-08-19 00:05:00.0	78°33.29’	9°27.94’	397	Conductivity Temperature Depth Probe with rosette watersampler | CTD/Ros	CTD/rosette water sampler	at depth, SL max. 396 m
MSM21/ 4-0553-1	CTD 7	2012-08-19 00:08:00.0	78°33.29’	9°27.94’	395.6	Conductivity Temperature Depth Probe with rosette watersampler | CTD/Ros	CTD/rosette water sampler	on deck
MSM21/ 4-0553-2	HF 5	2012-08-19 00:25:00.0	78°33.28’	9°27.99’	399.2	Heat Flow | HF	Heat Flow	surface
MSM21/ 4-0553-2	HF 5	2012-08-19 00:29:00.0	78°33.28’	9°27.99’	399.1	Heat Flow | HF	Heat Flow	at the bottom
MSM21/ 4-0553-2	HF 5	2012-08-19 00:32:00.0	78°33.28’	9°27.98’	399.6	Heat Flow | HF	Heat Flow	on deck
MSM21/ 4-0554-1	CTD 8	2012-08-19 01:21:00.0	78°33.30’	9°28.53’	389.4	Conductivity Temperature Depth Probe with rosette watersampler | CTD/Ros	CTD/rosette water sampler	surface
MSM21/ 4-0554-1	CTD 8	2012-08-19 01:25:00.0	78°33.30’	9°28.55’	390	Conductivity Temperature Depth Probe with rosette watersampler | CTD/Ros	CTD/rosette water sampler	at depth, SL max. 387 m
MSM21/ 4-0554-1	CTD 8	2012-08-19 01:35:00.0	78°33.30’	9°28.55’	390.4	Conductivity Temperature Depth Probe with rosette watersampler | CTD/Ros	CTD/rosette water sampler	on deck

Event label	Event	Time [UTC]	Latitude [N°]	Longitude [E°]	Water depth [mbsl]	Gear	Description	Remarks
MSM21/ 4-0554-2	HF 6	2012-08-19 01:39:00.0	78°33.30’	9°28.55’	389.8	Heat Flow | HF	Heat Flow	surface
MSM21/ 4-0554-2	HF 6	2012-08-19 01:46:00.0	78°33.30’	9°28.55’	389	Heat Flow | HF	Heat Flow	at the bottom
MSM21/ 4-0554-2	HF 6	2012-08-19 02:07:00.0	78°33.30’	9°28.61’	389.6	Heat Flow | HF	Heat Flow	on deck
MSM21/ 4-0555-1	CTD 9	2012-08-19 02:27:00.0	78°33.32’	9°28.69’	394.4	Conductivity Temperature Depth Probe with rosette watersampler | CTD/Ros	CTD/rosette water sampler	surface
MSM21/ 4-0555-1	CTD 9	2012-08-19 02:36:00.0	78°33.31’	9°28.73’	392.9	Conductivity Temperature Depth Probe with rosette watersampler | CTD/Ros	CTD/rosette water sampler	at depth, SL max. 389 m
MSM21/ 4-0555-1	CTD 9	2012-08-19 02:46:00.0	78°33.31’	9°28.73’	392.9	Conductivity Temperature Depth Probe with rosette watersampler | CTD/Ros	CTD/rosette water sampler	on deck
MSM21/ 4-0555-2	HF 7	2012-08-19 02:52:00.0	78°33.31’	9°28.73’	392.9	Heat Flow | HF	Heat Flow	surface
MSM21/ 4-0555-2	HF 7	2012-08-19 03:02:00.0	78°33.31’	9°28.73’	394.6	Heat Flow | HF	Heat Flow	at the bottom
MSM21/ 4-0555-2	HF 7	2012-08-19 03:22:00.0	78°33.31’	9°28.75’	392.8	Heat Flow | HF	Heat Flow	on deck
MSM21/ 4-0556-1	CTD 10	2012-08-19 03:44:00.0	78°33.33’	9°29.23’	389.2	Conductivity Temperature Depth Probe with rosette watersampler | CTD/Ros	CTD/rosette water sampler	surface
MSM21/ 4-0556-1	CTD 10	2012-08-19 03:52:00.0	78°33.33’	9°29.23’	389.2	Conductivity Temperature Depth Probe with rosette watersampler | CTD/Ros	CTD/rosette water sampler	at depth, SL max. 386 m
MSM21/ 4-0556-1	CTD 10	2012-08-19 04:03:00.0	78°33.33’	9°29.23’	388.8	Conductivity Temperature Depth Probe with rosette watersampler | CTD/Ros	CTD/rosette water sampler	on deck
MSM21/ 4-0556-2	HF 8	2012-08-19 04:05:00.0	78°33.33’	9°29.26’	388.6	Heat Flow | HF	Heat Flow	surface
MSM21/ 4-0556-2	HF 8	2012-08-19 04:15:00.0	78°33.33’	9°29.26’	388.8	Heat Flow | HF	Heat Flow	at the bottom
MSM21/ 4-0556-2	HF 8	2012-08-19 04:38:00.0	78°33.33’	9°29.26’	388.5	Heat Flow | HF	Heat Flow	on deck
MSM21/ 4-0557-1	CTD 11	2012-08-19 05:01:00.0	78°33.35’	9°29.83’	384	Conductivity Temperature Depth Probe with rosette watersampler | CTD/Ros	CTD/rosette water sampler	surface
MSM21/ 4-0557-1	CTD 11	2012-08-19 05:09:00.0	78°33.35’	9°29.83’	383.6	Conductivity Temperature Depth Probe with rosette watersampler | CTD/Ros	CTD/rosette water sampler	at depth, SL max. 381 m
MSM21/ 4-0557-1	CTD 11	2012-08-19 05:20:00.0	78°33.35’	9°29.83’	383.9	Conductivity Temperature Depth Probe with rosette watersampler | CTD/Ros	CTD/rosette water sampler	on deck

Event label	Event	Time [UTC]	Latitude [N°]	Longitude [E°]	Water depth [mbsl]	Gear	Description	Remarks
MSM21/ 4-0557-2	HF 9	2012-08-19 05:26:00.0	78°33.35’	9°29.83’	386.9	Heat Flow | HF	Heat Flow	surface
MSM21/ 4-0557-2	HF 9	2012-08-19 05:32:00.0	78°33.35’	9°29.83’	387	Heat Flow | HF	Heat Flow	at the bottom
MSM21/ 4-0557-2	HF 9	2012-08-19 05:56:00.0	78°33.35’	9°29.83’	383.8	Heat Flow | HF	Heat Flow	on deck
MSM21/ 4-0558-1	CTD 12	2012-08-19 06:14:00.0	78°33.38’	9°30.54’	377	Conductivity Temperature Depth Probe with rosette watersampler | CTD/Ros	CTD/rosette water sampler	surface
MSM21/ 4-0558-1	CTD 12	2012-08-19 06:22:00.0	78°33.38’	9°30.54’	377.6	Conductivity Temperature Depth Probe with rosette watersampler | CTD/Ros	CTD/rosette water sampler	at depth, SL max. 375 m
MSM21/ 4-0558-1	CTD 12	2012-08-19 06:32:00.0	78°33.38’	9°30.53’	377.1	Conductivity Temperature Depth Probe with rosette watersampler | CTD/Ros	CTD/rosette water sampler	on deck
MSM21/ 4-0558-2	HF 10	2012-08-19 06:36:00.0	78°33.38’	9°30.53’	376	Heat Flow | HF	Heat Flow	surface
MSM21/ 4-0558-2	HF 10	2012-08-19 06:42:00.0	78°33.38’	9°30.54’	374.1	Heat Flow | HF	Heat Flow	at the bottom
MSM21/ 4-0558-2	HF 10	2012-08-19 07:06:00.0	78°33.38’	9°30.54’	376.5	Heat Flow | HF	Heat Flow	on deck
MSM21/ 4-0559-1	CTD 13	2012-08-19 07:24:00.0	78°33.40’	9°31.40’	358.1	Conductivity Temperature Depth Probe with rosette watersampler | CTD/Ros	CTD/rosette water sampler	surface
MSM21/ 4-0559-1	CTD 13	2012-08-19 07:32:00.0	78°33.40’	9°31.39’	358.4	Conductivity Temperature Depth Probe with rosette watersampler | CTD/Ros	CTD/rosette water sampler	at depth, SL max. 355 m
MSM21/ 4-0559-1	CTD 13	2012-08-19 07:44:00.0	78°33.40’	9°31.39’	358.4	Conductivity Temperature Depth Probe with rosette watersampler | CTD/Ros	CTD/rosette water sampler	on deck
MSM21/ 4-0559-2	HF 11	2012-08-19 07:49:00.0	78°33.40’	9°31.39’	358.2	Heat Flow | HF	Heat Flow	surface
MSM21/ 4-0559-2	HF 11	2012-08-19 07:55:00.0	78°33.40’	9°31.39’	358.8	Heat Flow | HF	Heat Flow	at the bottom
MSM21/ 4-0559-2	HF 11	2012-08-19 08:25:00.0	78°33.41’	9°31.39’	358.8	Heat Flow | HF	Heat Flow	on deck
MSM21/ 4-0560-1	Survey S04	2012-08-19 09:49:00.0	78°33.42’	9°31.53’		Multibeam + Parasound | MB-PS	Multibeam and ParaSound	start of survey
MSM21/ 4-0560-1	Survey S04	2012-08-19 14:00:00.0	78°33.58’	9°33.85’	296.4	Multibeam + Parasound | MB-PS	Multibeam and ParaSound	end of survey
MSM21/ 4-0561-1	Gravity core 01	2012-08-19 14:33:00.0	78°33.28’	9°28.00’	396.1	Gravity Corer | GC	Gravity corer	surface

Event label	Event	Time [UTC]	Latitude [N°]	Longitude [E°]	Water depth [mbsl]	Gear	Description	Remarks
MSM21/ 4-0561-1	Gravity core 01	2012-08-19 14:42:00.0	78°33.28’	9°27.99’	396.1	Gravity Corer | GC	Gravity corer	at sea bottom
MSM21/ 4-0561-1	Gravity core 01	2012-08-19 14:54:00.0	78°33.28’	9°27.98’	397.1	Gravity Corer | GC	Gravity corer	on deck
MSM21/ 4-0561-2	Gravity core 02	2012-08-19 15:18:00.0	78°33.28’	9°28.00’	396.5	Gravity Corer | GC	Gravity corer	surface
MSM21/ 4-0561-2	Gravity core 02	2012-08-19 15:24:00.0	78°33.28’	9°28.02’	396.3	Gravity Corer | GC	Gravity corer	at sea bottom
MSM21/ 4-0561-2	Gravity core 02	2012-08-19 15:37:00.0	78°33.28’	9°27.99’	396.6	Gravity Corer | GC	Gravity corer	on deck
MSM21/ 4-0562-1	Seismic profile P200	2012-08-19 17:18:00.0	78°39.19’	9°20.05’	418.1	2D-Multi-Channel-Seismic | 2D-MCS	Seismic reflection profile	end deployment
MSM21/ 4-0562-1	Seismic profile P200	2012-08-19 17:25:00.0	78°38.96’	9°19.35’	426	2D-Multi-Channel-Seismic | 2D-MCS	Seismic reflection profile	start of profile
MSM21/ 4-0562-1	Seismic profile P201	2012-08-19 17:54:00.0	78°37.63’	9°10.43’	490.2	2D-Multi-Channel-Seismic | 2D-MCS	Seismic reflection profile	end of profile
MSM21/ 4-0562-1	Seismic profile P200	2012-08-19 17:54:00.0	78°37.63’	9°10.43’	490.2	2D-Multi-Channel-Seismic | 2D-MCS	Seismic reflection profile	start of profile
MSM21/ 4-0562-1	Seismic profile P202	2012-08-19 20:00:00.0	78°35.07’	8°19.38’	1032.1	2D-Multi-Channel-Seismic | 2D-MCS	Seismic reflection profile	end of profile
MSM21/ 4-0562-1	Seismic profile P201	2012-08-19 20:00:00.0	78°35.07’	8°19.38’	1032.1	2D-Multi-Channel-Seismic | 2D-MCS	Seismic reflection profile	start of profile
MSM21/ 4-0562-1	Seismic profile P202	2012-08-19 20:21:00.0	78°35.89’	8°11.95’	1050.9	2D-Multi-Channel-Seismic | 2D-MCS	Seismic reflection profile	end of profile
MSM21/ 4-0562-1	Seismic profile P203	2012-08-19 20:21:00.0	78°35.89’	8°11.95’	1050.9	2D-Multi-Channel-Seismic | 2D-MCS	Seismic reflection profile	start of profile
MSM21/ 4-0562-1	Seismic profile P204	2012-08-19 22:51:00.0	78°32.49’	7°11.85’	2122	2D-Multi-Channel-Seismic | 2D-MCS	Seismic reflection profile	end of profile
MSM21/ 4-0562-1	Seismic profile P203	2012-08-19 22:51:00.0	78°32.49’	7°11.85’	2122	2D-Multi-Channel-Seismic | 2D-MCS	Seismic reflection profile	start of profile
MSM21/ 4-0562-1	Seismic profile P204	2012-08-19 23:10:00.0	78°33.68’	7°08.64’	1891.1	2D-Multi-Channel-Seismic | 2D-MCS	Seismic reflection profile	end of profile
MSM21/ 4-0562-1	Seismic profile P205	2012-08-19 23:10:00.0	78°33.68’	7°08.64’	1891.1	2D-Multi-Channel-Seismic | 2D-MCS	Seismic reflection profile	start of profile
MSM21/ 4-0562-1	Seismic profile P205	2012-08-20 01:53:00.0	78°36.85’	8°10.05’	1017.3	2D-Multi-Channel-Seismic | 2D-MCS	Seismic reflection profile	end of profile

Event label	Event	Time [UTC]	Latitude [N°]	Longitude [E°]	Water depth [mbsl]	Gear	Description	Remarks
MSM21/ 4-0562-1	Seismic profile P206	2012-08-20 01:53:00.0	78°36.85’	8°10.05’	1017.3	2D-Multi-Channel-Seismic | 2D-MCS	Seismic reflection profile	start of profile
MSM21/ 4-0562-1	Seismic profile P207	2012-08-20 02:47:00.0	78°33.56’	8°17.82’	1158	2D-Multi-Channel-Seismic | 2D-MCS	Seismic reflection profile	end of profile
MSM21/ 4-0562-1	Seismic profile P206	2012-08-20 02:47:00.0	78°33.56’	8°17.82’	1158	2D-Multi-Channel-Seismic | 2D-MCS	Seismic reflection profile	start of profile
MSM21/ 4-0562-1	Seismic profile P207	2012-08-20 05:56:00.0	78°29.72’	7°15.54’	2837.7	2D-Multi-Channel-Seismic | 2D-MCS	Seismic reflection profile	end of profile
MSM21/ 4-0562-1	Seismic profile P208	2012-08-20 06:16:00.0	78°28.47’	7°14.06’	3065.1	2D-Multi-Channel-Seismic | 2D-MCS	Seismic reflection profile	start of profile
MSM21/ 4-0562-1	Seismic profile P208	2012-08-20 09:23:00.0	78°31.61’	8°20.46’	1296	2D-Multi-Channel-Seismic | 2D-MCS	Seismic reflection profile	end of profile
MSM21/ 4-0562-1	Survey S05	2012-08-20 09:23:00.0	78°31.61’	8°20.46’	1170.6	Multibeam + Parasound | MB-PS	Multibeam and ParaSound	start of survey
MSM21/ 4-0562-1	Seismic profile P208	2012-08-20 09:55:00.0	78°32.99’	8°21.26’	1170.6	2D-Multi-Channel-Seismic | 2D-MCS	Seismic reflection profile	end recovery
MSM21/ 4-0562-1	Survey S05	2012-08-20 11:50:00.0	78°33.29’	9°28.54’	388.3	Multibeam + Parasound | MB-PS	Multibeam and ParaSound	end of survey
MSM21/ 4-0563-1	Gravity core 03	2012-08-20 11:51:00.0	78°33.29’	9°28.54’	389.4	Gravity Corer | GC	Gravity corer	surface
MSM21/ 4-0563-1	Gravity core 03	2012-08-20 11:59:00.0	78°33.29’	9°28.53’	386.9	Gravity Corer | GC	Gravity corer	at sea bottom
MSM21/ 4-0563-1	Gravity core 03	2012-08-20 12:11:00.0	78°33.30’	9°28.51’	387.1	Gravity Corer | GC	Gravity corer	on deck
MSM21/ 4-0563-1	Survey S06	2012-08-20 12:20:00.0	78°33.30’	9°28.51’	387.9	Multibeam + Parasound | MB-PS	Multibeam and ParaSound	start of survey
MSM21/ 4-0563-1	Survey S06	2012-08-20 19:50:00.0	79°26.70’	5°26.79’	2358.4	Multibeam + Parasound | MB-PS	Multibeam and ParaSound	end of survey
MSM21/ 4-0564-1	HF Station 12	2012-08-20 19:53:00.0	79°26.94’	5°25.68’	2357.6	Heat Flow | HF	Heat Flow	surface
MSM21/ 4-0564-1	HF Station 12	2012-08-20 20:17:00.0	79°26.94’	5°25.68’	2361.6	Heat Flow | HF	Heat Flow	at sea bottom
MSM21/ 4-0564-1	HF Station 12	2012-08-20 20:22:00.0	79°26.94’	5°25.67’	2357.1	Heat Flow | HF	Heat Flow	start hieving
MSM21/ 4-0564-1	HF Station 12	2012-08-20 20:48:00.0	79°26.94’	5°25.69’	2359.1	Heat Flow | HF	Heat Flow	on deck

Event label	Event	Time [UTC]	Latitude [N°]	Longitude [E°]	Water depth [mbsl]	Gear	Description	Remarks
MSM21/ 4-0565-1	Seismic profile P300	2012-08-20 23:47:00.0	79°37.43’	6°59.69’	945.3	2D-Multi-Channel-Seismic | 2D-MCS	Seismic reflection profile	end deployment
MSM21/ 4-0565-1	Seismic profile P300	2012-08-20 23:55:00.0	79°37.90’	6°58.32’	945.6	2D-Multi-Channel-Seismic | 2D-MCS	Seismic reflection profile	start of profile
MSM21/ 4-0566-1	Survey S07	2012-08-21 02:13:00.0	79°46.77’	6°21.77’	985.8	Multibeam + Parasound | MB-PS	Multibeam and ParaSound	start of survey
MSM21/ 4-0565-1	Seismic profile P300	2012-08-21 02:13:00.0	79°46.77’	6°21.77’	985.8	2D-Multi-Channel-Seismic | 2D-MCS	Seismic reflection profile	end of profile
MSM21/ 4-0565-1	Seismic profile P300	2012-08-21 02:54:00.0	79°46.93’	6°20.10’	988.2	2D-Multi-Channel-Seismic | 2D-MCS	Seismic reflection profile	end recovery, streamer caught in ship's screw and cut off
MSM21/ 4-0566-1	Survey S07	2012-08-22 08:13:00.0	78°09.04’	13°43.11’		Multibeam + Parasound | MB-PS	Multibeam and ParaSound	end of survey
MSM21/ 4-0566-1	Survey S08	2012-08-22 22:36:00.0	78°32.68’	9°30.10’	390.9	Multibeam + Parasound | MB-PS	Multibeam and ParaSound	start of survey
MSM21/ 4-0566-1	Survey S08	2012-08-22 22:50:00.0	78°33.90’	9°27.17’	398.3	Multibeam + Parasound | MB-PS	Multibeam and ParaSound	end of survey
MSM21/ 4-0567-1	Gravity core 04	2012-08-22 23:27:00.0	78°33.32’	9°28.41’	389.8	Gravity Corer | GC	Gravity corer	surface
MSM21/ 4-0567-1	Gravity core 04	2012-08-22 23:35:00.0	78°33.32’	9°28.41’	389.4	Gravity Corer | GC	Gravity corer	at sea bottom
MSM21/ 4-0567-1	Gravity core 04	2012-08-22 23:35:00.0	78°33.32’	9°28.41’	389.4	Gravity Corer | GC	Gravity corer	start hieving
MSM21/ 4-0567-1	Gravity core 04	2012-08-22 23:47:00.0	78°33.33’	9°28.41’	388.8	Gravity Corer | GC	Gravity corer	on deck
MSM21/ 4-0568-1	HF Station 13	2012-08-23 01:14:00.0	78°36.61’	9°17.95’	449.7	Heat Flow | HF	Heat Flow	surface
MSM21/ 4-0568-1	HF Station 13	2012-08-23 01:24:00.0	78°36.61’	9°17.94’	451.1	Heat Flow | HF	Heat Flow	at the bottom
MSM21/ 4-0568-1	HF Station 13	2012-08-23 01:41:00.0	78°36.61’	9°17.95’	449.4	Heat Flow | HF	Heat Flow	on deck
MSM21/ 4-0569-1	HF Station 14	2012-08-23 02:02:00.0	78°36.63’	9°19.21’	437.7	Heat Flow | HF	Heat Flow	surface
MSM21/ 4-0569-1	HF Station 14	2012-08-23 02:08:00.0	78°36.62’	9°19.21’	437.7	Heat Flow | HF	Heat Flow	at the bottom

Event label	Event	Time [UTC]	Latitude [N°]	Longitude [E°]	Water depth [mbsl]	Gear	Description	Remarks
MSM21/ 4-0569-1	HF Station 14	2012-08-23 02:23:00.0	78°36.62’	9°19.21’	438.5	Heat Flow | HF	Heat Flow	on deck
MSM21/ 4-0570-1	HF Station 15	2012-08-23 02:49:00.0	78°36.64’	9°20.92’	427.6	Heat Flow | HF	Heat Flow	surface
MSM21/ 4-0570-1	HF Station 15	2012-08-23 02:55:00.0	78°36.64’	9°20.91’	427.7	Heat Flow | HF	Heat Flow	at the bottom
MSM21/ 4-0570-1	HF Station 15	2012-08-23 03:13:00.0	78°36.65’	9°20.92’	427.6	Heat Flow | HF	Heat Flow	on deck
MSM21/ 4-0571-1	HF Station 16	2012-08-23 03:34:00.0	78°36.66’	9°22.15’	418.5	Heat Flow | HF	Heat Flow	surface
MSM21/ 4-0571-1	HF Station 16	2012-08-23 03:40:00.0	78°36.66’	9°22.16’	417	Heat Flow | HF	Heat Flow	at the bottom
MSM21/ 4-0571-1	HF Station 16	2012-08-23 04:00:00.0	78°36.66’	9°22.24’	416.4	Heat Flow | HF	Heat Flow	on deck
MSM21/ 4-0572-1	HF Station 17	2012-08-23 04:23:00.0	78°36.67’	9°22.93’	406.9	Heat Flow | HF	Heat Flow	surface
MSM21/ 4-0572-1	HF Station 17	2012-08-23 04:30:00.0	78°36.67’	9°22.93’	409.1	Heat Flow | HF	Heat Flow	at the bottom
MSM21/ 4-0572-1	HF Station 17	2012-08-23 04:30:00.0	78°36.67’	9°22.93’	409.1	Heat Flow | HF	Heat Flow	probe fell over, hieving again
MSM21/ 4-0572-1	HF Station 17	2012-08-23 04:34:00.0	78°36.67’	9°22.93’	406.5	Heat Flow | HF	Heat Flow	at the bottom
MSM21/ 4-0572-1	HF Station 17	2012-08-23 04:44:00.0	78°36.67’	9°23.30’	397.2	Heat Flow | HF	Heat Flow	on deck
MSM21/ 4-0573-1	HF Station 18	2012-08-23 04:48:00.0	78°36.67’	9°23.51’	394.3	Heat Flow | HF	Heat Flow	surface
MSM21/ 4-0573-1	HF Station 18	2012-08-23 04:55:00.0	78°36.67’	9°23.51’	394.5	Heat Flow | HF	Heat Flow	at the bottom
MSM21/ 4-0573-1	HF Station 18	2012-08-23 05:16:00.0	78°36.68’	9°23.72’	392.6	Heat Flow | HF	Heat Flow	on deck
MSM21/ 4-0574-1	HF Station 19	2012-08-23 05:25:00.0	78°36.68’	9°24.30’	389	Heat Flow | HF	Heat Flow	surface
MSM21/ 4-0574-1	HF Station 19	2012-08-23 05:30:00.0	78°36.68’	9°24.30’	389	Heat Flow | HF	Heat Flow	at the bottom
MSM21/ 4-0574-1	HF Station 19	2012-08-23 05:51:00.0	78°36.69’	9°24.51’	387.7	Heat Flow | HF	Heat Flow	on deck

Event label	Event	Time [UTC]	Latitude [N°]	Longitude [E°]	Water depth [mbsl]	Gear	Description	Remarks
MSM21/ 4-0575-1	HF Station 20	2012-08-23 06:00:00.0	78°36.69’	9°25.03’	384.8	Heat Flow | HF	Heat Flow	surface
MSM21/ 4-0575-1	HF Station 20	2012-08-23 06:05:00.0	78°36.69’	9°25.03’	384.7	Heat Flow | HF	Heat Flow	at the bottom
MSM21/ 4-0575-1	HF Station 20	2012-08-23 06:27:00.0	78°36.70’	9°25.35’	381.5	Heat Flow | HF	Heat Flow	on deck
MSM21/ 4-0576-1	HF Station 21	2012-08-23 06:33:00.0	78°36.70’	9°25.50’	377.3	Heat Flow | HF	Heat Flow	surface
MSM21/ 4-0576-1	HF Station 21	2012-08-23 06:37:00.0	78°36.70’	9°25.51’	377.7	Heat Flow | HF	Heat Flow	at the bottom
MSM21/ 4-0576-1	HF Station 21	2012-08-23 06:38:00.0	78°36.70’	9°25.51’	378.2	Heat Flow | HF	Heat Flow	probe fell over, hieving again
MSM21/ 4-0576-1	HF Station 21	2012-08-23 06:42:00.0	78°36.70’	9°25.51’	377.6	Heat Flow | HF	Heat Flow	at the bottom
MSM21/ 4-0576-1	HF Station 21	2012-08-23 06:43:00.0	78°36.70’	9°25.51’	377.7	Heat Flow | HF	Heat Flow	probe fell over, hieving again, moving 50 m in 090°
MSM21/ 4-0576-1	HF Station 21	2012-08-23 07:02:00.0	78°36.70’	9°25.64’	377.3	Heat Flow | HF	Heat Flow	on deck, probe damaged
MSM21/ 4-0577-1	JAGO dive 02	2012-08-23 08:47:00.0	78°33.33’	9°28.40’	386.9	JAGO	JAGO Underwater Craft	weight to water
MSM21/ 4-0577-1	JAGO dive 02	2012-08-23 08:52:00.0	78°33.33’	9°28.40’	386.9	JAGO	JAGO Underwater Craft	JAGO to surface
MSM21/ 4-0577-1	JAGO dive 02	2012-08-23 09:12:00.0	78°33.33’	9°28.42’	386.9	JAGO	JAGO Underwater Craft	submerged
MSM21/ 4-0577-1	JAGO dive 02	2012-08-23 13:57:00.0	78°33.34’	9°28.47’	386.9	JAGO	JAGO Underwater Craft	back at surface
MSM21/ 4-0577-1	JAGO dive 02	2012-08-23 14:06:00.0	78°33.32’	9°28.33’	386.9	JAGO	JAGO Underwater Craft	connected to hook
MSM21/ 4-0577-1	JAGO dive 02	2012-08-23 14:10:00.0	78°33.31’	9°28.32’	386.9	JAGO	JAGO Underwater Craft	JAGO back on board
MSM21/ 4-0578-1	Survey S09	2012-08-23 15:02:00.0	78°33.25’	9°25.49’	420.8	Multibeam + Parasound | MB-PS	Multibeam and ParaSound	start of survey
MSM21/ 4-0578-1	Survey S09	2012-08-23 17:51:00.0	78°33.60’	9°30.77’	366.7	Multibeam + Parasound | MB-PS	Multibeam and ParaSound	end of survey

Event label	Event	Time [UTC]	Latitude [N°]	Longitude [E°]	Water depth [mbsl]	Gear	Description	Remarks
MSM21/ 4-0579-1	JAGO dive 03	2012-08-23 18:57:00.0	78°33.35’	9°28.40’		JAGO	JAGO Underwater Craft	weight to water
MSM21/ 4-0579-1	JAGO dive 03	2012-08-23 18:59:00.0	78°33.35’	9°28.40’		JAGO	JAGO Underwater Craft	JAGO to surface
MSM21/ 4-0579-1	JAGO dive 03	2012-08-23 19:18:00.0	78°33.36’	9°27.81’		JAGO	JAGO Underwater Craft	submerged
MSM21/ 4-0579-1	JAGO dive 03	2012-08-23 19:22:00.0	78°33.36’	9°27.81’		JAGO	JAGO Underwater Craft	JAGO at depth
MSM21/ 4-0579-1	JAGO dive 03	2012-08-23 21:40:00.0	78°33.44’	9°28.32		JAGO	JAGO Underwater Craft	back at surface
MSM21/ 4-0579-1	JAGO dive 03	2012-08-23 21:52:00.0	78°33.42’	9°28.26’		JAGO	JAGO Underwater Craft	connected to hook
MSM21/ 4-0579-1	JAGO dive 03	2012-08-23 21:56:00.0	78°33.42’	9°28.26’		JAGO	JAGO Underwater Craft	JAGO back on board
MSM21/ 4-0580-1	CTD 14	2012-08-23 22:38:00.0	78°33.34’	9°28.39’	389.6	Conductivity Temperature Depth Probe with rosette watersampler | CTD/Ros	CTD/rosette water sampler	surface
MSM21/ 4-0580-1	CTD 14	2012-08-23 22:47:00.0	78°33.34’	9°28.39’	389.6	Conductivity Temperature Depth Probe with rosette watersampler | CTD/Ros	CTD/rosette water sampler	at depth, SL max. 387 m
MSM21/ 4-0580-1	CTD 14	2012-08-23 22:59:00.0	78°33.34’	9°28.39’	389.6	Conductivity Temperature Depth Probe with rosette watersampler | CTD/Ros	CTD/rosette water sampler	on deck
MSM21/ 4-0581-1	CTD 15	2012-08-24 00:52:00.0	78°33.31’	9°28.49’	406	Conductivity Temperature Depth Probe with rosette watersampler | CTD/Ros	CTD/rosette water sampler	surface
MSM21/ 4-0581-1	CTD 15	2012-08-24 01:00:00.0	78°33.31’	9°28.49’	386.1	Conductivity Temperature Depth Probe with rosette watersampler | CTD/Ros	CTD/rosette water sampler	at depth, SL max. 384 m
MSM21/ 4-0581-1	CTD 15	2012-08-24 01:11:00.0	78°33.31’	9°28.49’	386.5	Conductivity Temperature Depth Probe with rosette watersampler | CTD/Ros	CTD/rosette water sampler	on deck
MSM21/ 4-0582-1	CTD 16	2012-08-24 02:25:00.0	78°33.33’	9°28.18’	390.4	Conductivity Temperature Depth Probe with rosette watersampler | CTD/Ros	CTD/rosette water sampler	surface
MSM21/ 4-0582-1	CTD 16	2012-08-24 02:35:00.0	78°33.33’	9°28.19’	390	Conductivity Temperature Depth Probe with rosette watersampler | CTD/Ros	CTD/rosette water sampler	at depth, SL max. 387 m
MSM21/ 4-0582-1	CTD 16	2012-08-24 02:44:00.0	78°33.33’	9°28.18’	389.8	Conductivity Temperature Depth Probe with rosette watersampler | CTD/Ros	CTD/rosette water sampler	on deck
MSM21/ 4-0583-1	CTD 17	2012-08-24 03:51:00.0	78°33.39’	9°28.27’	391.3	Conductivity Temperature Depth Probe with rosette watersampler | CTD/Ros	CTD/rosette water sampler	surface
MSM21/ 4-0583-1	CTD 17	2012-08-24 04:00:00.0	78°33.39’	9°28.27’	391.5	Conductivity Temperature Depth Probe with rosette watersampler | CTD/Ros	CTD/rosette water sampler	at depth, SL max. 388 m

Event label	Event	Time [UTC]	Latitude [N°]	Longitude [E°]	Water depth [mbsl]	Gear	Description	Remarks
MSM21/ 4-0583-1	CTD 17	2012-08-24 04:10:00.0	78°33.39’	9°28.27’	391.2	Conductivity Temperature Depth Probe with rosette watersampler | CTD/Ros	CTD/rosette water sampler	on deck
MSM21/ 4-0584-1	CTD 18	2012-08-24 05:15:00.0	78°33.37’	9°28.60’	388.4	Conductivity Temperature Depth Probe with rosette watersampler | CTD/Ros	CTD/rosette water sampler	surface
MSM21/ 4-0584-1	CTD 18	2012-08-24 05:23:00.0	78°33.37’	9°28.60’	388.3	Conductivity Temperature Depth Probe with rosette watersampler | CTD/Ros	CTD/rosette water sampler	at depth, SL max. 386 m
MSM21/ 4-0584-1	CTD 18	2012-08-24 05:31:00.0	78°33.37’	9°28.60’	388.1	Conductivity Temperature Depth Probe with rosette watersampler | CTD/Ros	CTD/rosette water sampler	on deck
MSM21/ 4-0585-1	JAGO dive 04	2012-08-24 08:41:00.0	78°33.35’	9°28.40’	389	JAGO	JAGO Underwater Craft	weight to water
MSM21/ 4-0585-1	JAGO dive 04	2012-08-24 08:56:00.0	78°33.35’	9°28.41’	388.7	JAGO	JAGO Underwater Craft	JAGO to surface
MSM21/ 4-0585-1	JAGO dive 04	2012-08-24 09:14:00.0	78°33.34’	9°28.31’	388.5	JAGO	JAGO Underwater Craft	submerged
MSM21/ 4-0585-1	JAGO dive 04	2012-08-24 12:49:00.0	78°33.43’	9°28.07’		JAGO	JAGO Underwater Craft	back at surface
MSM21/ 4-0585-1	JAGO dive 04	2012-08-24 12:54:00.0	78°33.43’	9°28.19’		JAGO	JAGO Underwater Craft	connected to hook
MSM21/ 4-0585-1	JAGO dive 04	2012-08-24 12:59:00.0	78°33.43’	9°28.19’		JAGO	JAGO Underwater Craft	JAGO back on board
MSM21/ 4-0586-1	Survey S10	2012-08-24 13:53:00.0	78°33.64’	9°31.86’	348.9	Multibeam + Parasound | MB-PS	Multibeam and ParaSound	start of survey
MSM21/ 4-0586-1	Survey S10	2012-08-24 16:46:00.0	78°33.47’	9°24.98’	423.5	Multibeam + Parasound | MB-PS	Multibeam and ParaSound	end of survey
MSM21/ 4-0587-1	JAGO dive 05	2012-08-24 17:17:00.0	78°33.35’	9°28.40’	389.3	JAGO	JAGO Underwater Craft	weight to water
MSM21/ 4-0587-1	JAGO dive 05	2012-08-24 17:21:00.0	78°33.35’	9°28.40’	392	JAGO	JAGO Underwater Craft	JAGO to surface
MSM21/ 4-0587-1	JAGO dive 05	2012-08-24 17:30:00.0	78°33.34’	9°28.38’	389.5	JAGO	JAGO Underwater Craft	submerged
MSM21/ 4-0587-1	JAGO dive 05	2012-08-24 20:16:00.0	78°33.43’	9°28.19’		JAGO	JAGO Underwater Craft	back at surface
MSM21/ 4-0587-1	JAGO dive 05	2012-08-24 20:22:00.0	78°33.42’	9°28.08’		JAGO	JAGO Underwater Craft	connected to hook
MSM21/ 4-0587-1	JAGO dive 05	2012-08-24 20:24:00.0	78°33.43’	9°28.12’		JAGO	JAGO Underwater Craft	JAGO back on board

Event label	Event	Time [UTC]	Latitude [N°]	Longitude [E°]	Water depth [mbsl]	Gear	Description	Remarks
MSM21/4-0588-1	HF Station 22	2012-08-24 21:56:00.0	78°26.85’	8°44.21’	1306.5	Heat Flow | HF	Heat Flow	surface
MSM21/4-0588-1	HF Station 22	2012-08-24 22:25:00.0	78°26.85’	8°44.22’	1311.5	Heat Flow | HF	Heat Flow	at the bottom
MSM21/4-0588-1	HF Station 22	2012-08-24 22:45:00.0	78°26.85’	8°44.24’	1307.5	Heat Flow | HF	Heat Flow	on deck
MSM21/4-0589-1	HF Station 23	2012-08-24 23:44:00.0	78°32.79’	9°16.54’	3963.9	Heat Flow | HF	Heat Flow	surface
MSM21/4-0589-1	HF Station 23	2012-08-24 23:55:00.0	78°32.79’	9°16.54’	3813.9	Heat Flow | HF	Heat Flow	at the bottom
MSM21/4-0589-1	HF Station 23	2012-08-25 00:18:00.0	78°32.79’	9°16.54’	4499.5	Heat Flow | HF	Heat Flow	on deck
MSM21/4-0590-1	HF Station 24	2012-08-25 00:48:00.0	78°33.03’	9°22.06’	463.4	Heat Flow | HF	Heat Flow	surface
MSM21/4-0590-1	HF Station 24	2012-08-25 00:58:00.0	78°33.03’	9°22.08’	461.1	Heat Flow | HF	Heat Flow	at the bottom
MSM21/4-0590-1	HF Station 24	2012-08-25 01:23:00.0	78°33.03’	9°22.08’	463.8	Heat Flow | HF	Heat Flow	on deck
MSM21/4-0591-1	HF Station 25	2012-08-25 01:51:00.0	78°33.27’	9°27.71’	411.7	Heat Flow | HF	Heat Flow	surface
MSM21/4-0591-1	HF Station 25	2012-08-25 02:02:00.0	78°33.27’	9°27.71’	411.5	Heat Flow | HF	Heat Flow	at the bottom
MSM21/4-0591-1	HF Station 25	2012-08-25 02:20:00.0	78°33.27’	9°27.71’	411.2	Heat Flow | HF	Heat Flow	on deck
MSM21/4-0592-1	HF Station 26	2012-08-25 02:35:00.0	78°33.29’	9°28.27’	405.2	Heat Flow | HF	Heat Flow	surface
MSM21/4-0592-1	HF Station 26	2012-08-25 02:40:00.0	78°33.29’	9°28.28’	400.9	Heat Flow | HF	Heat Flow	at the bottom
MSM21/4-0592-1	HF Station 26	2012-08-25 02:57:00.0	78°33.29’	9°28.27’	401.3	Heat Flow | HF	Heat Flow	on deck
MSM21/4-0593-1	HF Station 27	2012-08-25 03:14:00.0	78°33.32’	9°28.98’	401.2	Heat Flow | HF	Heat Flow	surface
MSM21/4-0593-1	HF Station 27	2012-08-25 03:18:00.0	78°33.32’	9°28.99’	403.6	Heat Flow | HF	Heat Flow	at the bottom
MSM21/4-0593-1	HF Station 27	2012-08-25 03:37:00.0	78°33.32’	9°29.06’	403.5	Heat Flow | HF	Heat Flow	on deck

Event label	Event	Time [UTC]	Latitude [N°]	Longitude [E°]	Water depth [mbsl]	Gear	Description	Remarks
MSM21/4-0594-1	HF Station 28	2012-08-25 03:46:00.0	78°33.35’	9°29.54’	395.2	Heat Flow | HF	Heat Flow	surface
MSM21/4-0594-1	HF Station 28	2012-08-25 03:51:00.0	78°33.35’	9°29.55’	395	Heat Flow | HF	Heat Flow	at the bottom
MSM21/4-0594-1	HF Station 28	2012-08-25 04:09:00.0	78°33.35’	9°29.55’	395.7	Heat Flow | HF	Heat Flow	on deck
MSM21/4-0595-1	HF Station 29	2012-08-25 04:19:00.0	78°33.37’	9°30.14’	390.6	Heat Flow | HF	Heat Flow	surface
MSM21/4-0595-1	HF Station 29	2012-08-25 04:24:00.0	78°33.37’	9°30.14’	390.2	Heat Flow | HF	Heat Flow	at the bottom
MSM21/4-0595-1	HF Station 29	2012-08-25 04:57:00.0	78°33.37’	9°30.14’	389.9	Heat Flow | HF	Heat Flow	on deck
MSM21/4-0596-1	Survey S11	2012-08-25 06:14:00.0	78°36.22’	9°23.90’	412.2	Multibeam + Parasound | MB-PS	Multibeam and ParaSound	start of survey
MSM21/4-0596-1	Survey S11	2012-08-25 07:47:00.0	78°36.71’	9°25.67’	373.6	Multibeam + Parasound | MB-PS	Multibeam and ParaSound	end of survey
MSM21/4-0597-1	JAGO dive 06	2012-08-25 08:22:00.0	78°36.65’	9°25.55’	379.3	JAGO	JAGO Underwater Craft	weight to water
MSM21/4-0597-1	JAGO dive 06	2012-08-25 08:34:00.0	78°36.65’	9°25.55’	388.2	JAGO	JAGO Underwater Craft	JAGO to surface
MSM21/4-0597-1	JAGO dive 06	2012-08-25 08:39:00.0	78°36.66’	9°25.53’	389	JAGO	JAGO Underwater Craft	submerged
MSM21/4-0597-1	JAGO dive 06	2012-08-25 09:10:00.0	78°36.66’	9°25.53’	389	JAGO	JAGO Underwater Craft	JAGO at depth
MSM21/4-0597-1	JAGO dive 06	2012-08-25 13:00:00.0	78°36.71’	9°25.35’	395.8	JAGO	JAGO Underwater Craft	back at surface
MSM21/4-0597-1	JAGO dive 06	2012-08-25 13:09:00.0	78°36.77’	9°25.25’	396.7	JAGO	JAGO Underwater Craft	connected to hook
MSM21/4-0597-1	JAGO dive 06	2012-08-25 13:11:00.0	78°36.77’	9°25.25’	394.4	JAGO	JAGO Underwater Craft	JAGO back on board
MSM21/4-0598-1	Survey S12	2012-08-25 14:34:00.0	78°36.66’	9°29.53’	283.4	Multibeam + Parasound | MB-PS	Multibeam and ParaSound	start of survey
MSM21/4-0598-1	Survey S12	2012-08-25 16:33:00.0	78°36.52’	9°22.93’	407.7	Multibeam + Parasound | MB-PS	Multibeam and ParaSound	end of survey
MSM21/4-0599-1	JAGO dive 07	2012-08-25 17:09:00.0	78°36.69’	9°25.50’	377.2	JAGO	JAGO Underwater Craft	weight to water

Event label	Event	Time [UTC]	Latitude [N°]	Longitude [E°]	Water depth [mbsl]	Gear	Description	Remarks
MSM21/ 4-0599-1	JAGO dive 07	2012-08-25 17:17:00.0	78°36.68’	9°25.50’	376.6	JAGO	JAGO Underwater Craft	JAGO to surface
MSM21/ 4-0599-1	JAGO dive 07	2012-08-25 17:24:00.0	78°36.67’	9°25.40’	381.1	JAGO	JAGO Underwater Craft	submerged
MSM21/ 4-0599-1	JAGO dive 07	2012-08-25 17:54:00.0	78°36.67’	9°25.40’	391.2	JAGO	JAGO Underwater Craft	JAGO at depth
MSM21/ 4-0599-1	JAGO dive 07	2012-08-25 21:05:00.0	78°36.75’	9°25.28’		JAGO	JAGO Underwater Craft	back at surface
MSM21/ 4-0599-1	JAGO dive 07	2012-08-25 21:10:00.0	78°36.76’	9°25.17’	404	JAGO	JAGO Underwater Craft	connected to hook
MSM21/ 4-0599-1	JAGO dive 07	2012-08-25 21:14:00.0	78°36.76’	9°25.16’		JAGO	JAGO Underwater Craft	JAGO back on board
MSM21/ 4-0600-1	Survey S13	2012-08-25 21:14:00.0	78°36.76’	9°25.16’		Multibeam + Parasound | MB-PS	Multibeam and ParaSound	start of survey
MSM21/ 4-0600-1	Survey S13	2012-08-25 23:48:00.0	79°00.38’	8°48.50’	213.9	Multibeam + Parasound | MB-PS	Multibeam and ParaSound	end of survey
MSM21/ 4-0600-1	Survey S14	2012-08-26 00:11:00.0	79°04.62’	8°40.80’	220.7	Multibeam + Parasound | MB-PS	Multibeam and ParaSound	start of survey
MSM21/ 4-0600-1	Survey S14	2012-08-26 02:06:00.0	79°25.94’	8°01.09’	392.1	Multibeam + Parasound | MB-PS	Multibeam and ParaSound	alter course
MSM21/ 4-0600-1	Survey S14	2012-08-26 04:47:00.0	79°34.21’	6°13.58’	1479.7	Multibeam + Parasound | MB-PS	Multibeam and ParaSound	Parasound failed
MSM21/ 4-0600-1	Survey S14	2012-08-26 04:53:00.0	79°34.42’	6°11.19’	1508.3	Multibeam + Parasound | MB-PS	Multibeam and ParaSound	alter course
MSM21/ 4-0600-1	Survey S14	2012-08-26 04:57:00.0	79°34.55’	6°09.91’	1524.3	Multibeam + Parasound | MB-PS	Multibeam and ParaSound	Parasound on again
MSM21/ 4-0600-1	Survey S14	2012-08-26 06:25:00.0	79°43.48’	5°30.45’	1684.6	Multibeam + Parasound | MB-PS	Multibeam and ParaSound	Parasound failed
MSM21/ 4-0600-1	Survey S14	2012-08-26 06:43:00.0	79°44.50’	5°26.02’	1627.5	Multibeam + Parasound | MB-PS	Multibeam and ParaSound	Parasound on again
MSM21/ 4-0600-1	Survey S14	2012-08-26 07:10:00.0	79°47.18’	5°13.96’	1564.5	Multibeam + Parasound | MB-PS	Multibeam and ParaSound	end of survey
MSM21/ 4-0600-1	Survey S15	2012-08-26 08:29:00.0	79°47.47’	5°12.69’	1542	Multibeam + Parasound | MB-PS	Multibeam and ParaSound	start of survey
MSM21/ 4-0600-1	Survey S15	2012-08-26 11:18:00.0	79°34.67’	3°34.53’	3317.3	Multibeam + Parasound | MB-PS	Multibeam and ParaSound	end of survey

Event label	Event	Time [UTC]	Latitude [N°]	Longitude [E°]	Water depth [mbsl]	Gear	Description	Remarks
MSM21/ 4-0601-1	CTD 19	2012-08-26 11:32:00.0	79°34.38’	3°32.36’	3256.5	Conductivity Temperature Depth Probe with rosette watersampler | CTD/Ros	CTD/rosette water sampler	surface
MSM21/ 4-0601-1	CTD 19	2012-08-26 12:12:00.0	79°34.39’	3°32.37’	3256.7	Conductivity Temperature Depth Probe with rosette watersampler | CTD/Ros	CTD/rosette water sampler	at depth, SL max. 1750 m
MSM21/ 4-0601-1	CTD 19	2012-08-26 12:47:00.0	79°34.37’	3°32.39’	3263.9	Conductivity Temperature Depth Probe with rosette watersampler | CTD/Ros	CTD/rosette water sampler	on deck
MSM21/ 4-0602-1	Survey S16	2012-08-26 13:03:00.0	79°34.55’	3°33.05’	3281.9	Multibeam + Parasound | MB-PS	Multibeam and ParaSound	start of survey
MSM21/ 4-0602-1	Survey S16	2012-08-26 13:30:00.0	79°36.79’	3°23.17’	3605.7	Multibeam + Parasound | MB-PS	Multibeam and ParaSound	alter course
MSM21/ 4-0602-1	Survey S16	2012-08-26 16:12:00.0	79°49.65’	4°55.18’	1619.1	Multibeam + Parasound | MB-PS	Multibeam and ParaSound	alter course
MSM21/ 4-0602-1	Survey S16	2012-08-26 16:30:00.0	79°51.42’	4°46.45’	1661.3	Multibeam + Parasound | MB-PS	Multibeam and ParaSound	alter course
MSM21/ 4-0602-1	Survey S16	2012-08-26 17:30:00.0	79°46.89’	4°10.00’	2629.6	Multibeam + Parasound | MB-PS	Multibeam and ParaSound	alter course
MSM21/ 4-0602-1	Survey S16	2012-08-26 17:52:00.0	79°48.74’	3°59.71’	2523.1	Multibeam + Parasound | MB-PS	Multibeam and ParaSound	alter course
MSM21/ 4-0602-1	Survey S16	2012-08-26 19:20:00.0	79°54.81’	4°48.31’	1422.5	Multibeam + Parasound | MB-PS	Multibeam and ParaSound	alter course
MSM21/ 4-0602-1	Survey S16	2012-08-26 21:37:00.0	79°42.47’	5°52.88’	1366.9	Multibeam + Parasound | MB-PS	Multibeam and ParaSound	alter course
MSM21/ 4-0602-1	Survey S16	2012-08-26 22:01:00.0	79°44.97’	6°00.93’	1172.8	Multibeam + Parasound | MB-PS	Multibeam and ParaSound	alter course
MSM21/ 4-0602-1	Survey S16	2012-08-26 23:14:00.0	79°51.70’	5°28.42’	1174.1	Multibeam + Parasound | MB-PS	Multibeam and ParaSound	alter course
MSM21/ 4-0602-1	Survey S16	2012-08-26 23:44:00.0	79°49.86’	5°14.98’		Multibeam + Parasound | MB-PS	Multibeam and ParaSound	end of survey
MSM21/ 4-0603-1	Gravity core 05	2012-08-26 23:50:00.0	79°49.87’	5°14.97’	1357.7	Gravity Corer | GC	Gravity corer	surface
MSM21/ 4-0603-1	Gravity core 05	2012-08-27 00:07:00.0	79°49.87’	5°14.98’	1355.4	Gravity Corer | GC	Gravity corer	at sea bottom
MSM21/ 4-0603-1	Gravity core 05	2012-08-27 00:32:00.0	79°49.87’	5°14.98’	1356.4	Gravity Corer | GC	Gravity corer	on deck
MSM21/ 4-0604-1	Survey S17	2012-08-27 00:50:00.0	79°49.89’	5°15.24’	1349.2	Multibeam + Parasound | MB-PS	Multibeam and ParaSound	start of survey

Event label	Event	Time [UTC]	Latitude [N°]	Longitude [E°]	Water depth [mbsl]	Gear	Description	Remarks
MSM21/ 4-0604-1	Survey S17	2012-08-27 02:06:00.0	79°43.79’	4°30.64’	2728.9	Multibeam + Parasound | MB-PS	Multibeam and ParaSound	end of survey
MSM21/ 4-0605-1	Gravity core 06	2012-08-27 02:24:00.0	79°44.15’	4°33.25’	2706.7	Gravity Corer | GC	Gravity corer	surface
MSM21/ 4-0605-1	Gravity core 06	2012-08-27 02:56:00.0	79°44.14’	4°33.25’	2706.1	Gravity Corer | GC	Gravity corer	at sea bottom
MSM21/ 4-0605-1	Gravity core 06	2012-08-27 03:35:00.0	79°44.14’	4°33.26’	2709.5	Gravity Corer | GC	Gravity corer	on deck
MSM21/ 4-0605-2	CTD 20	2012-08-27 03:41:00.0	79°44.14’	4°33.26’	2707.2	Conductivity Temperature Depth Probe with rosette watersampler | CTD/Ros	CTD/rosette water sampler	surface
MSM21/ 4-0605-2	CTD 20	2012-08-27 04:12:00.0	79°44.14’	4°33.25’	2708.4	Conductivity Temperature Depth Probe with rosette watersampler | CTD/Ros	CTD/rosette water sampler; SL max. 1500 m	at depth, SL max. 1500 m
MSM21/ 4-0605-2	CTD 20	2012-08-27 04:42:00.0	79°44.14’	4°33.25’	2712.9	Conductivity Temperature Depth Probe with rosette watersampler | CTD/Ros	CTD/rosette water sampler	on deck
MSM21/ 4-0605-2	Survey S18	2012-08-27 04:46:00.0	79°44.24’	4°33.38’	2700.3	Multibeam + Parasound | MB-PS	Multibeam and ParaSound	start of survey
MSM21/ 4-0605-2	Survey S18	2012-08-27 05:12:00.0	79°46.88’	4°11.51’	2616.7	Multibeam + Parasound | MB-PS	Multibeam and ParaSound	end of survey
MSM21/ 4-0606-1	Gravity core 07	2012-08-27 05:24:00.0	79°47.01’	4°10.92’	2624	Gravity Corer | GC	Gravity corer	surface
MSM21/ 4-0606-1	Gravity core 07	2012-08-27 05:55:00.0	79°47.02’	4°10.92’	2622.7	Gravity Corer | GC	Gravity corer	at sea bottom
MSM21/ 4-0606-1	Gravity core 07	2012-08-27 06:33:00.0	79°47.02’	4°10.92’	2625.4	Gravity Corer | GC	Gravity corer	on deck
MSM21/ 4-0607-1	Survey S19	2012-08-27 06:35:00.0	79°47.02’	4°10.92’	2623.8	Multibeam + Parasound | MB-PS	Multibeam and ParaSound	start of survey
MSM21/ 4-0607-1	Survey S19	2012-08-27 09:44:00.0	80°12.97’	3°12.50’	1456.9	Multibeam + Parasound | MB-PS	Multibeam and ParaSound	alter course
MSM21/ 4-0607-1	Survey S19	2012-08-27 10:24:00.0	80°15.35’	3°38.46’	1201.8	Multibeam + Parasound | MB-PS	Multibeam and ParaSound	alter course
MSM21/ 4-0607-1	Survey S19	2012-08-27 12:10:00.0	80°00.77’	4°21.66’	1431.6	Multibeam + Parasound | MB-PS	Multibeam and ParaSound	alter course
MSM21/ 4-0607-1	Survey S19	2012-08-27 13:12:00.0	80°01.32’	5°16.01’	1005.4	Multibeam + Parasound | MB-PS	Multibeam and ParaSound	end of survey
MSM21/ 4-0608-1	Seismic profile P400	2012-08-27 13:54:00.0	80°02.35’	5°28.18’	937.3	2D-Multi-Channel-Seismic | 2D-MCS	Seismic reflection profile	end deployment

Event label	Event	Time [UTC]	Latitude [N°]	Longitude [E°]	Water depth [mbsl]	Gear	Description	Remarks
MSM21/ 4-0608-1	Seismic profile P400	2012-08-27 14:16:00.0	80°01.85’	5°35.17’	922.1	2D-Multi-Channel-Seismic | 2D-MCS	Seismic reflection profile	start of profile
MSM21/ 4-0608-1	Seismic profile P400	2012-08-27 18:51:00.0	79°42.42’	4°27.89’	2802.2	2D-Multi-Channel-Seismic | 2D-MCS	Seismic reflection profile	end of profile, problems with airgun
MSM21/ 4-0608-1	Seismic profile P500	2012-08-27 20:00:00.0	79°44.23’	4°32.76’	2709.2	2D-Multi-Channel-Seismic | 2D-MCS	Seismic reflection profile	start of profile
MSM21/ 4-0608-1	Seismic profile P500	2012-08-27 22:16:00.0	79°34.93’	4°01.84’	4057.6	2D-Multi-Channel-Seismic | 2D-MCS [ ]	Seismic reflection profile	end of profile
MSM21/ 4-0608-1	Seismic profile P500	2012-08-27 22:32:00.0	79°34.31’	3°59.14’	4044.7	2D-Multi-Channel-Seismic | 2D-MCS	Seismic reflection profile	end recovery
MSM21/ 4-0609-1	Survey S20	2012-08-27 23:38:00.0	79°38.14’	4°41.99’	2921.1	Multibeam + Parasound | MB-PS	Multibeam and ParaSound	start of survey
MSM21/ 4-0609-1	Survey S20	2012-08-28 00:49:00.0	79°29.01’	5°25.02’	2473.4	Multibeam + Parasound | MB-PS	Multibeam and ParaSound	alter course
MSM21/ 4-0609-1	Survey S20	2012-08-28 01:01:00.0	79°27.28’	5°16.69’	2474.2	Multibeam + Parasound | MB-PS	Multibeam and ParaSound	alter course
MSM21/ 4-0609-1	Survey S20	2012-08-28 01:20:00.0	79°23.45’	5°09.90’	2342.3	Multibeam + Parasound | MB-PS	Multibeam and ParaSound	alter course
MSM21/ 4-0609-1	Survey S20	2012-08-28 06:44:00.0	78°34.92’	9°12.90’	498	Multibeam + Parasound | MB-PS	Multibeam and ParaSound	alter course
MSM21/ 4-0609-1	Survey S20	2012-08-28 06:44:00.0	78°34.92’	9°12.90’	498	Multibeam + Parasound | MB-PS	Multibeam and ParaSound	end of survey
MSM21/ 4-0610-1	Survey S21	2012-08-28 07:10:00.0	78°33.12’	9°30.14’	383.7	Multibeam + Parasound | MB-PS	Multibeam and ParaSound	start of survey
MSM21/ 4-0610-1	Survey S21	2012-08-28 07:44:00.0	78°33.10’	9°28.99’	391	Multibeam + Parasound | MB-PS	Multibeam and ParaSound	end of survey
MSM21/ 4-0611-1	JAGO dive 08	2012-08-28 09:17:00.0	78°33.18’	9°29.44’	391	JAGO	JAGO Underwater Craft	weight to water
MSM21/ 4-0611-1	JAGO dive 08	2012-08-28 09:34:00.0	78°33.18’	9°29.44’	390.6	JAGO	JAGO Underwater Craft	JAGO to surface
MSM21/ 4-0611-1	JAGO dive 08	2012-08-28 09:37:00.0	78°33.18’	9°29.46’	390.4	JAGO	JAGO Underwater Craft	submerged
MSM21/ 4-0611-1	JAGO dive 08	2012-08-28 10:17:00.0	78°33.18’	9°29.42’		JAGO	JAGO Underwater Craft	JAGO at depth

Event label	Event	Time [UTC]	Latitude [N°]	Longitude [E°]	Water depth [mbsl]	Gear	Description	Remarks
MSM21/ 4-0611-1	JAGO dive 08	2012-08-28 13:06:00.0	78°33.24’	9°29.37’		JAGO	JAGO Underwater Craft	back at surface
MSM21/ 4-0611-1	JAGO dive 08	2012-08-28 13:12:00.0	78°33.24’	9°29.35’		JAGO	JAGO Underwater Craft	connected to hook
MSM21/ 4-0611-1	JAGO dive 08	2012-08-28 13:15:00.0	78°33.24’	9°29.34’		JAGO	JAGO Underwater Craft	JAGO back on board
MSM21/ 4-0612-1	Survey S22	2012-08-28 14:24:00.0	78°33.00’	9°31.48’	365.8	Multibeam + Parasound | MB-PS	Multibeam and ParaSound	start of survey
MSM21/ 4-0612-1	Survey S22	2012-08-28 18:12:00.0	78°32.76’	9°29.54’	392.1	Multibeam + Parasound | MB-PS	Multibeam and ParaSound	end of survey
MSM21/ 4-0613-1	CTD 21	2012-08-28 19:04:00.0	78°33.31’	9°28.56’	391.2	Conductivity Temperature Depth Probe with rosette watersampler | CTD/Ros	CTD/rosette water sampler	surface
MSM21/ 4-0613-1	CTD 21	2012-08-28 19:13:00.0	78°33.31’	9°28.55’	388.5	Conductivity Temperature Depth Probe with rosette watersampler | CTD/Ros	CTD/rosette water sampler; SL max. 383 m	at depth, SL max. 383 m
MSM21/ 4-0613-1	CTD 21	2012-08-28 19:23:00.0	78°33.31’	9°28.56’	391.6	Conductivity Temperature Depth Probe with rosette watersampler | CTD/Ros	CTD/rosette water sampler	on deck
MSM21/ 4-0614-1	CTD 22	2012-08-28 21:02:00.0	78°36.63’	9°25.67’	377	Conductivity Temperature Depth Probe with rosette watersampler | CTD/Ros	CTD/rosette water sampler	surface
MSM21/ 4-0614-1	CTD 22	2012-08-28 21:12:00.0	78°36.63’	9°25.67’	375.5	Conductivity Temperature Depth Probe with rosette watersampler | CTD/Ros	CTD/rosette water sampler; SL max. 372 m	at depth, SL max. 372 m
MSM21/ 4-0614-1	CTD 22	2012-08-28 21:20:00.0	78°36.63’	9°25.68’	377.6	Conductivity Temperature Depth Probe with rosette watersampler | CTD/Ros	CTD/rosette water sampler	on deck
MSM21/ 4-0615-1	CTD 23	2012-08-28 22:10:00.0	78°34.73’	9°02.04’	601.4	Conductivity Temperature Depth Probe with rosette watersampler | CTD/Ros	CTD/rosette water sampler	surface
MSM21/ 4-0615-1	CTD 23	2012-08-28 22:23:00.0	78°34.73’	9°02.04’	599.2	Conductivity Temperature Depth Probe with rosette watersampler | CTD/Ros	CTD/rosette water sampler; SL max. 599 m	at depth, SL max. 599 m
MSM21/ 4-0615-1	CTD 23	2012-08-28 22:52:00.0	78°34.73’	9°02.04’	599.3	Conductivity Temperature Depth Probe with rosette watersampler | CTD/Ros	CTD/rosette water sampler	on deck
MSM21/ 4-0616-1	CTD 24	2012-08-29 00:18:00.0	78°32.45’	8°33.36’	1060.6	Conductivity Temperature Depth Probe with rosette watersampler | CTD/Ros	CTD/rosette water sampler	surface
MSM21/ 4-0616-1	CTD 24	2012-08-29 00:28:00.0	78°32.50’	8°33.13’	1058.6	Conductivity Temperature Depth Probe with rosette watersampler | CTD/Ros	CTD/rosette water sampler	technical problems
MSM21/ 4-0616-1	CTD 24	2012-08-29 01:02:00.0	78°32.69’	8°32.35’	1057.7	Conductivity Temperature Depth Probe with rosette watersampler | CTD/Ros	CTD/rosette water sampler	on deck
MSM21/ 4-0616-2	CTD 24-2	2012-08-29 01:56:00.0	78°32.45’	8°33.28’	1061.1	Conductivity Temperature Depth Probe with rosette watersampler | CTD/Ros	CTD/rosette water sampler	surface

Event label	Event	Time [UTC]	Latitude [N°]	Longitude [E°]	Water depth [mbsl]	Gear	Description	Remarks
MSM21/ 4-0616-2	CTD 24-2	2012-08-29 02:24:00.0	78°32.65’	8°32.42’	1054.5	Conductivity Temperature Depth Probe with rosette watersampler | CTD/Ros	CTD/rosette water sampler	at depth, SL max. 1054 m
MSM21/ 4-0616-2	CTD 24-2	2012-08-29 02:47:00.0	78°32.82’	8°31.76’	1053.3	Conductivity Temperature Depth Probe with rosette watersampler | CTD/Ros	CTD/rosette water sampler	on deck
MSM21/ 4-0617-1	CTD 25	2012-08-29 03:47:00.0	78°29.95’	8°01.69’	1704.3	Conductivity Temperature Depth Probe with rosette watersampler | CTD/Ros	CTD/rosette water sampler	surface
MSM21/ 4-0617-1	CTD 25	2012-08-29 04:19:00.0	78°30.05’	8°01.42’	1709.9	Conductivity Temperature Depth Probe with rosette watersampler | CTD/Ros	CTD/rosette water sampler	at depth, SL max. 1690 m
MSM21/ 4-0617-1	CTD 25	2012-08-29 04:54:00.0	78°30.05’	8°01.42’	1708.7	Conductivity Temperature Depth Probe with rosette watersampler | CTD/Ros	CTD/rosette water sampler	on deck
MSM21/ 4-0618-1	CTD 26	2012-08-29 06:00:00.0	78°26.19’	7°14.49’	3129.1	Conductivity Temperature Depth Probe with rosette watersampler | CTD/Ros	CTD/rosette water sampler	surface
MSM21/ 4-0618-1	CTD 26	2012-08-29 06:47:00.0	78°26.19’	7°14.48’	3128.8	Conductivity Temperature Depth Probe with rosette watersampler | CTD/Ros	CTD/rosette water sampler; SL max. 2500 m	at depth, SL max. 2500 m
MSM21/ 4-0618-1	CTD 26	2012-08-29 07:35:00.0	78°26.19’	7°14.48’	3128.3	Conductivity Temperature Depth Probe with rosette watersampler | CTD/Ros	CTD/rosette water sampler	on deck
MSM21/ 4-0619-1	Seismic profile P600	2012-08-29 08:22:00.0	78°26.07’	7°01.33’	3303.5	2D-Multi-Channel-Seismic | 2D-MCS	Seismic reflection profile	end deployment
MSM21/ 4-0619-1	Seismic profile P600	2012-08-29 08:39:00.0	78°25.31’	7°04.96’	3298	2D-Multi-Channel-Seismic | 2D-MCS	Seismic reflection profile	start of profile
MSM21/ 4-0619-1	Seismic profile P600	2012-08-29 15:08:00.0	78°37.39’	9°35.12’	174.7	2D-Multi-Channel-Seismic | 2D-MCS	Seismic reflection profile	end of profile
MSM21/ 4-0619-1	Seismic profile P600	2012-08-29 15:26:00.0	78°37.71’	9°39.99’	145.2	2D-Multi-Channel-Seismic | 2D-MCS	Seismic reflection profile	end recovery
MSM21/ 4-0620-1	JAGO dive 09	2012-08-29 16:18:00.0	78°39.31’	9°26.12’	245	JAGO	JAGO Underwater Craft	weight to water
MSM21/ 4-0620-1	JAGO dive 09	2012-08-29 16:27:00.0	78°39.31’	9°26.12’	243.1	JAGO	JAGO Underwater Craft	JAGO to surface
MSM21/ 4-0620-1	JAGO dive 09	2012-08-29 16:31:00.0	78°39.32’	9°26.14’	242.2	JAGO	JAGO Underwater Craft	submerged
MSM21/ 4-0620-1	JAGO dive 09	2012-08-29 16:53:00.0	78°39.32’	9°26.15’		JAGO	JAGO Underwater Craft	JAGO at depth
MSM21/ 4-0620-1	JAGO dive 09	2012-08-29 20:28:00.0	78°39.34’	9°26.17’		JAGO	JAGO Underwater Craft	back at surface
MSM21/ 4-0620-1	JAGO dive 09	2012-08-29 20:32:00.0	78°39.34’	9°26.06’		JAGO	JAGO Underwater Craft	connected to hook

Event label	Event	Time [UTC]	Latitude [N°]	Longitude [E°]	Water depth [mbsl]	Gear	Description	Remarks
MSM21/ 4-0620-1	JAGO dive 09	2012-08-29 20:36:00.0	78°39.34’	9°26.06’		JAGO	JAGO Underwater Craft	JAGO back on board
MSM21/ 4-0621-1	CTD 27 (test)	2012-08-29 20:55:00.0	78°39.34’	9°26.06’		Conductivity Temperature Depth Probe with rosette watersampler | CTD/Ros	CTD/rosette water sampler	surface
MSM21/ 4-0621-1	CTD 27 (test)	2012-08-29 20:59:00.0	78°39.34’	9°26.05’		Conductivity Temperature Depth Probe with rosette watersampler | CTD/Ros	CTD/rosette water sampler; SL max. 57 m	at depth, SL max. 57 m
MSM21/ 4-0621-1	CTD 27 (test)	2012-08-29 21:02:00.0	78°39.34’	9°26.07’		Conductivity Temperature Depth Probe with rosette watersampler | CTD/Ros	CTD/rosette water sampler	on deck
MSM21/ 4-0622-1	HF Station 30	2012-08-29 23:50:00.0	78°30.60’	7°07.09’	2941.5	Heat Flow | HF	Heat Flow	surface
MSM21/ 4-0622-1	HF Station 30	2012-08-30 00:47:00.0	78°30.60’	7°07.08’	2941.9	Heat Flow | HF	Heat Flow	at the bottom
MSM21/ 4-0622-1	HF Station 30	2012-08-30 01:42:00.0	78°30.60’	7°07.08’	2941.3	Heat Flow | HF	Heat Flow	on deck
MSM21/ 4-0623-1	HF Station 31	2012-08-30 02:23:00.0	78°31.15’	7°16.22’	2344	Heat Flow | HF	Heat Flow	surface
MSM21/ 4-0623-1	HF Station 31	2012-08-30 03:08:00.0	78°31.15’	7°16.23’	2335.7	Heat Flow | HF	Heat Flow	at the bottom
MSM21/ 4-0623-1	HF Station 31	2012-08-30 03:53:00.0	78°31.20’	7°17.00’	2272.7	Heat Flow | HF	Heat Flow	on deck
MSM21/ 4-0624-1	HF Station 32	2012-08-30 04:24:00.0	78°31.50’	7°21.89’	2051	Heat Flow | HF	Heat Flow	surface
MSM21/ 4-0624-1	HF Station 32	2012-08-30 05:07:00.0	78°31.50’	7°21.90’	2050.9	Heat Flow | HF	Heat Flow	at the bottom
MSM21/ 4-0624-1	HF Station 32	2012-08-30 05:53:00.0	78°31.50’	7°21.89’	2056.9	Heat Flow | HF	Heat Flow	on deck
MSM21/ 4-0625-1	HF Station 33	2012-08-30 06:39:00.0	78°33.27’	7°50.55’	1504.8	Heat Flow | HF	Heat Flow	surface
MSM21/ 4-0625-1	HF Station 33	2012-08-30 07:11:00.0	78°33.27’	7°50.55’	1508.6	Heat Flow | HF	Heat Flow	at the bottom
MSM21/ 4-0625-1	HF Station 33	2012-08-30 07:54:00.0	78°33.29’	7°50.66’	1503.1	Heat Flow | HF	Heat Flow	on deck
MSM21/ 4-0626-1	Gravity core 08	2012-08-30 11:01:00.0	78°33.54’	9°27.85’	392	Gravity Corer | GC	Gravity corer	surface
MSM21/ 4-0626-1	Gravity core 08	2012-08-30 11:08:00.0	78°33.54’	9°27.86’	392.6	Gravity Corer | GC	Gravity corer	at sea bottom

Event label	Event	Time [UTC]	Latitude [N°]	Longitude [E°]	Water depth [mbsl]	Gear	Description	Remarks
MSM21/ 4-0626-1	Gravity core 08	2012-08-30 11:19:00.0	78°33.54’	9°27.85’	393	Gravity Corer | GC	Gravity corer	on deck
MSM21/ 4-0626-2	Gravity core 09	2012-08-30 12:55:00.0	78°33.55’	9°27.80’	392.3	Gravity Corer | GC	Gravity corer	surface
MSM21/ 4-0626-2	Gravity core 09	2012-08-30 13:02:00.0	78°33.54’	9°27.86’	391.9	Gravity Corer | GC	Gravity corer	at sea bottom
MSM21/ 4-0626-2	Gravity core 09	2012-08-30 13:38:00.0	78°33.54’	9°27.86’	392.2	Gravity Corer | GC	Gravity corer	on deck
MSM21/ 4-0627-1	Gravity core 10	2012-08-30 14:02:00.0	78°33.52’	9°27.91’	393	Gravity Corer | GC	Gravity corer	surface
MSM21/ 4-0627-1	Gravity core 10	2012-08-30 14:08:00.0	78°33.52’	9°27.89’	393.3	Gravity Corer | GC	Gravity corer	at sea bottom
MSM21/ 4-0627-1	Gravity core 10	2012-08-30 14:18:00.0	78°33.52’	9°27.90’	392.1	Gravity Corer | GC	Gravity corer	on deck
MSM21/ 4-0628-1	Gravity core 11	2012-08-30 14:45:00.0	78°33.48’	9°28.14’	389.6	Gravity Corer | GC	Gravity corer	surface
MSM21/ 4-0628-1	Gravity core 11	2012-08-30 14:51:00.0	78°33.48’	9°28.13’	391.2	Gravity Corer | GC	Gravity corer	at sea bottom
MSM21/ 4-0628-1	Gravity core 11	2012-08-30 15:02:00.0	78°33.48’	9°28.14’	391.2	Gravity Corer | GC	Gravity corer	on deck
MSM21/ 4-0629-1	Gravity core 12	2012-08-30 15:35:00.0	78°33.45’	9°27.97’	394.4	Gravity Corer | GC	Gravity corer	surface
MSM21/ 4-0629-1	Gravity core 12	2012-08-30 15:42:00.0	78°33.45’	9°27.97’	393	Gravity Corer | GC	Gravity corer	at sea bottom
MSM21/ 4-0629-1	Gravity core 12	2012-08-30 15:53:00.0	78°33.45’	9°27.97’	392.5	Gravity Corer | GC	Gravity corer	on deck
MSM21/ 4-0630-1	Gravity core 13	2012-08-30 16:23:00.0	78°33.41’	9°28.20’	392.3	Gravity Corer | GC	Gravity corer	surface
MSM21/ 4-0630-1	Gravity core 13	2012-08-30 16:27:00.0	78°33.41’	9°28.20’	392	Gravity Corer | GC	Gravity corer	at sea bottom
MSM21/ 4-0630-1	Gravity core 13	2012-08-30 16:43:00.0	78°33.41’	9°28.20’	391.4	Gravity Corer | GC	Gravity corer	on deck
MSM21/ 4-0631-1	Gravity core 14	2012-08-30 17:30:00.0	78°33.42’	9°27.11’	400.4	Gravity Corer | GC	Gravity corer	surface
MSM21/ 4-0631-1	Gravity core 14	2012-08-30 17:35:00.0	78°33.42’	9°27.11’	401.2	Gravity Corer | GC	Gravity corer	at sea bottom

Event label	Event	Time [UTC]	Latitude [N°]	Longitude [E°]	Water depth [mbsl]	Gear	Description	Remarks
MSM21/ 4-0631-1	Gravity core 14	2012-08-30 17:49:00.0	78°33.42’	9°27.12’	400.8	Gravity Corer | GC	Gravity corer	on deck
MSM21/ 4-0632-1	Survey S23	2012-08-30 18:47:00.0	78°33.13’	9°25.14’	425.9	Multibeam + Parasound | MB-PS	Multibeam and ParaSound	start of survey
MSM21/ 4-0632-1	Survey S23	2012-08-30 19:02:00.0	78°33.42’	9°31.16’	412	Multibeam + Parasound | MB-PS	Multibeam and ParaSound	end of survey
MSM21/ 4-0633-1	CTD 28	2012-08-30 19:32:00.0	78°33.16’	9°25.40’	853.6	Conductivity Temperature Depth Probe with rosette watersampler | CTD/Ros	CTD/rosette water sampler	surface
MSM21/ 4-0633-1	CTD 28	2012-08-30 19:41:00.0	78°33.16’	9°25.39’		Conductivity Temperature Depth Probe with rosette watersampler | CTD/Ros	CTD/rosette water sampler; SL max. 422 m	at depth, SL max. 422 m
MSM21/ 4-0633-1	CTD 28	2012-08-30 20:04:00.0	78°33.16’	9°25.39’		Conductivity Temperature Depth Probe with rosette watersampler | CTD/Ros	CTD/rosette water sampler	on deck
MSM21/ 4-0633-2	HF Station 34	2012-08-30 20:27:00.0	78°33.16’	9°25.40’		Heat Flow | HF	Heat Flow	surface
MSM21/ 4-0633-2	HF Station 34	2012-08-30 20:38:00.0	78°33.16’	9°25.39’		Heat Flow | HF	Heat Flow	at sea bottom
MSM21/ 4-0633-2	HF Station 34	2012-08-30 20:44:00.0	78°33.16’	9°25.39’		Heat Flow | HF	Heat Flow	off bottom
MSM21/ 4-0633-2	HF Station 34	2012-08-30 20:56:00.0	78°33.16’	9°25.40’		Heat Flow | HF	Heat Flow	on deck
MSM21/ 4-0634-1	CTD 29	2012-08-30 21:17:00.0	78°33.23’	9°26.78’		Conductivity Temperature Depth Probe with rosette watersampler | CTD/Ros	CTD/rosette water sampler	surface
MSM21/ 4-0634-1	CTD 29	2012-08-30 21:27:00.0	78°33.24’	9°26.78’		Conductivity Temperature Depth Probe with rosette watersampler | CTD/Ros	CTD/rosette water sampler; SL max. 404 m	at depth, SL max. 404 m
MSM21/ 4-0634-1	CTD 29	2012-08-30 21:36:00.0	78°33.24’	9°26.78’		Conductivity Temperature Depth Probe with rosette watersampler | CTD/Ros	CTD/rosette water sampler	on deck
MSM21/ 4-0634-2	HF Station 35	2012-08-30 21:40:00.0	78°33.23’	9°26.72’		Heat Flow | HF	Heat Flow	surface
MSM21/ 4-0634-2	HF Station 35	2012-08-30 21:51:00.0	78°33.24’	9°26.78’		Heat Flow | HF	Heat Flow	at sea bottom
MSM21/ 4-0634-2	HF Station 35	2012-08-30 22:05:00.0	78°33.24’	9°26.78’		Heat Flow | HF	Heat Flow	off bottom
MSM21/ 4-0634-2	HF Station 35	2012-08-30 22:12:00.0	78°33.23’	9°26.78’		Heat Flow | HF	Heat Flow	on deck

Event label	Event	Time [UTC]	Latitude [N°]	Longitude [E°]	Water depth [mbsl]	Gear	Description	Remarks
MSM21/ 4-0635-1	CTD 30	2012-08-30 22:39:00.0	78°33.25’	9°27.33’		Conductivity Temperature Depth Probe with rosette watersampler | CTD/Ros	CTD/rosette water sampler	surface
MSM21/ 4-0635-1	CTD 30	2012-08-30 22:48:00.0	78°33.26’	9°27.34’		Conductivity Temperature Depth Probe with rosette watersampler | CTD/Ros	CTD/rosette water sampler; SL max. 400	at depth, SL max. 400
MSM21/ 4-0635-1	CTD 30	2012-08-30 22:57:00.0	78°33.26’	9°27.34’		Conductivity Temperature Depth Probe with rosette watersampler | CTD/Ros	CTD/rosette water sampler	on deck
MSM21/ 4-0635-2	HF Station 36	2012-08-30 23:02:00.0	78°33.26’	9°27.34’		Heat Flow | HF	Heat Flow	surface
MSM21/ 4-0635-2	HF Station 36	2012-08-30 23:12:00.0	78°33.26’	9°27.34’		Heat Flow | HF	Heat Flow	at sea bottom
MSM21/ 4-0635-2	HF Station 36	2012-08-30 23:25:00.0	78°33.26’	9°27.34’		Heat Flow | HF	Heat Flow	off bottom
MSM21/ 4-0635-2	HF Station 36	2012-08-30 23:32:00.0	78°33.26’	9°27.34’		Heat Flow | HF	Heat Flow	on deck
MSM21/ 4-0636-1	CTD 31	2012-08-30 23:51:00.0	78°33.29’	9°27.96’		Conductivity Temperature Depth Probe with rosette watersampler | CTD/Ros	CTD/rosette water sampler	surface
MSM21/ 4-0636-1	CTD 31	2012-08-31 00:02:00.0	78°33.29’	9°27.97’		Conductivity Temperature Depth Probe with rosette watersampler | CTD/Ros	CTD/rosette water sampler; SL max. 393 m	at depth, SL max. 393 m
MSM21/ 4-0636-1	CTD 31	2012-08-31 00:12:00.0	78°33.29’	9°27.97’		Conductivity Temperature Depth Probe with rosette watersampler | CTD/Ros	CTD/rosette water sampler	on deck
MSM21/ 4-0636-2	HF Station 37	2012-08-31 00:18:00.0	78°33.29’	9°27.97’	396.3	Heat Flow | HF	Heat Flow	surface
MSM21/ 4-0636-2	HF Station 37	2012-08-31 00:28:00.0	78°33.29’	9°27.97’	394.2	Heat Flow | HF	Heat Flow	at sea bottom
MSM21/ 4-0636-2	HF Station 37	2012-08-31 00:55:00.0	78°33.29’	9°28.00’	397	Heat Flow | HF	Heat Flow	on deck
MSM21/ 4-0637-1	CTD 32	2012-08-31 01:05:00.0	78°33.31’	9°28.53’	389	Conductivity Temperature Depth Probe with rosette watersampler | CTD/Ros	CTD/rosette water sampler	surface
MSM21/ 4-0637-1	CTD 32	2012-08-31 01:15:00.0	78°33.31’	9°28.53’	387.5	Conductivity Temperature Depth Probe with rosette watersampler | CTD/Ros	CTD/rosette water sampler; SL max. 401 m	at depth, SL max. 401 m
MSM21/ 4-0637-1	CTD 32	2012-08-31 01:23:00.0	78°33.31’	9°28.53’	390.5	Conductivity Temperature Depth Probe with rosette watersampler | CTD/Ros	CTD/rosette water sampler	on deck
MSM21/ 4-0637-2	HF Station 38	2012-08-31 01:29:00.0	78°33.31’	9°28.53’	390	Heat Flow | HF	Heat Flow	surface
MSM21/ 4-0637-2	HF Station 38	2012-08-31 01:38:00.0	78°33.31’	9°28.53’	390	Heat Flow | HF	Heat Flow	at sea bottom

Event label	Event	Time [UTC]	Latitude [N°]	Longitude [E°]	Water depth [mbsl]	Gear	Description	Remarks
MSM21/ 4-0637-2	HF Station 38	2012-08-31 01:59:00.0	78°33.31’	9°28.53’	388.6	Heat Flow | HF	Heat Flow	on deck
MSM21/ 4-0638-1	CTD 33	2012-08-31 02:35:00.0	78°33.32’	9°28.73’	390.5	Conductivity Temperature Depth Probe with rosette watersampler | CTD/Ros	CTD/rosette water sampler	surface
MSM21/ 4-0638-1	CTD 33	2012-08-31 02:45:00.0	78°33.32’	9°28.73’	390	Conductivity Temperature Depth Probe with rosette watersampler | CTD/Ros	CTD/rosette water sampler; SL max. 389 m	at depth, SL max. 389 m
MSM21/ 4-0638-1	CTD 33	2012-08-31 02:55:00.0	78°33.32’	9°28.73’	389.8	Conductivity Temperature Depth Probe with rosette watersampler | CTD/Ros	CTD/rosette water sampler	on deck
MSM21/ 4-0638-2	HF Station 39	2012-08-31 03:02:00.0	78°33.32’	9°28.72’	390.4	Heat Flow | HF	Heat Flow	surface
MSM21/ 4-0638-2	HF Station 39	2012-08-31 03:12:00.0	78°33.32’	9°28.73’	391.5	Heat Flow | HF	Heat Flow	at sea bottom
MSM21/ 4-0638-2	HF Station 39	2012-08-31 03:35:00.0	78°33.32’	9°28.73’	390.4	Heat Flow | HF	Heat Flow	on deck
MSM21/ 4-0639-1	CTD 34	2012-08-31 03:53:00.0	78°33.34’	9°29.22’	386.9	Conductivity Temperature Depth Probe with rosette watersampler | CTD/Ros	CTD/rosette water sampler	surface
MSM21/ 4-0639-1	CTD 34	2012-08-31 04:02:00.0	78°33.34’	9°29.22’	389.4	Conductivity Temperature Depth Probe with rosette watersampler | CTD/Ros	CTD/rosette water sampler; SL max. 383 m	at depth, SL max. 383 m
MSM21/ 4-0639-1	CTD 34	2012-08-31 04:12:00.0	78°33.34’	9°29.23’	386.9	Conductivity Temperature Depth Probe with rosette watersampler | CTD/Ros	CTD/rosette water sampler	on deck
MSM21/ 4-0639-2	HF Station 40	2012-08-31 04:16:00.0	78°33.34’	9°29.23’	389.3	Heat Flow | HF	Heat Flow	surface
MSM21/ 4-0639-2	HF Station 40	2012-08-31 04:25:00.0	78°33.34’	9°29.23’	387.4	Heat Flow | HF	Heat Flow	at sea bottom
MSM21/ 4-0639-2	HF Station 40	2012-08-31 04:49:00.0	78°33.35’	9°29.35’	385.4	Heat Flow | HF	Heat Flow	on deck
MSM21/ 4-0640-1	CTD 35	2012-08-31 05:00:00.0	78°33.36’	9°29.79’	381.9	Conductivity Temperature Depth Probe with rosette watersampler | CTD/Ros	CTD/rosette water sampler	surface
MSM21/ 4-0640-1	CTD 35	2012-08-31 05:10:00.0	78°33.36’	9°29.80’	381.5	Conductivity Temperature Depth Probe with rosette watersampler | CTD/Ros	CTD/rosette water sampler; SL max. 378 m	at depth, SL max. 378 m
MSM21/ 4-0640-1	CTD 35	2012-08-31 05:20:00.0	78°33.36’	9°29.79’	383.5	Conductivity Temperature Depth Probe with rosette watersampler | CTD/Ros	CTD/rosette water sampler	on deck
MSM21/ 4-0640-2	HF Station 41	2012-08-31 05:26:00.0	78°33.36’	9°29.80’	382	Heat Flow | HF	Heat Flow	surface
MSM21/ 4-0640-2	HF Station 41	2012-08-31 05:35:00.0	78°33.36’	9°29.80’	381.2	Heat Flow | HF	Heat Flow	at sea bottom

Event label	Event	Time [UTC]	Latitude [N°]	Longitude [E°]	Water depth [mbsl]	Gear	Description	Remarks
MSM21/ 4-0640-2	HF Station 41	2012-08-31 05:57:00.0	78°33.36’	9°29.80’	382.1	Heat Flow | HF	Heat Flow	on deck
MSM21/ 4-0641-1	CTD 36	2012-08-31 06:17:00.0	78°33.38’	9°30.50’	377.7	Conductivity Temperature Depth Probe with rosette watersampler | CTD/Ros	CTD/rosette water sampler	surface
MSM21/ 4-0641-1	CTD 36	2012-08-31 06:26:00.0	78°33.38’	9°30.50’	374.6	Conductivity Temperature Depth Probe with rosette watersampler | CTD/Ros	CTD/rosette water sampler; SL max. 370 m	at depth, SL max. 370 m
MSM21/ 4-0641-1	CTD 36	2012-08-31 06:37:00.0	78°33.38’	9°30.50’	373.1	Conductivity Temperature Depth Probe with rosette watersampler | CTD/Ros	CTD/rosette water sampler	on deck
MSM21/ 4-0641-2	HF Station 42	2012-08-31 06:41:00.0	78°33.38’	9°30.50’	374.9	Heat Flow | HF	Heat Flow	surface
MSM21/ 4-0641-2	HF Station 42	2012-08-31 06:51:00.0	78°33.38’	9°30.50’	374.7	Heat Flow | HF	Heat Flow	at sea bottom
MSM21/ 4-0641-2	HF Station 42	2012-08-31 07:14:00.0	78°33.38’	9°30.50’	375.1	Heat Flow | HF	Heat Flow	on deck
MSM21/ 4-0642-1	CTD 37	2012-08-31 07:51:00.0	78°33.41’	9°31.35’	357.4	Conductivity Temperature Depth Probe with rosette watersampler | CTD/Ros	CTD/rosette water sampler	surface
MSM21/ 4-0642-1	CTD 37	2012-08-31 08:02:00.0	78°33.41’	9°31.36’	358	Conductivity Temperature Depth Probe with rosette watersampler | CTD/Ros	CTD/rosette water sampler; SL max. 352 m	at depth, SL max. 352 m
MSM21/ 4-0642-1	CTD 37	2012-08-31 08:15:00.0	78°33.41’	9°31.36’	359.2	Conductivity Temperature Depth Probe with rosette watersampler | CTD/Ros	CTD/rosette water sampler	on deck
MSM21/ 4-0642-2	HF Station 43	2012-08-31 08:21:00.0	78°33.41’	9°31.36’	359.9	Heat Flow | HF	Heat Flow	surface
MSM21/ 4-0642-2	HF Station 43	2012-08-31 08:30:00.0	78°33.41’	9°31.36’	358.1	Heat Flow | HF	Heat Flow	at sea bottom
MSM21/ 4-0642-2	HF Station 43	2012-08-31 08:43:00.0	78°33.41’	9°31.36’	359.4	Heat Flow | HF	Heat Flow	off bottom
MSM21/ 4-0642-2	HF Station 43	2012-08-31 08:58:00.0	78°33.48’	9°31.75’	352.8	Heat Flow | HF	Heat Flow	on deck
MSM21/ 4-0643-1	Gravity core 15	2012-08-31 10:11:00.0	78°36.99’	9°18.65’	441.2	Gravity Corer | GC	Gravity corer	surface
MSM21/ 4-0643-1	Gravity core 15	2012-08-31 10:30:00.0	78°37.03’	9°19.02’	437.2	Gravity Corer | GC	Gravity corer	at sea bottom
MSM21/ 4-0643-1	Gravity core 15	2012-08-31 10:44:00.0	78°37.05’	9°19.14’	434.6	Gravity Corer | GC	Gravity corer	on deck
MSM21/ 4-0644-1	Gravity core 16	2012-08-31 11:08:00.0	78°36.99’	9°18.71’	441.7	Gravity Corer | GC	Gravity corer	surface

Event label	Event	Time [UTC]	Latitude [N°]	Longitude [E°]	Water depth [mbsl]	Gear	Description	Remarks
MSM21/ 4-0644-1	Gravity core 16	2012-08-31 11:39:00.0	78°37.01’	9°19.06’	436.2	Gravity Corer | GC	Gravity corer	at sea bottom
MSM21/ 4-0644-1	Gravity core 16	2012-08-31 11:56:00.0	78°37.04’	9°19.34’	433.1	Gravity Corer | GC	Gravity corer	on deck
MSM21/ 4-0644-2	Gravity core 17	2012-08-31 13:29:00.0	78°37.01’	9°19.08’	435.5	Gravity Corer | GC	Gravity corer	surface
MSM21/ 4-0644-2	Gravity core 17	2012-08-31 13:56:00.0	78°37.00’	9°19.08’	435	Gravity Corer | GC	Gravity corer	at sea bottom
MSM21/ 4-0644-2	Gravity core 17	2012-08-31 14:12:00.0	78°37.00’	9°19.13’	435	Gravity Corer | GC	Gravity corer	on deck
MSM21/ 4-0645-1	Survey S24	2012-08-31 15:50:00.0	78°36.40’	9°20.38’	430.1	Multibeam + Parasound | MB-PS	Multibeam and ParaSound	start of survey
MSM21/ 4-0645-1	Survey S24	2012-08-31 18:46:00.0	78°15.74’	8°13.13’	2167.3	Multibeam + Parasound | MB-PS	Multibeam and ParaSound	alter course
MSM21/ 4-0645-1	Survey S24	2012-08-31 20:11:00.0	78°26.48’	8°08.26’	1988.1	Multibeam + Parasound | MB-PS	Multibeam and ParaSound	alter course
MSM21/ 4-0645-1	Survey S24	2012-08-31 22:10:00.0	78°13.66’	7°54.01’	2487.5	Multibeam + Parasound | MB-PS	Multibeam and ParaSound	alter course
MSM21/ 4-0645-1	Survey S24	2012-09-01 00:08:00.0	78°26.28’	7°37.27’	2833.9	Multibeam + Parasound | MB-PS	Multibeam and ParaSound	alter course
MSM21/ 4-0645-1	Survey S24	2012-09-01 02:20:00.0	78°13.10’	7°22.38’	3250	Multibeam + Parasound | MB-PS	Multibeam and ParaSound	alter course
MSM21/ 4-0645-1	Survey S24	2012-09-01 03:44:00.0	78°20.34’	7°02.47’	3135.9	Multibeam + Parasound | MB-PS	Multibeam and ParaSound	alter course
MSM21/ 4-0645-1	Survey S24	2012-09-01 07:39:00.0	78°13.15’	6°44.38’	2397.1	Multibeam + Parasound | MB-PS	Multibeam and ParaSound	alter course
MSM21/ 4-0645-1	Survey S24	2012-09-01 10:31:00.0	78°31.36’	6°20.59’	2312.6	Multibeam + Parasound | MB-PS	Multibeam and ParaSound	alter course
MSM21/ 4-0645-1	Survey S24	2012-09-01 13:27:00.0	78°11.97’	6°07.91’	1766.2	Multibeam + Parasound | MB-PS	Multibeam and ParaSound	alter course
MSM21/ 4-0645-1	Survey S24	2012-09-01 13:54:00.0	78°11.81’	5°51.27’	1723.9	Multibeam + Parasound | MB-PS	Multibeam and ParaSound	alter course
MSM21/ 4-0645-1	Survey S24	2012-09-01 16:37:00.0	78°32.77’	5°44.92’	1803	Multibeam + Parasound | MB-PS	Multibeam and ParaSound	end of survey
MSM21/ 4-0646-1	Seismic profile P700	2012-09-01 18:07:00.0	78°25.23’	6°14.56’	1907.6	2D-Multi-Channel-Seismic | 2D-MCS	Seismic reflection profile	end deployment

Event label	Event	Time [UTC]	Latitude [N°]	Longitude [E°]	Water depth [mbsl]	Gear	Description	Remarks
MSM21/ 4-0646-1	Seismic profile P700	2012-09-01 19:06:00.0	78°26.84’	6°21.85’	2002.1	2D-Multi-Channel-Seismic | 2D-MCS	Seismic reflection profile	start of profile
MSM21/ 4-0646-1	Seismic profile P700	2012-09-01 21:55:00.0	78°37.18’	7°09.08’	1526.7	2D-Multi-Channel-Seismic | 2D-MCS	Seismic reflection profile	end of profile
MSM21/ 4-0646-1	Seismic profile P701	2012-09-01 21:55:00.0	78°37.18’	7°09.08’	1526.7	2D-Multi-Channel-Seismic | 2D-MCS	Seismic reflection profile	start of profile
MSM21/ 4-0646-1	Seismic profile P702	2012-09-01 23:07:00.0	78°36.45’	7°38.32’	1284.1	2D-Multi-Channel-Seismic | 2D-MCS	Seismic reflection profile	end of profile
MSM21/ 4-0646-1	Seismic profile P701	2012-09-01 23:07:00.0	78°36.45’	7°38.32’	1284.1	2D-Multi-Channel-Seismic | 2D-MCS	Seismic reflection profile	start of profile
MSM21/ 4-0646-1	Seismic profile P703	2012-09-02 01:31:00.0	78°24.89’	7°44.25’	2759.9	2D-Multi-Channel-Seismic | 2D-MCS	Seismic reflection profile	end of profile
MSM21/ 4-0646-1	Seismic profile P702	2012-09-02 01:31:00.0	78°24.89’	7°44.25’	2759.9	2D-Multi-Channel-Seismic | 2D-MCS	Seismic reflection profile	start of profile
MSM21/ 4-0646-1	Seismic profile P703	2012-09-02 01:55:00.0	78°24.67’	7°35.49’	2856.1	2D-Multi-Channel-Seismic | 2D-MCS	Seismic reflection profile	airgun recovered for repair, end of profile
MSM21/ 4-0646-1	Seismic profile P704	2012-09-02 03:54:00.0	78°24.69’	7°35.47’		2D-Multi-Channel-Seismic | 2D-MCS	Seismic reflection profile	start of profile
MSM21/ 4-0646-1	Seismic profile P704	2012-09-02 06:55:00.0	78°26.92’	6°21.39’	2024.3	2D-Multi-Channel-Seismic | 2D-MCS	Seismic reflection profile	end of profile
MSM21/ 4-0646-1	Seismic profile P705	2012-09-02 06:55:00.0	78°26.92’	6°21.39’	2024.3	2D-Multi-Channel-Seismic | 2D-MCS	Seismic reflection profile	start of profile
MSM21/ 4-0646-1	Seismic profile P705	2012-09-02 08:09:00.0	78°24.08’	6°42.50’	2938.8	2D-Multi-Channel-Seismic | 2D-MCS	Seismic reflection profile	end of profile
MSM21/ 4-0646-1	Seismic profile P706	2012-09-02 08:09:00.0	78°24.08’	6°42.50’	2938.8	2D-Multi-Channel-Seismic | 2D-MCS	Seismic reflection profile	start of profile
MSM21/ 4-0646-1	Seismic profile P706	2012-09-02 11:25:00.0	78°37.41’	7°25.49’	1356.6	2D-Multi-Channel-Seismic | 2D-MCS	Seismic reflection profile	end of profile
MSM21/ 4-0646-1	Seismic profile P706	2012-09-02 11:48:00.0	78°37.12’	7°31.14’	1310	2D-Multi-Channel-Seismic | 2D-MCS	Seismic reflection profile	end recovery
MSM21/ 4-0647-1	JAGO dive 10	2012-09-02 14:35:00.0	78°33.35’	9°28.44’	388.6	JAGO	JAGO Underwater Craft	weight to water
MSM21/ 4-0647-1	JAGO dive 10	2012-09-02 15:01:00.0	78°33.35’	9°28.52’		JAGO	JAGO Underwater Craft	JAGO to surface

Event label	Event	Time [UTC]	Latitude [N°]	Longitude [E°]	Water depth [mbsl]	Gear	Description	Remarks
MSM21/ 4-0647-1	JAGO dive 10	2012-09-02 15:37:00.0	78°33.35’	9°28.53’		JAGO	JAGO Underwater Craft	JAGO at depth
MSM21/ 4-0647-1	JAGO dive 10	2012-09-02 17:41:00.0	78°33.54’	9°27.57’		JAGO	JAGO Underwater Craft	back at surface
MSM21/ 4-0647-1	JAGO dive 10	2012-09-02 17:56:00.0	78°33.57’	9°26.70’		JAGO	JAGO Underwater Craft	connected to hook
MSM21/ 4-0647-1	JAGO dive 10	2012-09-02 17:59:00.0	78°33.57’	9°26.73’		JAGO	JAGO Underwater Craft	JAGO back on board
MSM21/ 4-0648-1	CTD 38	2012-09-02 18:40:00.0	78°33.34’	9°28.41’	387.1	Conductivity Temperature Depth Probe with rosette watersampler | CTD/Ros	CTD/rosette water sampler	surface
MSM21/ 4-0648-1	CTD 38	2012-09-02 18:49:00.0	78°33.34’	9°28.41’	387.1	Conductivity Temperature Depth Probe with rosette watersampler | CTD/Ros	CTD/rosette water sampler; SL max. 388 m	at depth, SL max. 388 m
MSM21/ 4-0648-1	CTD 38	2012-09-02 19:02:00.0	78°33.35’	9°28.44’	387.1	Conductivity Temperature Depth Probe with rosette watersampler | CTD/Ros	CTD/rosette water sampler	on deck
MSM21/ 4-0648-2	Gravity core 18	2012-09-02 19:11:00.0	78°33.35’	9°28.44’	386.9	Gravity Corer | GC	Gravity corer	surface
MSM21/ 4-0648-2	Gravity core 18	2012-09-02 19:33:00.0	78°33.34’	9°28.46’	386.9	Gravity Corer | GC	Gravity corer	at sea bottom
MSM21/ 4-0648-2	Gravity core 18	2012-09-02 19:48:00.0	78°33.34’	9°28.46’	386.9	Gravity Corer | GC	Gravity corer	on deck
MSM21/ 4-0648-3	Gravity core 19	2012-09-02 20:08:00.0	78°33.34’	9°28.46’		Gravity Corer | GC	Gravity corer	surface
MSM21/ 4-0648-3	Gravity core 19	2012-09-02 20:26:00.0	78°33.34’	9°28.47’		Gravity Corer | GC	Gravity corer	at sea bottom
MSM21/ 4-0648-3	Gravity core 19	2012-09-02 20:42:00.0	78°33.34’	9°28.46’		Gravity Corer | GC	Gravity corer	on deck
MSM21/ 4-0649-1	CTD 39	2012-09-02 21:28:00.0	78°36.68’	9°25.53’		Conductivity Temperature Depth Probe with rosette watersampler | CTD/Ros	CTD/rosette water sampler	surface
MSM21/ 4-0649-1	CTD 39	2012-09-02 21:38:00.0	78°36.68’	9°25.54’		Conductivity Temperature Depth Probe with rosette watersampler | CTD/Ros	CTD/rosette water sampler; SL max. 375 m	at depth, SL max. 375 m
MSM21/ 4-0649-1	CTD 39	2012-09-02 21:48:00.0	78°36.68’	9°25.53’		Conductivity Temperature Depth Probe with rosette watersampler | CTD/Ros	CTD/rosette water sampler	on deck
MSM21/ 4-0650-1	CTD 40	2012-09-02 22:24:00.0	78°39.31’	9°26.07’		Conductivity Temperature Depth Probe with rosette watersampler | CTD/Ros	CTD/rosette water sampler	surface
MSM21/ 4-0650-1	CTD 40	2012-09-02 22:31:00.0	78°39.31’	9°26.07’		Conductivity Temperature Depth Probe with rosette watersampler | CTD/Ros	CTD/rosette water sampler; SL max. 239 m	at depth, SL max. 239 m

Event label	Event	Time [UTC]	Latitude [N°]	Longitude [E°]	Water depth [mbsl]	Gear	Description	Remarks
MSM21/ 4-0650-1	CTD 40	2012-09-02 22:38:00.0	78°39.31’	9°26.07’		Conductivity Temperature Depth Probe with rosette watersampler | CTD/Ros	CTD/rosette water sampler	on deck
MSM21/ 4-0651-1	Seismic profile P800	2012-09-03 02:18:00.0	78°21.21’	7°07.12’	3174.8	2D-Multi-Channel-Seismic | 2D-MCS	Seismic reflection profile	end deployment
MSM21/ 4-0651-1	Seismic profile P800	2012-09-03 02:38:00.0	78°22.59’	7°10.29’	3247.9	2D-Multi-Channel-Seismic | 2D-MCS	Seismic reflection profile	start of profile
MSM21/ 4-0651-1	Seismic profile P801	2012-09-03 07:26:00.0	78°45.07’	7°46.92’	1044.9	2D-Multi-Channel-Seismic | 2D-MCS	Seismic reflection profile	end of profile
MSM21/ 4-0651-1	Seismic profile P800	2012-09-03 07:26:00.0	78°45.07’	7°46.92’	1044.9	2D-Multi-Channel-Seismic | 2D-MCS	Seismic reflection profile	start of profile
MSM21/ 4-0651-1	Seismic profile P801	2012-09-03 10:26:00.0	78°46.44’	6°34.13’	1810.5	2D-Multi-Channel-Seismic | 2D-MCS	Seismic reflection profile	end of profile
MSM21/ 4-0651-1	Seismic profile P802	2012-09-03 10:26:00.0	78°46.44’	6°34.13’	1810.5	2D-Multi-Channel-Seismic | 2D-MCS	Seismic reflection profile	start of profile
MSM21/ 4-0651-1	Seismic profile P802	2012-09-03 13:07:00.0	78°34.66’	6°02.81’	2269.8	2D-Multi-Channel-Seismic | 2D-MCS	Seismic reflection profile	end of profile
MSM21/ 4-0651-1	Seismic profile P803	2012-09-03 13:07:00.0	78°34.66’	6°02.81’	2269.8	2D-Multi-Channel-Seismic | 2D-MCS	Seismic reflection profile	start of profile
MSM21/ 4-0651-1	Seismic profile P804	2012-09-03 14:17:00.0	78°32.13’	6°28.17’	2421.2	2D-Multi-Channel-Seismic | 2D-MCS	Seismic reflection profile	end of profile
MSM21/ 4-0651-1	Seismic profile P803	2012-09-03 14:17:00.0	78°32.13’	6°28.17’	2421.2	2D-Multi-Channel-Seismic | 2D-MCS	Seismic reflection profile	start of profile
MSM21/ 4-0651-1	Seismic profile P805	2012-09-03 16:31:00.0	78°41.86’	6°54.60’	1450.1	2D-Multi-Channel-Seismic | 2D-MCS	Seismic reflection profile	end of profile
MSM21/ 4-0651-1	Seismic profile P804	2012-09-03 16:31:00.0	78°41.86’	6°54.60’	1450.1	2D-Multi-Channel-Seismic | 2D-MCS	Seismic reflection profile	start of profile
MSM21/ 4-0651-1	Seismic profile P805	2012-09-03 17:08:00.0	78°39.52’	6°57.65’	1517.8	2D-Multi-Channel-Seismic | 2D-MCS	Seismic reflection profile	end of profile
MSM21/ 4-0651-1	Seismic profile P805	2012-09-03 17:37:00.0	78°39.55’	7°01.71’	1460.8	2D-Multi-Channel-Seismic | 2D-MCS	Seismic reflection profile	end recovery
MSM21/ 4-0652-1	Gravity core 20	2012-09-03 18:06:00.0	78°40.84’	6°57.50’	1449.5	Gravity Corer | GC	Gravity corer	surface
MSM21/ 4-0652-1	Gravity core 20	2012-09-03 18:23:00.0	78°40.84’	6°57.50’	1450.6	Gravity Corer | GC	Gravity corer	at sea bottom
MSM21/ 4-0653-1	Gravity core 21	2012-09-03 20:30:00.0	78°33.36’	7°52.20’	1480.1	Gravity Corer | GC	Gravity corer	on deck

Event label	Event	Time [UTC]	Latitude [N°]	Longitude [E°]	Water depth [mbsl]	Gear	Description	Remarks
MSM21/ 4-0653-1	Gravity core 21	2012-09-03 21:01:00.0	78°33.31’	7°51.95’	1490	Gravity Corer | GC	Gravity corer	surface
MSM21/ 4-0653-1	Gravity core 21	2012-09-03 21:25:00.0	78°33.31’	7°51.94’	1485.9	Gravity Corer | GC	Gravity corer	at sea bottom
MSM21/ 4-0653-2	CTD 41	2012-09-03 21:44:00.0	78°33.31’	7°51.95’	1490	Conductivity Temperature Depth Probe with rosette watersampler | CTD/Ros	CTD/rosette water sampler	surface
MSM21/ 4-0653-2	CTD 41	2012-09-03 22:11:00.0	78°33.31’	7°51.95’	1486.9	Conductivity Temperature Depth Probe with rosette watersampler | CTD/Ros	CTD/rosette water sampler	at depth, SL max. 1400 m
MSM21/ 4-0653-2	CTD 41	2012-09-03 22:38:00.0	78°33.31’	7°51.95’	1488.9	Conductivity Temperature Depth Probe with rosette watersampler | CTD/Ros	CTD/rosette water sampler	on deck
MSM21/ 4-0654-1	CTD 42	2012-09-04 00:46:00.0	78°33.34’	9°28.40’	390.7	Conductivity Temperature Depth Probe with rosette watersampler | CTD/Ros	CTD/rosette water sampler	surface
MSM21/ 4-0654-1	CTD 42	2012-09-04 00:55:00.0	78°33.34’	9°28.39’	390.5	Conductivity Temperature Depth Probe with rosette watersampler | CTD/Ros	CTD/rosette water sampler	at depth, SL max. 387 m
MSM21/ 4-0654-1	CTD 42	2012-09-04 01:05:00.0	78°33.34’	9°28.39’	389.9	Conductivity Temperature Depth Probe with rosette watersampler | CTD/Ros	CTD/rosette water sampler	on deck
MSM21/ 4-0655-1	CTD 43	2012-09-04 02:02:00.0	78°36.67’	9°25.48’	380.5	Conductivity Temperature Depth Probe with rosette watersampler | CTD/Ros	CTD/rosette water sampler	surface
MSM21/ 4-0655-1	CTD 43	2012-09-04 02:09:00.0	78°36.67’	9°25.48’	380.3	Conductivity Temperature Depth Probe with rosette watersampler | CTD/Ros	CTD/rosette water sampler	at depth, SL max. 376 m
MSM21/ 4-0655-1	CTD 43	2012-09-04 02:18:00.0	78°36.68’	9°25.47’	379.7	Conductivity Temperature Depth Probe with rosette watersampler | CTD/Ros	CTD/rosette water sampler	on deck
MSM21/ 4-0656-1	CTD 44	2012-09-04 03:05:00.0	78°39.30’	9°26.02’	244.7	Conductivity Temperature Depth Probe with rosette watersampler | CTD/Ros	CTD/rosette water sampler	surface
MSM21/ 4-0656-1	CTD 44	2012-09-04 03:11:00.0	78°39.30’	9°26.01’	244.1	Conductivity Temperature Depth Probe with rosette watersampler | CTD/Ros	CTD/rosette water sampler	at depth, SL max. 236 m
MSM21/ 4-0656-1	CTD 44	2012-09-04 03:18:00.0	78°39.30’	9°26.01’	243.1	Conductivity Temperature Depth Probe with rosette watersampler | CTD/Ros	CTD/rosette water sampler	on deck
MSM21/ 4-0657-1	Gravity core 22	2012-09-04 04:33:00.0	78°33.34’	9°28.38’	388.1	Gravity Corer | GC	Gravity corer	surface
MSM21/ 4-0657-1	Gravity core 22	2012-09-04 04:45:00.0	78°33.34’	9°28.38’	388.4	Gravity Corer | GC	Gravity corer	at sea bottom
MSM21/ 4-0657-1	Gravity core 22	2012-09-04 05:00:00.0	78°33.34’	9°28.38’	389.5	Gravity Corer | GC	Gravity corer	on deck
MSM21/ 4-0658-1	CTD 45	2012-09-04 06:52:00.0	78°18.82’	9°41.65’	307.7	Conductivity Temperature Depth Probe with rosette watersampler | CTD/Ros	CTD/rosette water sampler	surface

Event label	Event	Time [UTC]	Latitude [N°]	Longitude [E°]	Water depth [mbsl]	Gear	Description	Remarks
MSM21/ 4-0658-1	CTD 45	2012-09-04 06:59:00.0	78°18.82’	9°41.65’	306.9	Conductivity Temperature Depth Probe with rosette watersampler | CTD/Ros	CTD/rosette water sampler	at depth, SL ma. 303 m
MSM21/ 4-0658-1	CTD 45	2012-09-04 07:08:00.0	78°18.82’	9°41.59’	307.4	Conductivity Temperature Depth Probe with rosette watersampler | CTD/Ros	CTD/rosette water sampler	on deck
MSM21/ 4-0658-1	Survey S25	2012-09-04 07:08:00.0	78°18.82’	9°41.59’	307.4	Multibeam + Parasound | MB-PS	Multibeam and ParaSound	start of survey
MSM21/ 4-0659-1	Survey S26	2012-09-06 17:06:00.0	67°08.03’	4°40.93’	1354	Multibeam + Parasound | MB-PS	Multibeam and ParaSound	end of survey
MSM21/ 4-0658-1	Survey S25	2012-09-06 17:06:00.0	67°08.03’	4°40.93’	1354	Multibeam + Parasound | MB-PS	Multibeam and ParaSound	start of survey
MSM21/ 4-0659-1	Survey S26	2012-09-06 17:44:00.0	67°06.72’	4°41.56’	1352.2	Multibeam + Parasound | MB-PS	Multibeam and ParaSound	end of survey
MSM21/ 4-0660-1	Gravity core 23	2012-09-06 18:24:00.0	67°06.67’	4°41.74’	1348	Gravity Corer | GC	Gravity corer	surface
MSM21/ 4-0660-1	Gravity core 23	2012-09-06 18:52:00.0	67°06.68’	4°41.74’	1348	Gravity Corer | GC	Gravity corer	at sea bottom
MSM21/ 4-0660-1	Gravity core 23	2012-09-06 19:19:00.0	67°06.68’	4°41.74’	1348	Gravity Corer | GC	Gravity corer	on deck
MSM21/ 4-0661-1	Gravity core 24	2012-09-06 19:59:00.0	67°06.67’	4°41.63’	1344	Gravity Corer | GC	Gravity corer	surface
MSM21/ 4-0661-1	Gravity core 24	2012-09-06 20:31:00.0	67°06.64’	4°41.64’	1344	Gravity Corer | GC	Gravity corer	at sea bottom
MSM21/ 4-0661-1	Survey S27	2012-09-06 20:57:00.0	67°06.64’	4°41.64’	1344	Multibeam + Parasound | MB-PS	Multibeam and ParaSound	start of survey
MSM21/ 4-0661-1	Gravity core 24	2012-09-06 20:57:00.0	67°06.64’	4°41.64’	1344	Gravity Corer | GC	Gravity corer	on deck
MSM21/ 4-0661-1	Survey S27	2012-09-07 11:15:00.0	64°42.31’	4°58.38’	799.5	Multibeam + Parasound | MB-PS	Multibeam and ParaSound	end of survey
MSM21/ 4-0662-1	Gravity core 25	2012-09-07 11:15:00.0	64°42.31’	4°58.38’	799.5	Gravity Corer | GC	Gravity corer	surface
MSM21/ 4-0662-1	Gravity core 25	2012-09-07 11:30:00.0	64°42.31’	4°58.38’	798.4	Gravity Corer | GC	Gravity corer	at sea bottom
MSM21/ 4-0662-1	Gravity core 25	2012-09-07 11:49:00.0	64°42.31’	4°58.38’	799.1	Gravity Corer | GC	Gravity corer	on deck
MSM21/ 4-0663-1	Gravity core 26	2012-09-07 13:36:00.0	64°35.11’	4°45.76’	1149.1	Gravity Corer | GC	Gravity corer	surface

Event label	Event	Time [UTC]	Latitude [N°]	Longitude [E°]	Water depth [mbsl]	Gear	Description	Remarks
MSM21/ 4-0663-1	Gravity core 26	2012-09-07 13:50:00.0	64°35.12’	4°45.76’	1143.9	Gravity Corer | GC	Gravity corer	at sea bottom
MSM21/ 4-0663-1	Gravity core 26	2012-09-07 14:13:00.0	64°35.10’	4°45.75’	1143	Gravity Corer | GC	Gravity corer	on deck
MSM21/ 4-0664-1	Survey S28	2012-09-09 05:14:00.0	58°36.11’	2°06.90’	92.4	Multibeam + Parasound | MB-PS	Multibeam and ParaSound	start of survey
MSM21/ 4-0664-1	Survey S28	2012-09-09 05:35:00.0	58°35.95’	2°05.36’	92.9	Multibeam + Parasound | MB-PS	Multibeam and ParaSound	end of survey
MSM21/ 4-0665-1	Lander deployment	2012-09-09 07:21:00.0	58°35.76’	2°05.36’	91.8	Lander | LANDER	Bottom lander	surface
MSM21/ 4-0665-1	Lander deployment	2012-09-09 07:33:00.0	58°35.76’	2°05.35’	91.8	Lander | LANDER	Bottom lander	released

8 Data and Sample Storage and Availability

A Cruise Summary Report (CRS) was compiled and submitted to DOD (Deutsches Ozeanographisches Datenzentrum), BSH, Hamburg, immediately after the cruise.

Concerning data storage a joint data management team of GEOMAR and Kiel University organizes and supervises data storage and publication by marine science projects in a web based multi-user system. In a first phase, data are only available to the project user groups. After a three year proprietary time the data management team will publish these data by dissemination to national and international data archives, i.e. the data will be submitted to PANGAEA no later than September, 2015. Digital object identifiers (DOIs) are automatically assigned to data sets archived in the PANGAEA Open Access library making them publically retrievable, citable and reusable for the future.

All metadata are immediately available publically via the following link pointing at the GEOMAR portal (https://portal.geomar.de/metadata/leg/show/315696).
In addition the portal provides a single downloadable KML formatted file (https://portal.geomar.de/metadata/leg/kmlexport/315696) which retrieves and combines up-to-date cruise (MSM21-4) related information, links to restricted data and to published data for visualization e.g. in GoogleEarth. Cruise related data can be found on PANGAEA at: http://www.pangaea.de/search?q=campaign%3A"MSM21/4"

Data availability

Data type	Database	Available	Contact
Seismic data	Pangaea/GEOMAR	10.9.2015	Dirk Klaeschen
Parasound data	Pangaea/GEOMAR	10.9.2015	Dirk Klaeschen
Multi-beam data	Pangaea/GEOMAR	10.9.2015	Ingo Klaucke
Heat flow data	Pangaea	1.1.2014	Tom Feseker
Geochemistry	Pangaea	1.1.2014	Tina Treude
Water chemistry	Pangaea	10.9.2015	Helge Niemann
Sediment cores	Pangaea/GEOMAR	10.9.2015	Joachim Schönfeld
Air samples	Pangaea/RHUL	10.9.2015	Euan Nisbet/RHUL

9 Acknowledgements

We like to thank captain Klaus Bergmann, his officers and crew of RV Maria S. Merian for their professional support of our science programme and for very pleasant company on board. We also like to thank our technical engineer Gero Wetzel for his dedication to making things work.

The ship time of RV Maria S. Merian was provided by the Deutsche Forschungsgemeinschaft within the core program METEOR/MERIAN. Financial support for the different projects carried out during the cruise was provided through the Excellence Cluster Future Ocean and funding through the institutions involved. We gratefully appreciate all this support.

10 References

Archer, D., Buffett, B. (2005). "Time-dependent response of the global ocean clathrate reservoir to climatic and anthropogenic forcing." Geochemistry Geophysics Geosystems. 6 (3).

Berndt, C., Bünz, S., Clayton, T., Mienert, J. and Saunders, M. (2004). "Seismic character of bottom simulating reflectors: Examples from the mid-Norwegian margin." Marine and Petroleum Geology, 21 (6), pp. 723-733.

Berndt, C., Brune, S., Nisbet, E., Zschau, J. and Sobolev, S. V. (2009). "Tsunami modeling of a submarine landslide in Fram Strait." Geochemistry Geophysics Geosystems, 10 (4).

Buffett, B. and D. Archer (2004). "Global inventory of methane clathrate: sensitivity to changes in the deep ocean." Earth and Planetary Science Letters, vol. 227(3-4): 185-199.

Biastoch, A., T. Treude, L. H. Rüpke, U. Riebesell, C. Roth, E. B. Burwicz, W. Park, C. W. Böning, M. Latif, G. Madec and K. Wallmann (2011). "Rising Arctic Ocean temperatures cause gas hydrate destabilization and ocean acidification." Geophysical Research Letters, 38.

Boetius. A.. K. Ravenschlag. et al. (2000). "A marine microbial consortium apparently mediating anaerobic oxidation of methane." Nature, vol. 407(6804): 623-626.

Bünz, S., J. Petersen, et al. (2008). "Environmentally-sensitive gas hydrates on the W-Svalbard margin at the gateway to the Arctic Ocean." Proceedings of the 6th International Conference on Gas Hydrates (ICGH 2008), July 6-10, Vancouver, British Columbia. Canada.

Dickson, R. R. (1999). "All change in the Arctic." Nature. vol. 397: 389-391.

Dimitrov, L. (2002). "Contribution to atmospheric methane by natural seepages on the Bulgarian continental shelf." Continental Shelf Research**,** vol. 22(16): 2429-2442.

Ekström, G., M. Nettles, et al. (2003). "Glacial earthquakes." Science, vol. 302(5654): 622-624.

Feseker, T., Wetzel, G., Heesemann, B. (2012). "Introducing the T-Stick: A new device for high precision in situ sediment temperature profile measurements". Limnol. Oceanogr-Meth. 10, 31-40.

Fisher, R. E., S. Sriskantharajah, et al. (2011). "Arctic methane sources: Isotopic evidence for atmospheric inputs." Geophysical Research Letters, 38(21).

Hassol, S. J. (2004). "Impacts of a warming Arctic - Arctic climate impact assessment." Cambridge. Cambridge University Press.

Harvey, L. D. and Z. Huang (1995). "Evaluation of the potential impact of methane clathrate destabilization on future global warming." Journal of Geophysical Research, vol. 100(D2): 2905-2926.

Hill, J. C., N. W. Driscoll, et al. (2004). "Large-scale elongated gas blowouts along the U.S. Atlantic margin." Journal of Geophysical Research, vol. 10(9): 2969.

Hinrichs, K. U. and A. Boetius (2002). "The anaerobic oxidation of methane: new insights in microbial ecology and biogeochemistry." Ocean Margin Systems. G. Wefer. D. S. M. Billet. D. Hebbeln. B. B. Jørgensen and M. Schlüter. Heidelberg, Springer**:** 457-477.

IPCC (2001). Third annual report of the Intergovernmental Panel on Climate Change, Geneva, Switzerland, World Meteorological Organization.

Johannessen, O. M., L. Bengtsson, et al. (2004). "Arctic climate change: observed and modelled temperature and sea-ice variability." Tellus, vol. 56(A(4)): 328-341.

Judd, A. G., M. Hovland, et al. (2002). "The geological methane budget at continental margins and its influence on climate change." Geofluids, vol. 2: 109-126.

Jung, W.-Y. and P. R. Vogt (2004). "Effects of bottom water warming and sea level rise on Holocene hydrate dissociation and mass wasting along the Norwegian-Barents Continental Margin." Journal of Geophysical Research, vol. 109(B06104).

Kastner, M., D. Bartlett, et al. (2005). "CH_4 fluxes across the seafloor at three distinct gas hydrate fields: Impacts on ocean and atmosphere chemistry." International Gas Hydrate Conference, Trondheim.

Kennett. J. P., K. G. Cannariato, et al. (2003). "Methane Hydrates in Quaternary Climate Change: The Clathrate Gun Hypothesis." Washington, D.C., American Geophysical Union.

Knies. J., E. Damm, et al. (2004). "Near-surface hydrocarbon anomalies in shelf sediments off Spitsbergen: Evidences for past seepages." Geochemistry Geophysics Geosystems, vol. 5.

Luff. R., Wallmann, K. (2003). "Fluid flow. methane fluxes. carbonate precipitation and biogeochemical turnover in gas hydrate-bearing sediments at Hydrate Ridge. Cascadia Margin: Numerical modeling and mass balances.“ Geochimica et Cosmochimica Acta, vol. 67 (18), pp 3403-3421.

Knittel. K. and A. Boetius. (2009). Anaerobic Oxidation of Methane: Progress with an Unknown Process, Annual Review of Microbiology 63: 311-334.

Kvalstad. T. J., L. Andresen, et al. (2005). "The Storegga slide: evaluation of triggering sources and slide mechanics." Marine and Petroleum Geology, vol. 22(1-2): 245-256.

Kvenvolden. K.A. and Rogers. B.W. (2005). „Gaia’s breath – global methane exhalations.“ Marine and Petroleum Geology 22: 579-590.

Landvik. J., Ó. Ingólfsson, et al. (2005). "Rethinking Late Weichselian ice-sheet dynamics in coastal NW Svalbard." Boreas, vol. 34: 7-24.

Landvik. J. Y., Bondevik. S., Elverhøi. A., Fjeldskaar. W., Mangerud. J., Salvigsen. O., Siegert. M. J., Svendsen. J. I. and Vorren. T. O. (1998). "The last glacial maximum of Svalbard and the Barents Sea area: ice sheet extent and configuration.“ Quaternary Science Reviews 17, 43_75.

Mangerud. J., Dokken. T., Hebbeln. D. (1998). "Fluctuations of the Svalbard Barents Sea ice sheet during the last 150.000 years.“ Quaternary Science Reviews, vol. 17 (1-3), pp 11-42.

Mienert. J., M. Vanneste, et al. (2005). "Ocean warming and gas hydrate stability on the mid-Norwegian margin at the Storegga Slide." Marine and Petroleum Geology, vol. 22(1-2): 233-244.

Mienert. J., Vanneste. M., Haflidason. H., and Bünz. S. (2010). Norwegian margin outer shelf cracking: a consequence of climate-induced gas hydrate dissociation? International Journal for Earth Sciences, DOI 10.1007/s00531-010-0536-z.

Milkov. A. V. (2004). "Global estimates of hydrate-bound gas in marine sediments: how much is really out there?" Earth Science Reviews, vol. 66(3-4): 183-197.

Nauhaus. K., Albrecht. M., Elvert. M., et al. (2007). "In vitro cell growth of marine archaeal-bacterial consortia during anaerobic oxidation of methane with sulfate.“ Environmental Microbiology, vol. 9 (1), pp 187-196.

Niemann. H., J. Duarte, et al. (2006). "Microbial methane turnover at mud volcanoes of the Gulf of Cadiz." Geochemica et Cosmochimica Acta, vol. 70: 5336-5355.

Ottesen. D., J. A. Dowdeswell, et al. (2007). "Dynamics of the Late Weichselian ice sheet on Svalbard inferred from high-resolution sea-floor morphology." Boreas, vol. 36(3): 286-306.

Reeburgh, W. S. (2007). "Oceanic methane biogeochemistry". Chemical Reviews 107: 486-513.

Ritzmann. O. and W. Jokat (2003). "Crustal structure of northwestern Svalbard and the adjacent Yermak Plateau: evidence for Oligocene detachment tectonics and non-volcanic breakup." Geophysical Journal International, vol. 152: 139-159.

Ritzmann. O., Jokat. W., Czuba. W., Guterch. A., Mjelde. R. and Nishimura. Y.. (2004). "A deep seismic transect from Hovgård Ridge to northwestern Svalbard across the continental-ocean transition: A sheared margin study." Geophysical Journal International, vol. 157, pp. 683–702.

Sahling. H., Rickert. D., Lee. R.W., et al. (2002). "Macrofaunal community structure and sulfide flux at gas hydrate deposits from the Cascadia convergent margin. NE Pacific." Marine Ecology Progress Series, vol. 231, pp 121-138.

Sato. T., J. Okuno, et al. (2006). "A geophysical interpretation of the secular displacement and gravity rates observed at Ny-Ålesund. Svalbard in the Arctic; effects of post-glacial rebound and present-day ice melting." Geophysical Journal International, vol. 165(3): 729-743.

Shindell. D.T., Faluvegi. G., Koch. D.M., Schmidt. G.A., Unger. N., Bauer. S.E. (2009). "Improved attribution of climate forcing to emissions." Science, Vol. 326 no. 5953, pp 716-718.

Sloan Jr., E. D. (1998). Physical/chemical properties of gas hydrates and application to world margin stability and climatic change. Gas Hydrates: Relevance to World Margin Stability and Climate Change. J.-P. Henriet and J. Mienert, Geological Society of London, vol. 137**:** 31-50.

Svendsen. J. I., H. Alexanderson, et al. (2004). "Late Quaternary ice sheet history of northern Eurasia." Quaternary Science Reviews, vol. 23(11-13): 1229-1271.

Thiede. J. and Myhre. A.M.. (1996). Introduction to the North Atlantic - Arctic Gateways: Plate tectonic - paleoceanographic history and significance. In: J. Thiede, A.M. Myhre, J.V. Firth, G.L. Johnson and W.F. Ruddiman (Editors). Proceedings on ODP. scientific results, Ocean Drilling Program, TX, USA, pp. 3-23. Weitemeyer, K.A., S. C. Constable, K. W. Key, and J. P. Behrens (2006). First results from a marine controlled-source electromagnetic survey to detect gas hydrates offshore Oregon. GEOPHYs. RES. LETTERS, 33, doi:10.1029/2005GL024896.

Tishchenko. P., Hensen. C., Wallmann, K., and Wong, C. S. (2005). Calculation of the stability and solubility of methane hydrate in seawater. Chemical Geology, 219(1-4). 37-52.

Treude. T., Boetius, A., Knittel, K., Wallmann, K. and Jorgensen. B. B. (2003). "Anaerobic oxidation of methane above gas hydrates" Marine Ecology Progress Series, 264, pp. 1-14.

Treude, T., Krüger, M., Boetius, A., Jørgensen, B.B. (2005). "Environmental control on anaerobic oxidation of methane in the gassy sediments of Eckernförde Bay (German Baltic)." Limnol. Oceanogr. 50, 1771-1786.

Vanneste, M., S. Guidard, et al. (2005). "Bottom-simulating reflections and geothermal gradients across the western Svalbard margin." Terra Nova, vol. 17(6): 510-516.

Villinger. H., and E. E. Davis. (1987). A new reduction algorithm for marine heat flow measurements. J. Geophys. Res. 92(B12):12846-12856.

Valentine, D.L., Blanton, D.C., Reeburgh, W.S., and Kastner, M. (2001). "Water column methane oxidation adjacent to an area of active gas hydrate dissociation." Eel River Basin, Geochim Cosmochim Acta 65: 2633-2640.

Vogt, P. R., K. Crane, et al. (1994). "Methan-generated(?) pockmarks on young. thickly sedimented oceanic crust in the Arctic: Vestnesa Ridge, Fram strait." Geology (22): 255-258.

Vogt, P. R. and W.-Y. Jung (2002). "Holocene mass wasting on upper non-polar continental slopes - due to post-glacial ocean warming and hydrate dissociation?" Geophysical Research Letters, vol. 29(9).

Wegener, G., Boetius, A. (2008). "Short-term changes in anaerobic oxidation of methane in response to varying methane and sulphate fluxes." Biogeosciences Discussions.

Westbrook, G. K., et al. (2008). "Estimation of gas-hydrate concentration from multi-component seismic data at sites on the continental margins of NW Svalbard and the Storegga region of Norway." Mar. Pet. Geol., 25, 744– 758.

Westbrook, G. K., R. Exley, T. Minshull, H. Nouzé, A. Gailler, T. Jose, S. Ker and A. Plaza (2008b). "High-resolution 3D seismic investigations of hydrate-bearing fluid escape chimneys in the Nyegga region of the Voring Plateau. Norway". Proc. 6th Int. Conf. on Natural Gas Hydrates, paper 5597.

Westbrook, G.K., Thatcher, K.E., Rohling, E.J., Piotrowski, A.M., Pälike, H., Osborne, A.H., Nisbet, E.G., Minshull, T.A., Lanoisellé, M., James, R.H., Hühnerbach, V., Green, D., Fisher, R.E., Crocker, A.J., Chabert, A., Bolton, C., Beszczynska-Möller, A., Berndt, C., and Aquilina, A. (2009). "Escape of methane gas from the sea bed along the West Spitsbergen continental margin." Geophysical Research Letters, v. GL039191.

Winkelmann, D., W. Jokat, et al. (2006). "Age and extent of the Yermak Slide north of Spitsbergen. Arctic Ocean." Geochemistry, Geophysics, Geosystems**,** vol. 7(6).

Winkelmann, D. and R. Stein (2007). "Triggering of the Hinlopen/Yermak megaslide in relation to paleoceanography and climate history of the continental margin north of Spitsbergen." Geochemistry, Geophysics, Geosystems, vol. 8(6): Q06018.